Chapter 7

Canopy Spectral Invariants: Shabanov et al.

(Re)View: Stenberg et al.

(Re)View: Wang et al.

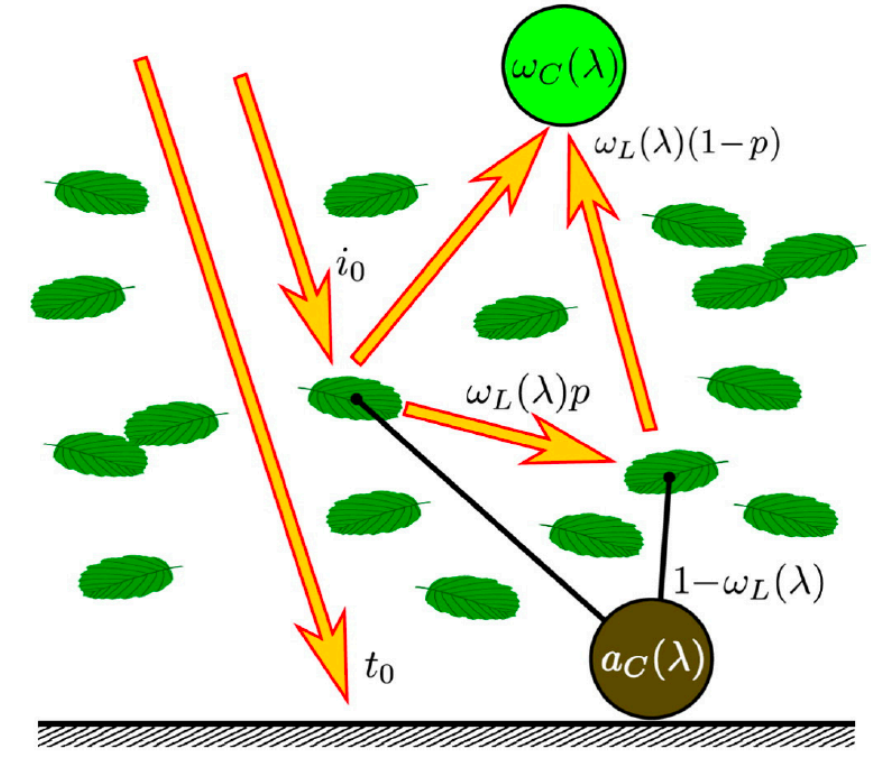

Chapter 7

Canopy Spectral Invariants

1. Introduction

The *shortwave radiation budget* describes how the fraction of radiation absorbed by or scattered out from the canopy to the underlying background or back to space are related to the structural and optical properties of canopy and background. Operational remote sensing or climate applications of the model of shortwave radiation budget naturally require that such model should build upon a canopy representation with only a small set of basic parameters which govern the radiation budget with sufficient accuracy.

The interaction of solar radiation with the vegetation canopy is fully described by the three-dimensional (3D) RT equation. The scale of the elementary volume of the equation (scale of leaves, branches, twigs, etc.) is large compared to the wavelength of solar radiation, and, according to principles of physics, the photon free path between two successive interactions is independent of the wavelength. Namely, while the scattering and absorption processes are different at different wavelengths, the interaction probabilities for photons in vegetation media (interaction cross-section or extinction coefficient) are determined by the structure of the canopy rather than photon wavelength or the optics of the canopy.

This feature of the RT equation allowed formulation of the concept of canopy *spectral invariants*. This concept states that simple algebraic combinations of leaf and canopy spectral transmittance and reflectance become wavelength independent and determine a small set of canopy structure specific variables. The set of structural variables includes *canopy interceptance*, *recollision* and *escape probabilities*. These variables specify the spectral response of a vegetation canopy to the incident solar radiation and allow for a simple and accurate parameterization of the partitioning of the incoming radiation into canopy transmission, reflection and absorption at any wavelength in the solar spectrum. In addition to the spectral invariance property, these variables poses fundamental scaling property, allowing to scale RT parameters over full range of landscape scales from leaf internals, through leaf, shoots, crowns to whole canopy. Thus, the spectral invariant approach provides a compact alternative to the full 3D RT equation for operational remote sensing or climate applications.

This chapter is organized as follows. We start by introducing basic physical principles of the spectral invariants and supporting field measurements. Next, we present rigorous mathematical formulation of the spectral invariants based on the method Successive Orders of Scattering approximations (SOSA) or Neumann series and eigenvalue/eigenvector theory of functional analysis. Finally, we discuss the scaling properties of spectral invariants and illustrate this fundamental feature with two case studies: (a) scaling from needles to shoots in the needle leaf canopies and (b) scaling form leaf internals to leaf.

2. Physical Principles of Spectral Invariants

Radiation Fluxes at Leaf and Canopy Scale: The 3D RT equation can be interpreted as the link between leaf and canopy scale radiation fluxes (Chapter 3 and 4). At the *leaf scale* the radiation fluxes are described in terms of spectral leaf transmittance and reflectance. The *leaf transmittance* (reflectance) is the portion of radiation flux density incident on the leaf surface that the leaf transmits (reflects) (Chapter 3). The leaf albedo, $\omega(\lambda)$, is the sum of the leaf reflectance, $\rho_L(\lambda)$, and transmittance, $\tau_L(\lambda)$,

$$\omega(\lambda) = \rho_L(\lambda) + \tau_L(\lambda). \quad (1)$$

The fluxes at the *canopy scale* are described in terms of spectral canopy interceptance, absorptance, reflectance and transmittance. The canopy *interceptance (absorptance)* is the ratio of the mean flux density intercepted (absorbed) by canopy leaves to the downward radiation flux density above the canopy. Similarly, *canopy transmittance* (*reflectance*) is the ratio of the mean downward radiation flux density at the canopy bottom (mean upward radiation flux density at the canopy top) to the downward radiation flux density above the canopy. According to RT theory (Chapter 3), the canopy interceptance, $i(\lambda)$, absorptance, $a(\lambda)$, reflectance, $r(\lambda)$, and transmittance, $t(\lambda)$, are defined as follows:

$$i(\lambda) \equiv \int_V d\underline{r} \int_{4\pi} d\underline{\Omega}\, \sigma(\underline{r},\underline{\Omega})\, I(\lambda,\underline{r},\underline{\Omega}), \tag{2a}$$

$$a(\lambda) \equiv \int_V d\underline{r} \int_{4\pi} d\underline{\Omega}\, \sigma_a(\underline{r},\underline{\Omega})\, I(\lambda,\underline{r},\underline{\Omega}), \tag{2b}$$

$$r(\lambda) \equiv \int_{2\pi+} d\underline{\Omega}\, \mu(\underline{\Omega}) I(\lambda,\underline{r}=0,\underline{\Omega}), \tag{2c}$$

$$t(\lambda) \equiv \int_{2\pi-} d\underline{\Omega}\, \mu(\underline{\Omega}) I(\lambda,\underline{r}=H,\underline{\Omega}). \tag{2d}$$

In the above, $I(\lambda,\underline{r},\underline{\Omega})$ is the radiation intensity at wavelength λ, spatial location $\underline{r}$, and in direction $\underline{\Omega}$, $\sigma(\underline{r},\underline{\Omega})$ is the interaction cross-section, and $\sigma_a(\underline{r},\underline{\Omega})$ is the absorption cross-section. The interaction cross-section is treated as wavelength independent considering the size of the scattering elements (leaves, branches, twigs, etc.) relative to the wavelength of solar radiation [Ross, 1981]. The interaction cross-section, $\sigma(\underline{r},\underline{\Omega})$, consist of absorption, $\sigma_a(\underline{r},\underline{\Omega})$ and scattering, $\sigma'_s(\underline{r},\underline{\Omega})$, cross-sections (cf. Chapter 3):

$$\sigma(\underline{r},\underline{\Omega}) = \sigma_a(\underline{r},\underline{\Omega}) + \sigma'_s(\underline{r},\underline{\Omega}), \tag{3a}$$

where

$$\sigma_a(\underline{r},\underline{\Omega}) = [1-\omega(\lambda)]\sigma(\underline{r},\underline{\Omega}), \tag{3b}$$

$$\sigma_s'(\underline{r},\underline{\Omega}) \equiv \int_{4\pi} d\underline{\Omega}'\,\sigma_s(\underline{r},\underline{\Omega}\rightarrow\underline{\Omega}') = \omega(\lambda)\sigma(\underline{r},\underline{\Omega}). \tag{3c}$$

In the above $\sigma_s(\underline{r},\underline{\Omega}\rightarrow\underline{\Omega}')$ is the differential scattering cross-section. Thus, combining Eqs. (2) and (3) we have,

$$a(\lambda) = [1-\omega(\lambda)]\,i(\lambda). \tag{4}$$

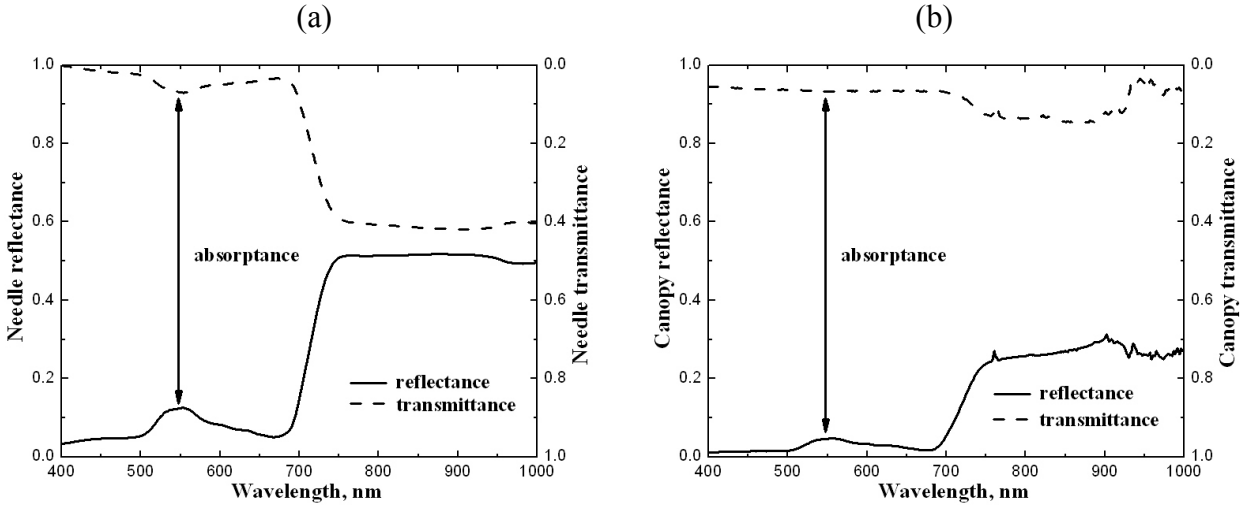

Figure 1. Needle (Panel a) and canopy (Panel b) spectral reflectance (vertical axis on the left side) and transmittance (vertical axis on the right side) for a Norway spruce (*Picea abies (L.) Karst*) stand at Flakaliden site in Sweden. Arrows show needle and canopy absorptance. The effective LAI at the site was 4.37. The needle transmittance, τ_L, and albedo, ω, follow the regression line $\tau_L = 0.47\omega - 0.02$.

The canopy absorptance, reflectance and transmittance are the three components of the shortwave energy conservation law which describes canopy spectral response to incident solar radiation at the *canopy scale*. If reflectance of the ground below the vegetation is zero (black soil, cf. Chapter 4), the portion of radiation absorbed, $a(\lambda)$, transmitted, $t(\lambda)$, or reflected, $r(\lambda)$, by the canopy totals to unity, i.e.,

$$t(\lambda) + r(\lambda) + a(\lambda) = 1. \quad (5)$$

The key reference data set for this Chapter will be field data collected in Flakaliden site in Sweden [Huang et al., 2007]. Other ancillary sources will be mentioned as appropriate. Canopy spectral transmittance and reflectance, soil and understorey reflectance spectra, needle optical properties, shoot structure and LAI were collected in six 50x50 m plots composed of Norway spruce (*Picea abies* (L.) Karst) located at Flakaliden research area ($64^0 14'$N, $19^0 46'$E), operated by the Swedish University of Agricultural Studies. The spectral measurements of canopy and needles were taken by ASD Field spec Pro handheld spectroradiometer. Needle spectral reflectances and transmittances of an average needle were obtained by averaging 50 measured spectra with highest weight given to the 2-year-old needles (80%) and equal weights to the current (10%) and 1-year (10%) needles. Figure 1 shows needle and canopy transmittance, reflectance and absorptance spectra at the Flakaliden site.

Mechanism of Scattering: Consider the following basic scheme of the relationship between leaf and canopy scales radiation fluxes. We assume that canopy is illuminated from the top by monodirectional unit flux. Canopy bottom is assumed to be absolutely absorbing, such that photons hit background will not re-enter, but exit canopy. The incident unit flux undergo multiple interactions with phytoelements and ultimately is partitioned into absorbed, $a(\lambda)$, transmitted, $t(\lambda)$, and reflected, $r(\lambda)$, portions. To analyze multiple scattering, we separate the radiation flux incident on vegetation canopy into two components (Fig. 2): directly intercepted by leaves and available for future interaction events (*zero-order interceptance*, i_0), and directly transited to the canopy bottom without hitting a leaf (*zero-order transmittance*, t_0):

$$1 = i_0 + t_0. \quad (6a)$$

The intercepted photons, i_0, will participate in the multiple scattering and ultimately will be either absorbed, $a(\lambda)$, or scattered outside of canopy, $s(\lambda)$:

$$i_0 = a(\lambda) + s(\lambda). \quad (6b)$$

Thus,

$$1 = a(\lambda) + s(\lambda) + t_0 . \qquad (6c)$$

Note, i_0 and t_0 are zero-order scattering quantities, while $a(\lambda)$ and $s(\lambda)$ are total quantities, accumulated over multiple events of scattering. While $a(\lambda)$ and $s(\lambda)$ are wavelength dependent, i_0 and t_0 don't depend on wavelength, that is, they are function of overall canopy structure/architecture and illumination geometry, but not leaf optical properties.

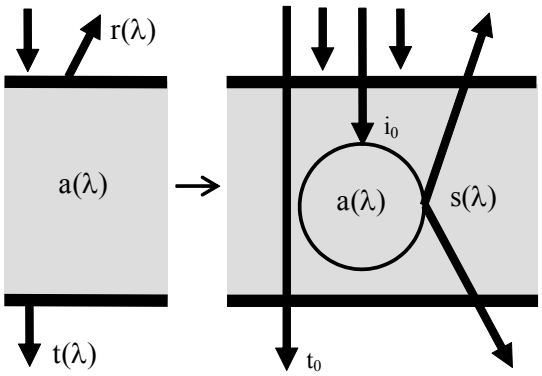

Figure 2. Partitioning of the incoming flux between canopy absorptance, $a(\lambda)$, transmittance, $t(\lambda)$, and reflectance, $r(\lambda)$, (left panel) as the result of the scattering process (right panel). The incoming flux is intercepted by canopy, (zero-order intrerceptance, i_0) or directly transmitted through canopy (zero-order transmittance, t_0). The intersepted flux participates in multiple scattering and is further subdivided between absorptance, $a(\lambda)$, and scattering out of canopy, $s(\lambda)$.

The scheme of multiple scattering is as follows. At each individual event of interaction in the sequence of multiple scattering, the $\omega(\lambda)$ portion of intercepted photons is scattered and $1 - \omega(\lambda)$ portion is absorbed (Fig. 3). In turn, the scattered portion, $\omega(\lambda)$, can be further subdivided into two parts: with probability p (*recollision probability*) photon will further participate in multiple scattering and will hit new leaf again, while with the probability 1-p the photon will be removed from canopy. Thus, the three components of the radiation budget for the singe photon-phytoelement interaction event are (Fig. 3):

[Absorbed] + [Re-scattered] + [Scattered out of canopy] =

$$= \left[1-\omega(\lambda)\right] + \left[p\omega(\lambda)\right] + \left[(1-p)\omega(\lambda)\right] \equiv 1. \qquad (7)$$

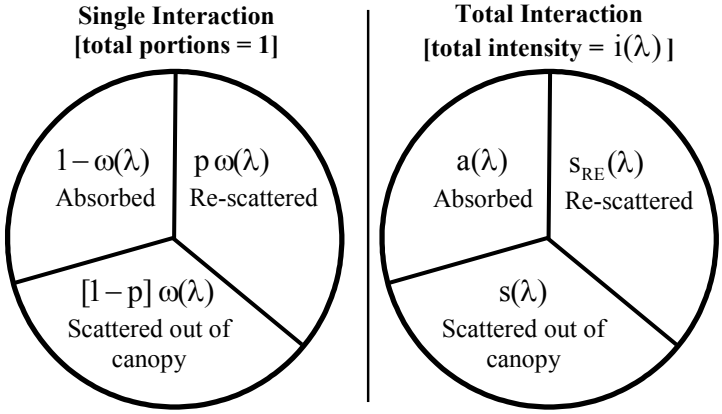

Figure 3. Partitioning of energy between absorbed, scattered out of canopy and rescattered within canopy portions is preserved through the individual scattering events (left panel). This leads to the same proportions for the total radiation regime (right panel).

Consider the sequence of scattering events generating the total observed radiation regime as detailed in Fig. 4. Part of the incoming intensity in the amount of t_0 is directly transmitted to the canopy bottom and will not participate in the process of multiple scattering. The remaining part of the incoming radiation, i_0, will be intercepted by canopy and become the source of the first interaction event resulting in the first-order absorptance, $a_1 = [1-\omega(\lambda)]\cdot i_0$, scattering out of canopy, $s_1 = [1-p]\omega(\lambda)\cdot i_0$ and re-scattering, $s_{RE,1} = \omega(\lambda)p\cdot i_0$, all are in proportions as shown in Fig. 3. The re-scattered portion will serve as a source for the second-order interaction events, and so on. Referring to Fig. 4, the canopy total *interceptance,* $i(\lambda)$, absorptance, $a(\lambda)$, scattering, $s(\lambda)$, and rescattering, $s_{RE}(\lambda)$ are calculated as the sum of contributions of individual scattering events:

$$i(\lambda) \equiv i_0 + i_1(\lambda) + i_2(\lambda) + ... = i_0 \sum_{k=0}^{\infty} \left[\omega(\lambda)p\right]^k = \frac{1}{1-p\omega(\lambda)} \cdot i_0 \equiv n_{eff}(\lambda)\cdot i_0, \qquad (8a)$$

$$a(\lambda) = i_0[1-\omega(\lambda)] \sum_{k=0}^{\infty} \left[\omega(\lambda)p\right]^k = \frac{1-\omega(\lambda)}{1-p\omega(\lambda)} \cdot i_0, \qquad (8b)$$

$$s(\lambda) = i_0[1-p]\omega(\lambda) \sum_{k=0}^{\infty} \left[\omega(\lambda)p\right]^k = \frac{[1-p]\omega(\lambda)}{1-p\omega(\lambda)} \cdot i_0, \qquad (8c)$$

$$s_{RE}(\lambda) = i_0 p\omega(\lambda)\sum_{k=0}^{\infty}\left[\omega(\lambda)p\right]^k = \frac{p\omega(\lambda)}{1-p\omega(\lambda)}\cdot i_0. \qquad (8d)$$

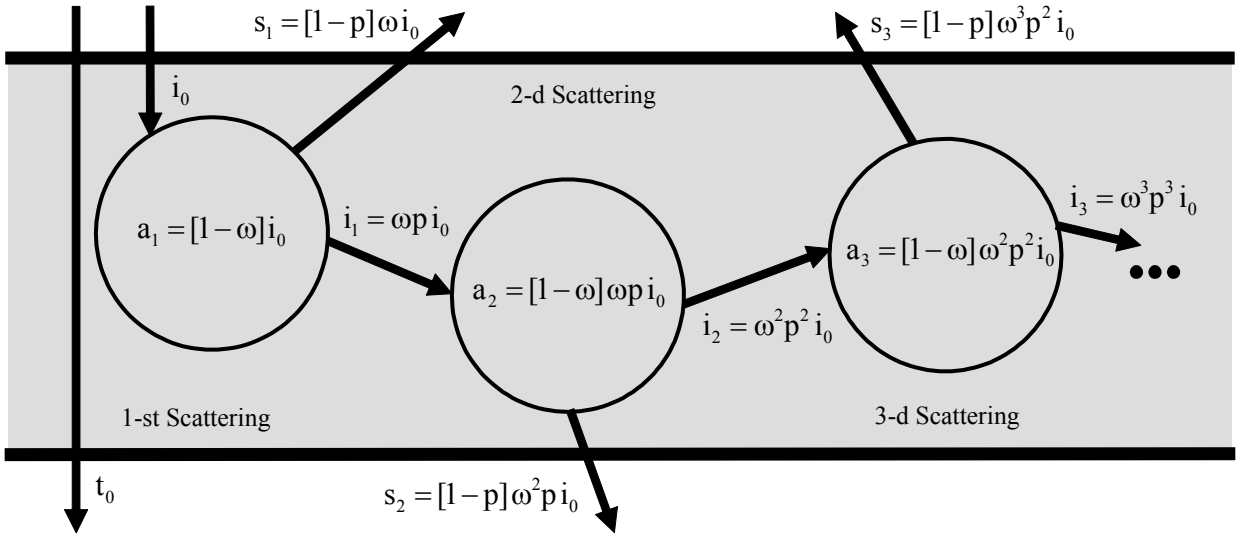

Figure 4. Quantitative presentation of the scattering scheme shown in Fig. 2. The sequence of cicles represents sequence of scattering events. The energy budget for each individual scattering event (intercepted, absorbed, scattered out of canopy and rescattered within the canopy portions) is according to Fig.3.

Refer to Fig. 5, which explains the meaning of the effective number of photon-phytoelement interactions, n_{eff}, appearing in Eq. (8a). According to the definition, the total intercepted by phytoelements radiation is the infinite sum of the amounts of intercepted radiation of decreasing intensity, corresponding to infinite series of photon-phytoelement interactions [Eq. (8a)] Alternatively, the contribution of infinite series can be represented by finite number of photon-phytoelement interactions, n_{eff}, assuming each has constant interceptance of i_0. Also note the following notations. Sometimes, the normalized versions of absorptance and scattering are used in the literature: *canopy absorption (scattering) coefficient*, $a(\lambda)/i_0$ ($s(\lambda)/i_0$), is the portion of intercepted photons that canopy absorb (escape canopy in upward and downward directions).

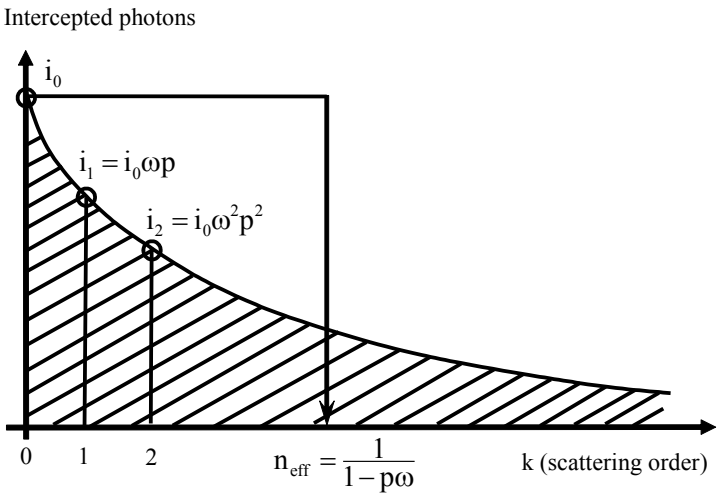

Figure 5. Derivation of the effective number of scattering events, n_{eff}. The total canopy interceptance is accumulated with the infinte number of scattering events, k, with declining interceptance, i_k. Effectively this can be represented as the contribution of finite number, n_{eff}, of interactions with constant interceptance, i_0. The numer n_{eff} is derived from the condition that area of rectange $n_{eff} \times i_0$ is equal to the area under curve i_k.

Refer to Eq. (8) and Figs. 3 and 6, and note the following properties of interceptance, absorptance, scattering out of canopy and rescattering. First, the series for interceptance, $i(\lambda)$, are unique in terms that the first term (zero-order interceptance) does not depends on wavelength. Second, the relationship between interceptance, absorptance, scattering out of canopy and rescattering is

$$\begin{cases} i(\lambda) = i_0 + s_{RE}(\lambda), \\ i_0 = a(\lambda) + s(\lambda). \end{cases} \Rightarrow \quad i(\lambda) = a(\lambda) + s(\lambda) + s_{RE}(\lambda). \tag{9}$$

Thus, the total canopy interceptance, $i(\lambda)$, consist of fixed component (absorptance and scattering out of canopy) and transit component (rescattering). The transit component is volatile, energy transferred from one scattering to another will ultimately be either absorbed or scattered out of canopy. Third, the relationship between energy fluxes at leaf and canopy are established with the following ratios:

$$\frac{i(\lambda)}{a(\lambda)} = \frac{1}{1-\omega(\lambda)}, \quad \frac{s(\lambda)}{a(\lambda)} = \frac{[1-p]\omega(\lambda)}{1-\omega(\lambda)}, \quad \frac{s_{RE}(\lambda)}{a(\lambda)} = \frac{p\,\omega(\lambda)}{1-\omega(\lambda)}. \tag{10}$$

The physical meaning of ratios in Eq. (10) is as follows [cf. Fig. 3]. In view that at each individual photon-phytoelement interaction the intercepted energy is distributed between absorptance, scattering out of canopy and rescattering in the constant proportion, independent on scattering order, this same proportion will be preserved at the whole canopy scale. For instance, the scattering out of canopy constitute $[1-p]\omega(\lambda)$ portion, while absorptance constitutes $1-\omega$ portion, and this holds true both at phytoelement and canopy scales.

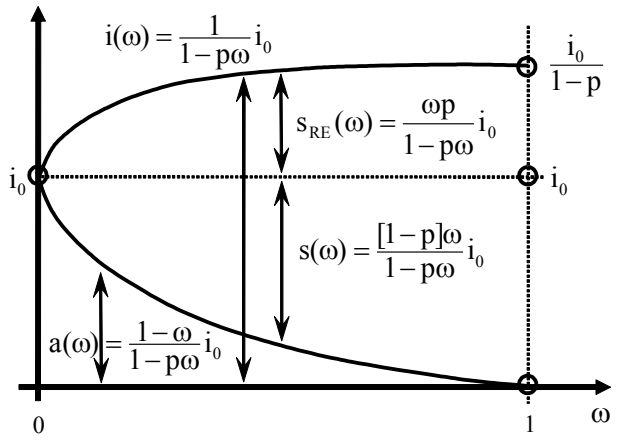

Figure 6. Functional dependance of canopy inteceptance, $i(\omega)$, absorptance, $a(\omega)$, scattering out of canopy, $s(\omega)$, and rescattering within canopy, $s_{RE}(\omega)$, on single scattering albedo, ω. Here, i_0 is the zero-order canopy interceptance and p is the recollision probability.

Next, consider functional dependence of interceptance, absorptance, and two scattering quantities on single scattering albedo, ω [cf. Fig. 6]. Note, zero-order quantities and the same quantities at $\omega = 0$ convey a distinct meaning and should not be used interchangeably. In the case of interceptance, i_0 and $i(\omega = 0)$ coincide, but the definition of i_0 does not require ω equal zero, as it is constant for all values of ω. In contrast, in the case of absorptance, a_0 and $a(\omega = 0)$ are different, and a_0 depends on ω. As ω increases, total interceptance increases starting from i_0 due to contribution of multiple scattering. In contrast, total absorptance is highest for black leaves ($\omega = 0$) and decreases with ω, because multiple scattering removes energy out of canopy. The two scattering quantities (scattering out of canopy and rescattering) are equal to zero at $\omega = 0$, but increase with increasing ω. The overall functional dependence and specific limits of all above quantities are shown in Fig. 6. Finally, note the consistency between series of scattering formulation [Eq. (10)] and RT equation [Eq. (4)].

Canopy Spectral Invariant for Interceptance: Consider total canopy interceptance at two independent wavelengths, $i(\lambda_1) = i_0/[1 - p\omega(\lambda_1)]$ and $i(\lambda_2) = i_0/[1 - p\omega(\lambda_2)]$ for $\lambda_1 \neq \lambda_2$ [cf. Eq. (8a)]. The system of the above two equations can be solved for the recollision probability:

$$p = \frac{i(\lambda_1) - i(\lambda_2)}{i(\lambda_1)\omega(\lambda_1) - i(\lambda_2)\omega(\lambda_2)}. \tag{11}$$

This equation expresses the principle of spectral invariance with respect to canopy interceptance. Recall [cf. Eqs. (7) and (9)] the total canopy interceptance, $i(\lambda)$, is partitioned between total canopy absorptance, $a(\lambda) = [1 - \omega(\lambda)]i(\lambda)$, and total canopy scattering, $s(\lambda) + s_{RE}(\lambda) = \omega(\lambda)i(\lambda)$. The principle of spectral invariance states that the ratio between difference in the amount of intercepted photons, $i(\lambda_1) - i(\lambda_2)$, and those of scattered photons, $\omega(\lambda_1)i(\lambda_1) - \omega(\lambda_2)i(\lambda_2)$, is spectrally invariant with respect to any wavelength λ_1 and λ_2, and is equal to the recollision probability. Figure 7 shows amount of photons intercepted, $i(\lambda)$, and scattered, $\omega(\lambda)i(\lambda)$, by canopy as function of wavelengths derived from measurements at Flakaliden site. Also shown is the frequency of values of the recollision probability, p, corresponding to all combinations of λ and λ_0. The sharp peak of the distribution suggests that the recollision probability, p, is invariant with respect to the wavelength with sufficiently high accuracy. The minor spread of the distribution is due to measurements errors and ignoring surface contribution.

(a) (b)

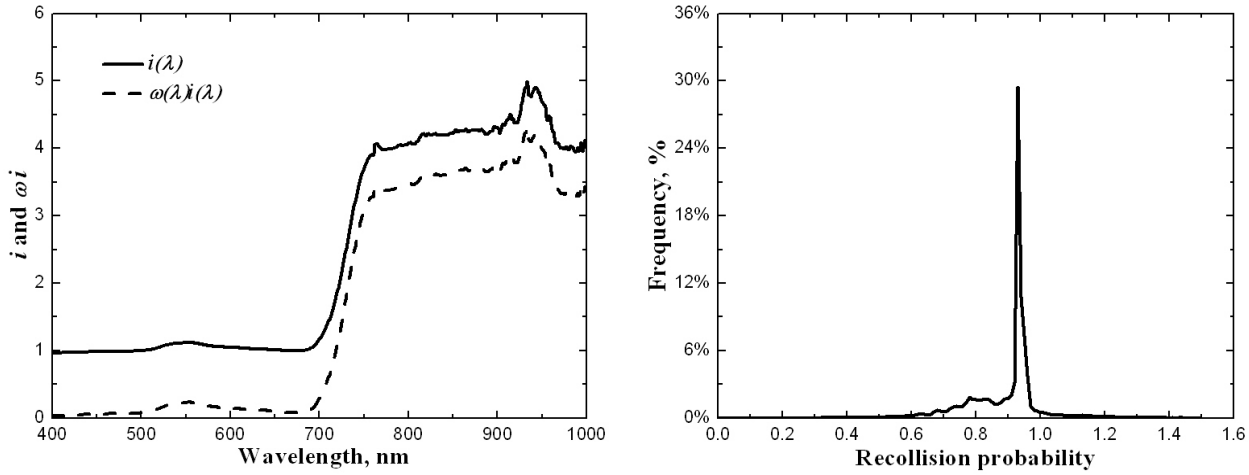

Figure 7. Retrieval of the recollision probability, p, from Flakaliden field data (Fig. 1). Panel (a) shows total canopy interceptance, $i(\lambda)$ (solid line), and total canopy scattering, $s(\lambda) + s_{RE}(\lambda) = \omega(\lambda) i(\lambda)$ (dashed line). Panel (b) shows frequency of values of the recollision probability derived according to Eq. (11).

The Equation (11) can be rearranged to a different form, which we use to derive p and i_0 $(= i(\omega = 0))$ from field data, namely,

$$\frac{1}{i(\lambda)} = \frac{1}{i_0} - \frac{p}{i_0}\omega(\lambda) .$$

If the reciprocal of the total canopy interceptance calculated from measured canopy absorption and needle albedo is plotted versus measured needle albedo, a linear relationship is obtained (Fig. 8). The recollision probability, p, and canopy interceptance, i_0, can be inferred from the slope and intercept.

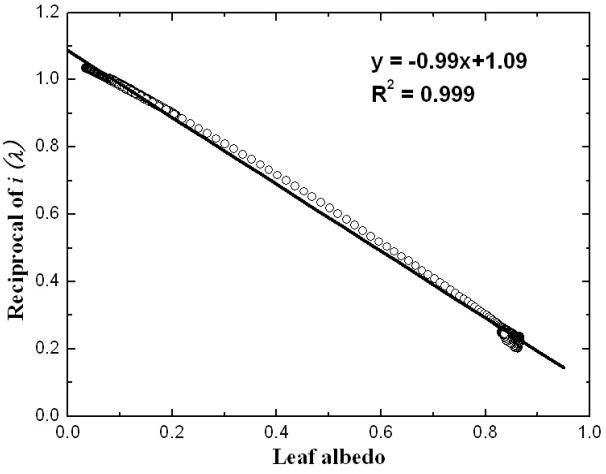

Figure 8. Reciprocal of $i(\lambda)$ and (b) $\omega(\lambda)/[i(\lambda) - i_0]$ versus leaf albedo $\omega(\lambda)$ derived from Flakaliden field data (Fig. 1). The recollision probability, p=0.91, and canopy interceptance, i_0=0.92, are derived from the slope and intercept of the line.

The key properties of the recollision probability are as follows. The recollision probability establishes the link between leaf and canopy scales, and thus it is a scaling parameter in RT theory for vegetation. This parameter accounts for the effect of the canopy structure on RT regime across range of scales. The parameter is wavelength independent. Monte Carlo simulations [Smolander and Stenberg, 2005] suggest that the recollision probability is minimally

sensitive to rather large changes in the direction of the incident beam. However, other numerical simulations [Lewis and Disney, 2007] indicate that the recollision probability depends on scattering order and LAI (Fig. 9). Thus, one should discriminate between the *actual recollision probability*, p_{actual}, which is function of scattering order, its *asymptotic value*, p_{inf}, a plateau, reached under condition of infinite scattering, and *effective value*, p_{efff}, evaluated over scattering events.

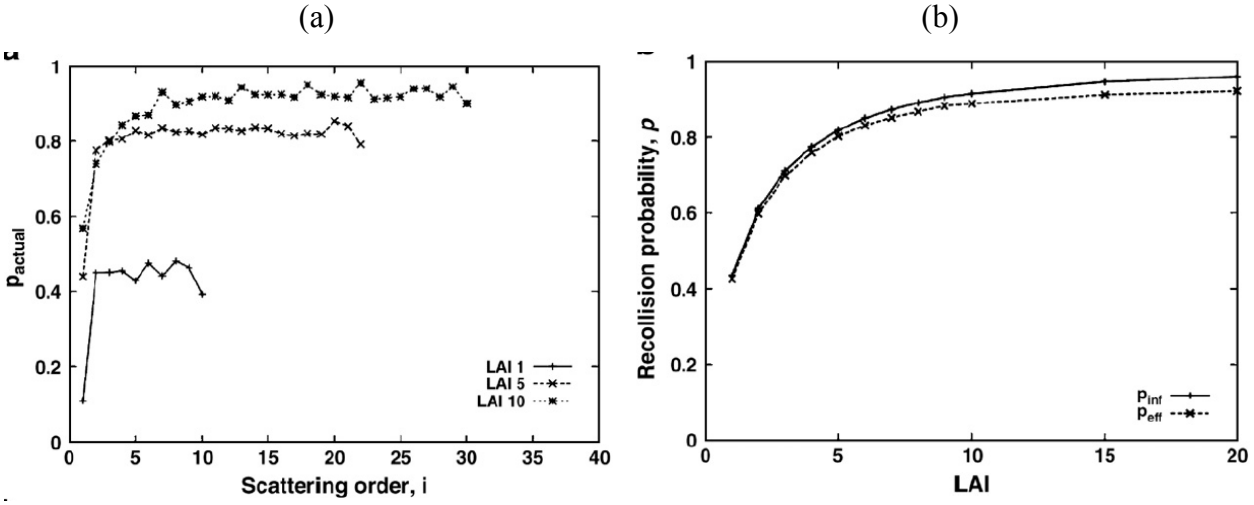

Figure 9. Recollision probability, p_{actual}, as a function of scattering order calculated for canopies with LAI 1, 5, 10. Infinite scattering order recollision probability (p_{inf}) and effective recollision probability (p_{efff}) as a function of LAI. Monte-Carlo simulations are performed for canopies composed of randomly located non-overlapping disks with a spherical leaf angle distribution (from Lewis and Disney, [2007]).

Canopy Spectral Invariant for Reflectance and Transmittance: The total canopy scattering consist of rescattering between phytoelements, $s_{RE}(\lambda)$, and scattering out of canopy, $s(\lambda)$. The rescattering term, $s_{RE}(\lambda)$, is characterized by recollision probability, p. The scattering out of canopy term, $s(\lambda)$, can be subdivided further into upward and downward components to derive reflectance and transmittance. The probability that scattered photon will escape the vegetation canopy through the upper (or lower) boundary is called *escape probabilities* ρ and τ, respectively. At each individual event of photon-phytoelement interaction, all possible outcomes of scattering are limited to photon escaping canopy in upward, or downward direction, or colliding another phytoelement, thus,

$$\rho + \tau + p = 1. \tag{12}$$

As in the case of recollision probability, p, the escape probabilities, ρ and τ, depend, in general, on scattering order, but reach constant value (plateau) after several iterations. The number of interaction events before this plateau is reached depends on the canopy structure and the needle transmittance-albedo ratio. Monte Carlo simulations suggest that the recollision and escape probabilities saturate after two-three photon-canopy interactions for low to moderate LAI canopies [Lewis and Disney, 2007]. This result underlies the approximation to the canopy reflectance, $r(\lambda)$, proposed by Disney and Lewis [2005],

$$r(\lambda) = \omega(\lambda)R_1 + \frac{\omega(\lambda)^2 R_2}{1 - p_r\omega(\lambda)}, \tag{13a}$$

where coefficients R_1, R_2 and p_r are determined by fitting Eq. (13a) to measured reflectance spectrum. Under assumption that the recollision, p, and escape probability, τ, remains constant in successive interactions,

$$R_1 \to \rho i_0, \quad R_2 \to \rho p i_0, \quad p_r \to p. \tag{13b}$$

The first term evaluates the portion of photons from the intercepted flux, i_0 that escape the vegetation canopy in upward directions as a result of one interaction with phytoelements. The second term accounts for photons that have undergone two and more interactions. Violation of the above condition results in a transformation of ρi_0, $\rho p i_0$, and p to some effective values R_1, R_2 and p_r as the result of the fitting procedure. The difference between actual and effective values of the escape probabilities depends on its speed of convergence as the number of interactions increases. A detailed analysis of this effect will be presented in Section 3. A simplified expression, $R_2 = p_r R_1$, can also be used, with a reduction in accuracy of the approximation [Disney and Lewis, 2005].

Figure 10 shows correlation between measured and evaluated according to Eq. (13) canopy reflectance over Flakaliden site. Overall close agreement supports the approximation of Disney and Lewis. In this example the selected values for R_1 and p_r give the best fit to the measured reflectance spectrum. These coefficients can also be evaluated from the slope and intercept of the regression line, derived from values of the needle albedo, $\omega(\lambda)$, and the reciprocal of $r(\lambda)/\omega(\lambda)$ at wavelengths [700 - 750 nm]. At those wavelengths values of $\omega(\lambda)$ are uniformly distributed in the interval [0.1, 0.9] and the canopy reflectance exhibits a strong correlation with $\omega(\lambda)$. These features allow reducing the impact of ground reflectance and measurement uncertainties on the specification of R_1 and p_r from the regression line.

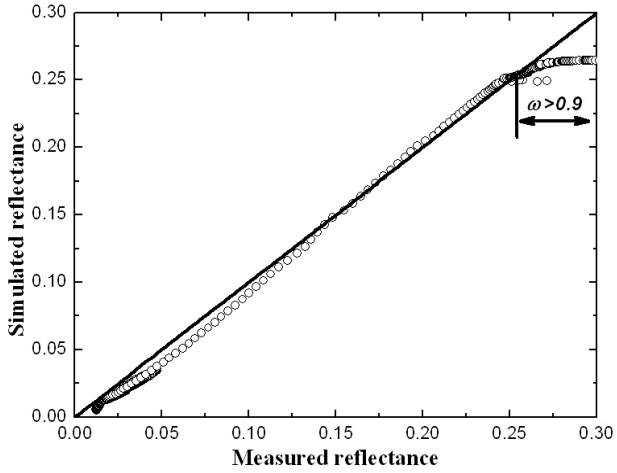

Figure 10. Correlation between measured canopy reflectance and canopy reflectance evaluated using Eq. (13) with $R_1 = 0.15$, $p_r = 0.59$, and $R_2 = p_r R_1 = 0.09$ for the spectral interval $400 \le \lambda \le 900$ nm. The arrow indicates a range of reflectance values corresponding to $\omega \ge 0.9$. Field data are from Flakaliden site (Fig. 1).

Analogous to Eq. (13) for canopy reflectance, a similar relationship can be established between canopy transmittance and phytoelements albedo, namely

$$t(\lambda) = t_0 + \frac{T_1\,\omega(\lambda)}{1 - p_t\omega(\lambda)}, \qquad (14a)$$

where the values of coefficients t_0, T_1 and p_t are chosen by fitting Eq. (14a) to the measured spectrum of canopy transmittance. Analogous to Eq. (13b), the coefficients T_1 and p_t are effective values and under assumption that the recollision, p, and escape probability, τ, remains constant in successive interactions,

$$T_1 \to \tau i_0, \quad p_t \to p. \tag{14b}$$

Under the above assumption, the value of t_0 converges to zero-order transmittance [cf. Eq. (6)]. Figure 11 shows correlation between measured and evaluated according to Eq. (14) canopy transmittance over Flakaliden site. A theoretical analysis of this approximation will be presented in Section 3. It should be noted that canopy transmittance is sensitive to the needle transmittance to albedo ratio $\tau_L(\lambda)/\omega(\lambda)$ [Panferov et al., 2001]. This may imbue wavelength dependence to the escape probabilities for low order photon scattering.

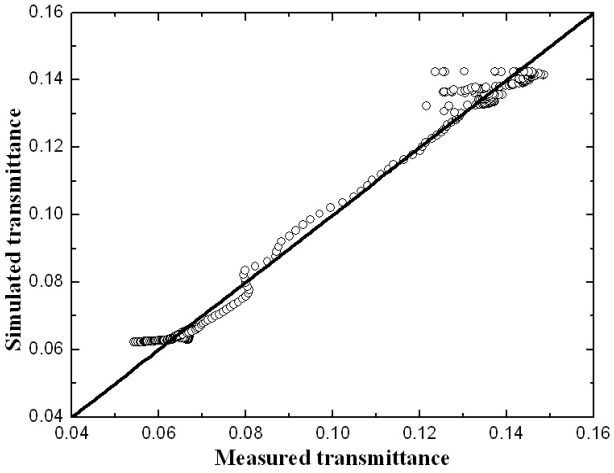

Figure 11. Correlation between measured canopy transmittance and canopy transmittance simulated using Eq. (14) with $t_0 = 0.06$, $T_1 = 0.017$ and $p_t = 0.94$. Energy conservations for i_0 and t_0 is preserved with good accuracy, i.e., $i_0 + t_0 = 0.92+0.06=0.98$. Field data are from Flakaliden site (Fig. 1).

Impact of Soil Reflectance: The total canopy transmittance, $t(\lambda)$, reflectance, $r(\lambda)$, and absorptance, $a(\lambda)$, for the general RT problem of canopy above soil background can be represented by contribution of black-soil and soil sub-problems as follows (cf. Chapter 4):

$$t(\lambda) = \frac{t_{BS}(\lambda)}{1-\rho_{soil}(\lambda)r_S(\lambda)} = t_{BS}(\lambda) + t(\lambda)\rho_{soil}(\lambda)r_S(\lambda), \tag{42a}$$

$$r(\lambda) = r_{BS}(\lambda) + t(\lambda)\rho_{soil}(\lambda)t_S(\lambda), \tag{42b}$$

$$a(\lambda) = a_{BS}(\lambda) + t(\lambda)\rho_{soil}(\lambda)a_S(\lambda). \tag{42c}$$

Here, ρ_{soil} is the hemispherical reflectance of the canopy ground. Variables r_{BS} and r_S; t_{BS} and t_S; a_{BS} and a_S denote canopy reflectance, transmittance, and absorptance calculated for a vegetation canopy (1) illuminated from above by the incident radiation and bounded from below by a non reflecting surface (subscript "BS", for black soil); and (2) illuminated from the bottom by normalized isotropic sources and bounded from above by a non-reflecting boundary (subscript "S"). These variables are related via the energy conservation law, i.e.,

$$a_i(\lambda) + r_i(\lambda) + t_i(\lambda) = 1, \quad \text{i=BS or S-problem.}$$

The canopy spectral invariants are formulated for r_{BS}, t_{BS} and a_{BS}. The measured spectral transmittance, t, and reflectance, r, are taken as estimates of r_{BS}, t_{BS}. The absorptance a_{BS} is approximated using Eq. (5). It follows from Eq. (42) that the relative errors, Δ_a, Δ_t and Δ_r, and in a_{BS}, t_{BS}, and r_{BS} due to the neglecting of surface reflection can be estimated in terms of measured t, r and ρ_{soil} as:

$$\Delta_a \equiv \frac{a_{BS} - a}{a} = \frac{t}{1 - t - r}\rho_{ssoil}(1 - t_S - r_S) \le \frac{t}{1 - t - r}\rho_{soil}, \tag{43a}$$

$$\Delta_t \equiv \frac{t - t_{BS}}{t} = \rho_{soil}\, r_S \le \rho_{soil}, \tag{43b}$$

$$\Delta_r \equiv \frac{r - r_{BS}}{r} = \frac{t}{r}\rho_{soil}\, t_S \le \frac{t}{r}\rho_{soil}, \tag{43c}$$

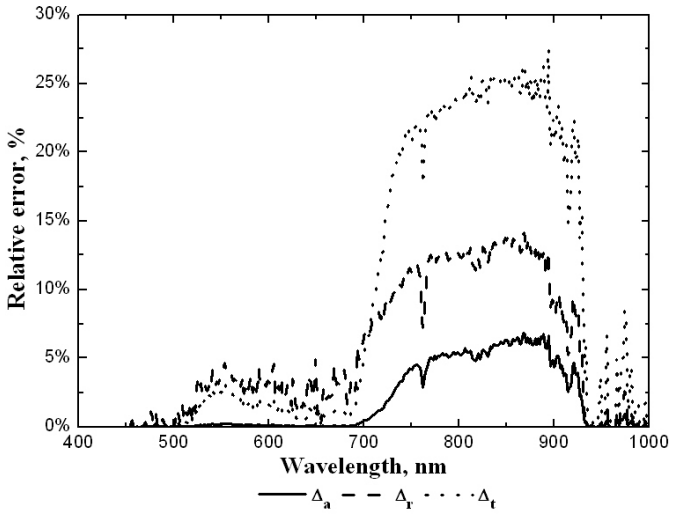

Figure 12. Upper limits of the relative errors Δ_t, Δ_r, and Δ_a in the estimates of t_{BS}, r_{BS} and a_{BS}, arising due to the effect of non-black soil reflectance. Reference field data are from Flakaliden site in Sweden (Fig. 1).

Thus, neglecting contribution of soil, results in overestimation of reflectance and transmittances and underestimation of absorptances. Figure 12 shows upper limits of the relative errors Δ_t, Δ_r,and Δ_a.as a function of the wavelength for Flakaliden data. It follows from the above analysis that measured canopy absorptance approximates a_{BS} with an accuracy of about 5%. Deviations of measured canopy transmittance and reflectance from t_{BS} and r_{BS} in the interval $400 \le \lambda \le 700$ nm do not exceed 5%, however they increase substantially in the interval $700 \le \lambda \le 900$ nm.

Major Assumptions for Spectral Invariants: We summarize key assumptions of the theory of spectral invariants along three categories. (1) Boundary conditions assumptions: a vegetation canopy is illuminated from above by a wavelength independent parallel beam and bounded from below by a non-reflecting (black) surface. The last assumption is required to avoid re-entrance of photons exiting through background. (2) Phytoelements scattering properties assumptions: the interaction cross-section, $\sigma(\underline{r},\underline{\Omega})$, is treated as wavelength independent considering the size of the scattering elements (leaves, branches, twigs, etc.) relative to the wavelength of solar radiation. (3) Effective values assumptions: the recollision and escape probabilities (p, ρ, τ) are generally dependant on the scattering order, but tend to reach plateau and could be replaced with corresponding effective values. The uncertainties of retrievals of interceptance (or absorptance) are relatively low, as those variables depend on recollision probability only, while

uncertainties for transmittance and reflectance are higher as those variables depend both on recollision and escape probabilities.

3. RT Theory of Spectral Invariants

Successive Orders of Scattering Approximation: Below we formulate the rigorous mathematical basis underlying the principle of spectral invariance, introduced in the previous section. We adopt functional analysis formulation of the transport equation (Vladimirov [1963], Marchuk et al [1980]). Let V and δV be the domain where radiative transfer occurs and its boundary, respectively. The domain V can be a shoot, tree crown, tree stand, etc. Let L and S_λ be the *streaming-collision* and *scattering* linear operators (Chapter 2),

$$LI_\lambda \equiv \underline{\Omega}\nabla I_\lambda(\underline{r},\underline{\Omega}) + \sigma(\underline{r},\underline{\Omega})I_\lambda(\underline{r},\underline{\Omega}), \tag{15a}$$

$$S_\lambda I_\lambda \equiv \int_{4\pi} \sigma_{s,\lambda}(\underline{r},\underline{\Omega}' \to \underline{\Omega})I_\lambda(\underline{r},\underline{\Omega}')d\underline{\Omega}', \tag{15b}$$

where $I_\lambda(\underline{r},\underline{\Omega})$ is the radiation intensity at wavelength λ, spatial location $\underline{r}$ and direction $\underline{\Omega}$; σ and σ_S are extinction and differential scattering coefficients, respectively. In the following we assume that single scattering albedo, $\omega(\lambda)$, does not depend on $\underline{r}$ and $\underline{\Omega}$. The 3D radiative transfer equation (Chapter 4) can be formulated in operator notations as follows

$$LI_\lambda = S_\lambda I_\lambda. \tag{16a}$$

The boundary conditions include canopy top to be illuminated from above by unit beam in direction $\underline{\Omega}_0$ and canopy bottom to be absolutely absorbing,

$$I_\lambda(\underline{r}_{top},\Omega) = \delta(\Omega - \Omega_0), \quad \underline{r}_{top} \in \delta V, \quad \mu(\underline{\Omega}) < 0, \tag{16b}$$

$$I_\lambda(\underline{r}_{bottom},\underline{\Omega}) = 0, \quad \underline{r}_{bottom} \in \delta V, \quad \mu(\underline{\Omega}) > 0. \tag{16c}$$

We solve Eq. (16) with method of successive order of scattering approximations (SOSA). The total radiation intensity is represented as the sum of uncollided, Q_0, and collided, components (cf. Chapter 2),

$$I_\lambda = Q_0(\underline{r},\underline{\Omega}) + I_\lambda^{dif}(\underline{r},\underline{\Omega}). \tag{17}$$

By definition, Q_0 is the radiation intensity of photons in the incident flux that will arrive at $\underline{r}$ along direction $\underline{\Omega}$ without suffering a collision. This is a wavelength independent parameter. Q_0 satisfies the equation

$$LQ_0 = 0, \tag{18}$$

and the original boundary conditions, Eq. (16b-c). $I_\lambda^{dif}(\underline{r},\underline{\Omega})$ is the collided (or diffuse) radiation intensity, that is, radiation generated by photons scattered one or more times. This is a wavelength dependant parameter. Combining Eqs. (16)-(18) one can verify that $I_\lambda^{dif}(\underline{r},\underline{\Omega})$ satisfies the following equation,

$$LI_\lambda^{dif} = SQ_0 + SI_\lambda^{dif}, \tag{19}$$

and zero boundary conditions at the top and bottom of canopy. Finally, by combining Eq. (17) and (19), the Eq. (16a) can be rewritten in the form of the following integral radiative transfer equation,

$$I_\lambda = Q_0 + TI_\lambda, \tag{20}$$

where operator $T \equiv L^{-1}S$. The SOSA method states that the solution of Eq. (20) is given by

$$I_\lambda = \sum_{m=0}^{\infty} Q_m, \quad \text{where } Q_m = TQ_{m-1} = T^m Q_0, \ m = [1,\infty]. \tag{21}$$

One can verify the validity of solution given by Eq. (21) by substituting it in Eq. (20) and taking into account properties of operator T. The physical meaning of Eq. (21) is as follows. Q_m is the radiation intensity of photons, scattered m times. The uncollided photons with intensity Q_0, serve as the source for the photons scattered one time with intensity Q_1, which in turn serve as a source of photons scattered two times, and so on (cf. Fig. 4). In Monte Carlo simulations, operator T corresponds to a procedure, which inputs Q_0, simulates the scattering event, calculates the photon free path and outputs the distribution, Q_1, of photons just before their next interaction with phytoelements; the procedure is repeated with the source of photons evaluated as output at the previous step.

Spectral Invariant for Canopy Interceptance: Let $\|f\|$ be the norm of 3D radiation field $f(\underline{r},\underline{\Omega})$ in the domain $V \times 4\pi$, according to notations of functional analysis [Vladimirov, 1963; and Marchuk et al., 1980],

$$\| f \| = \int_V d\underline{r} \int_{4\pi} d\underline{\Omega}\, \sigma(\underline{r},\underline{\Omega}) \, | f(\underline{r},\underline{\Omega}) | , \tag{22}$$

In terms of these notations, the total canopy interceptance, $i(\lambda)$, and m-order canopy interceptance, i_m, are $\|I_\lambda\|$ and $\|Q_m\|$, respectively [cf. Eqs. (2a) and (8a)]. The distribution of probability, $e_m(\underline{r},\underline{\Omega})$, that a photon scattered m times will arrive at $\underline{r}$ along the direction $\underline{\Omega}$ without suffering a collision can be expressed as the radiation intensity of the photons, scattered m times, normalized by its norm

$$e_m(\underline{r},\underline{\Omega}) \equiv \frac{Q_m(\underline{r},\underline{\Omega})}{\| Q_m \|}, \quad \| e_m \| = 1. \tag{23}$$

The normalization is required, as $Q_m(\underline{r},\underline{\Omega})$ is the radiation intensity, whose norm, interceptance, i_m, decreases with order of scattering m (cf. Fig. 5), while $e_m(\underline{r},\underline{\Omega})$ is the distribution of probability, whose norm is required to be unity.

The recollision probability can be expressed in terms of $\|Q_m\|$. The recollision probability, p_m, at the step m of scattering is the ratio of radiation intensity rescattered inside of canopy to the total intensity of scattering (i.e., rescattered inside of canopy and escaped canopy) [cf. Figs. 3-4 and Eq. (7)]. The radiation intensity scattered m-1 times is Q_{m-1}, therefore, $\|Q_{m-1}\|$ will be intercepted and $\omega\|Q_{m-1}\|$ will be available for the total scattering at the current step m of scattering. The total radiation available for scattering originates the radiation intensity Q_m at current step m of scattering. The rescattered intensity at the current step m is equal to the intercepted intensity at the next step m+1, $\|Q_m\|$. Therefore,

$$p_m = \frac{\| Q_m \|}{\omega \| Q_{m-1} \|}. \tag{24}$$

For convenience of the following derivations we will use $\gamma_m \equiv p_m \omega$. Taking into account Eqs. (21), (23) and (24), the distributions $e_{m-1}(\underline{r},\underline{\Omega})$ and $e_m(\underline{r},\underline{\Omega})$ between successive orders of scattering m-1 and m are related as

$$Te_{m-1}(\underline{r},\underline{\Omega}) = T\frac{Q_{m-1}(\underline{r},\underline{\Omega})}{\|Q_{m-1}\|} = \frac{\|Q_m\|}{\|Q_{m-1}\|} \times \frac{Q_m(\underline{r},\underline{\Omega})}{\|Q_m\|} = \gamma_m e_m(\underline{r},\underline{\Omega}). \tag{25}$$

The above equation explicitly states the nature of operator T: it converts the probability distribution of photons from previous to the next order of scattering and evaluates recollision probability.

The set $(\gamma_m,\ e_m(\underline{r},\underline{\Omega}))$, $m = [0,\infty]$, derived from operator T according to SOSA method poses one fundamental property established in *eigenvalues/eigenvectors theory* of functional analysis

[Vladimirov, 1963]. An eigenvalue of the radiative transfer equation is a number χ such that there exist a function $\psi(\underline{r},\underline{\Omega})$ that satisfies the equation

$$T\psi(\underline{r},\underline{\Omega}) = \chi\,\psi(\underline{r},\underline{\Omega}) \tag{26}$$

and zero boundary conditions. Under some general conditions [Vladimirov, 1963], the set of eigenvalues and eigenvectors $(\chi_m, \psi_m(\underline{r},\underline{\Omega}))$ is a discrete set. Since the eigenvalue and eigenvector problem is formulated for zero boundary conditions, χ and $\psi(\underline{r},\underline{\Omega})$ are independent on the incoming radiation. The radiative transfer equation has a *unique positive eigenvalue*, χ^*, that corresponds to a *unique positive eigenvector*, ψ^* [Vladimirov, 1963],

$$T\psi^*(\underline{r},\underline{\Omega}) = \chi^*\psi^*(\underline{r},\underline{\Omega}), \quad \| \psi^* \| = 1.$$

It should be emphasized that set $(\chi_m, \psi_m(\underline{r},\underline{\Omega}))$, derived according to eigenvalue problem [Eq. (26)] is different from $(\gamma_m, e_m(\underline{r},\underline{\Omega}))$, derived according SOSA method [Eq. (25)]. In general, $(\gamma_m,\ e_m(\underline{r},\underline{\Omega}))$ vary with the scattering order m. However, they tend to converge to plateaus as the number of interactions increases according to numerical results [Lewis and Disney, 1998]. Further, according to general principles of functional analysis [Riesz and Sz.-Nagy, 1990; Vladimirov, 1963] the set $(\gamma_m, e_m(\underline{r},\underline{\Omega}))$ converges to the unique positive eigenvector/eigenvalue of operator T, as number of scattering increases,

$$\lim_{m\to\infty} \gamma_m = \chi^*, \quad \lim_{m\to\infty} e_m(\underline{r},\underline{\Omega}) = \psi^*(\underline{r},\underline{\Omega}). \tag{27}$$

Assuming negligible variation in γ_m and $e_m(\underline{r},\underline{\Omega})$ for the scattering order m and higher and accounting for Eqs. (21) and (23), the radiation field, $I_\lambda(\underline{r},\underline{\Omega})$, can be approximated as follows

$$I_\lambda(\underline{r},\underline{\Omega}) = \sum_{k=0}^{\infty} \| Q_k \| e_k = \sum_{k=0}^{m} \| Q_k \| e_k + \sum_{k=m+1}^{\infty} \| Q_k \| e_k$$

$$= \sum_{k=0}^{m} \| Q_k \| e_k + \sum_{\ell=0}^{\infty} \gamma_{m+1}^{\ell} \| Q_{m+1} \| e_{m+1} + \delta_m$$

$$= \sum_{k=0}^{m} \| Q_k \| e_k + \| Q_m \| \frac{\gamma_{m+1}}{1-\gamma_{m+1}} e_{m+1} + \delta_m$$

$$\equiv I_{\lambda,m}(\underline{r},\underline{\Omega}) + \delta_m . \tag{28}$$

That is, radiation field, $I_\lambda(\underline{r},\underline{\Omega})$, is approximated with $I_{\lambda,m}(\underline{r},\underline{\Omega})$, for which the contribution of the first m scattering orders is calculated exactly and contribution of higher order scattering is approximated assuming that γ_k and $e_k(\underline{r},\underline{\Omega})$ are constant with respect to k for $k \geq m+1$. The error of this approximation is δ_m.

Following the above approach, we examine the accuracy of the approximation of the canopy interceptance as a function of the scattering order m. It follows form Eq. (28) that the m-th approximation, $i_m(\lambda)$, to $i(\lambda)$ is

$$i_m(\lambda) \equiv \left\| I_{\lambda,m}(\underline{r},\underline{\Omega}) \right\| = \sum_{k=0}^{m} \| Q_k \| + \| Q_m \| \frac{\gamma_{m+1}}{1-\gamma_{m+1}} = i_0 \left(\sum_{k=0}^{m} \theta_k + \frac{\theta_{m+1}}{1-\gamma_{m+1}} \right). \tag{29}$$

Here $i_0 \equiv \| Q_0 \|$ is the zero-order canopy interceptance; $\theta_0 = 1$, and

$$\theta_k \equiv \frac{\| Q_k \|}{\| Q_0 \|} = \frac{\| Q_k \|}{\| Q_{k-1} \|} \times \frac{\| Q_{k-1} \|}{\| Q_{k-2} \|} \times \ldots \times \frac{\| Q_1 \|}{\| Q_0 \|} = \gamma_1 \gamma_2 \ldots \gamma_k , \quad k \geq 1. \tag{30}$$

The error, $\delta i_m(\lambda)$, in the m-th approximation is given by [Huang et al., 2007]

$$| \delta i_m | = \left| i(\lambda) - i_m(\lambda) \right| \leq \varepsilon_{\gamma,m+1} \frac{\theta_{m+1}}{1-\gamma_{m+1}} s_{m+1} i_0 , \tag{31}$$

where

$$\varepsilon_{\gamma,m+1} = \max_{k \geq 1} \frac{| \gamma_{m+1+k} - \gamma_{m+1} |}{\gamma_{m+1+k}}, \quad s_{m+1} = \sum_{k=1}^{\infty} \frac{\theta_{m+1+k}}{\theta_{m+1}} . \tag{32}$$

Note that $\lim_{m\to\infty} \sqrt[m]{\theta_m} = \gamma_\infty$. If m is large enough, i.e. $\sqrt[m+1]{\theta_{m+1}} \approx \gamma_\infty$, the ratio $\theta_{m+1+k} / \theta_{m+1}$ can be approximated by γ_∞^k. Substituting this relationship into Eq. (32) one obtains $s_m \approx \gamma_\infty /(1-\gamma_\infty)$.

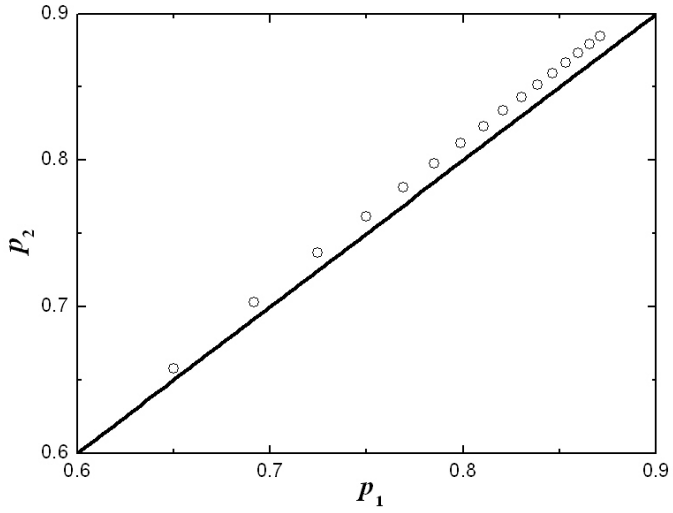

Figure 13. Correlation between first and second scattering order recollision probabilities (p_1 and p_2) for a range of LAI. The RT simulations were performed with the stochastic RT model for a canopy modeled with identical cylindrical "trees" uniformly distributed over black background. Crown height=1, ground cover=variable and plant LAI=10, SZA=30^0.

Two factors determine the accuracy of the m-th approximation of canopy interceptance. The first is the difference between successive approximations γ_{m+1} and γ_{m+1+k}; that is, the smaller this difference, the more accurate the approximation is. The second factor is the contribution of photons scattered m+1 or more times to the canopy radiation field. Their contribution is given by $\theta_{m+1} /(1-\gamma_{m+1}) \approx \gamma_\infty^{m+1} /(1-\gamma_\infty)$ which depends on the recollision probability, p_∞, and the single scattering albedo, ω; that is, the higher $\gamma_\infty = p_\infty \omega$ is, the higher order of approximation is needed to estimate the canopy interceptance. This is illustrated in Fig. 13. The variations in the recollision probability as function of scattering order reaches its maximum at high values of p (here the recollision probabilities for the first and second order of scattering were compared). The spectral invariant can not be derived if $p_\infty \omega = 1$ since the Neumann series (24) do not converge in this case.

Spectral Invariants for the Canopy Transmittance and Reflectance: Let the domain V be a layer $0 \le z \le H$. The surfaces S, $z = 0$ and $z = H$ constitute its upper and lower boundaries, respectively. Let $\|f\|_r$ and $\|f\|_t$ be norms of 3D radiation field $f(\underline{r}, \underline{\Omega})$ in the domain $S \times 2\pi$,

$$\| f \|_r = \int_{z=0} d\underline{r} \int_{2\pi^+} d\underline{\Omega} f(r,\underline{\Omega}) |\mu|,$$

$$\| f \|_t = \int_{z=H} d\underline{r} \int_{2\pi^-} d\underline{\Omega} f(r,\underline{\Omega}) |\mu|, \tag{33}$$

where the first integral is taken over the top boundary and in upward direction, while second is taken over lower boundary in downward directions. In terms of notations of Eq. (33), the canopy reflectance, $r(\lambda)$, and transmittance, $t(\lambda)$, are given by $\|I_\lambda\|_r$ and $\|I_\lambda\|_t$. Recall, according to notations of Eq. (22) canopy interceptance, $i(\lambda)$, is given by $\|I_\lambda\|$. The relationship between reflectance, transmittance and interceptance for some order of scattering m can be derived as follows. Recall, $Q_m = TQ_{m-1}$ [cf. Eq. (21)], or, in terms of operators L and S [cf. Eq. (15)], $LQ_m = SQ_{m-1}$. Integrating the last equation over the domain $V \times 4\pi$, we have:

$$\int_{4\pi} d\underline{\Omega} \int_V dV \Omega \nabla Q_m(\underline{r},\underline{\Omega}) + \int_{4\pi} d\underline{\Omega} \int_V dV \sigma(\underline{\Omega}) Q_m(\underline{r},\underline{\Omega}) = \int_{4\pi} d\underline{\Omega} \int_V dV \int_{4\pi} d\underline{\Omega}' \sigma_S(\underline{\Omega}' \to \underline{\Omega}) Q_{m-1}(\underline{r},\underline{\Omega}'),$$

$$\Rightarrow \quad \int_{4\pi} d\underline{\Omega} \int_S d\underline{S}\underline{\Omega} Q_m(\underline{r},\underline{\Omega}) + \int_{4\pi} d\underline{\Omega} \int_V dV \sigma(\underline{\Omega}) Q_m(\underline{r},\underline{\Omega}) = \omega \int_{4\pi} d\underline{\Omega} \int_V dV \sigma(\underline{\Omega}) Q_{m-1}(\underline{r},\underline{\Omega}'),$$

$$\Rightarrow \quad \|Q_m\|_r + \|Q_m\|_t + \|Q_m\| = \omega \|Q_{m-1}\|. \tag{34}$$

In the above derivations we accounted for definition of norms [Eqs. (22) and (33)], relationship between extinction coefficient, $\sigma(\underline{\Omega})$, and differential scattering coefficient, $\sigma_S(\underline{\Omega}' \to \underline{\Omega})$, [Eq. (3)] and Gauss theorem for converting volume integral to the surface integral for some scalar function. Normalizing Eq. (34) by $\omega\|Q_{m-1}\|$ we finally have

$$\rho_m + \tau_m + p_m = 1, \tag{35a}$$

where ρ_m and τ_m are escape probabilities for reflectance transmittance and p_m is the recollision probability for the m-th order of scattering,

$$\rho_m \equiv \frac{\| Q_m \|_r}{\omega \| Q_{m-1} \|}, \quad \tau_m \equiv \frac{\| Q_m \|_t}{\omega \| Q_{m-1} \|}, \quad p_m \equiv \frac{\|Q_m\|}{\omega \|Q_{m-1}\|}. \tag{35b}$$

The physical interpretation of Eqs. (34) and (35) follows those given for Eq. (24). The recollision probability, p_m (escape probability in upward, ρ_m, and downward, τ_m, directions) at the step m of scattering is the ratio of radiation intensity rescattered inside of canopy (escaped canopy in upward and downward directions) to the total intensity of scattering. The total intensity available for scattering at the current step m of scattering is $\omega\|Q_{m-1}\|$. This total intensity is distributed between rescattered intensity at current step m, $\|Q_m\|$, escaped canopy in upward directions, $\|Q_m\|_r$, and escaped canopy in downward direction, $\|Q_m\|_t$. This explains Eq. (34). The ratio of above quantities according to definition of recollision and escape probabilities explains Eq. (35b). The escape and recollision probabilities correspond to portions of all possible events of scattering (escaped upward, downward or rescattered), which explains Eq. (35a). Note also, the escape probabilities vary with the scattering order, but, as in the case of recollision probabilities, they reach plateaus (ρ_∞ and τ_∞) as the number of interactions increases.

It follows from Eq. (28) that the m-th approximation, $r_m(\lambda)$ and $t_m(\lambda)$, to the canopy reflectance and transmittance are

$$r_m(\lambda) \equiv \| I_{\lambda,m} \|_r = \left[\sum_{k=1}^{m} \rho_k \theta_{k-1} + \frac{\theta_m \rho_{m+1}}{1-\gamma_{m+1}} \right] \omega i_0 , \tag{36a}$$

$$t_m(\lambda) \equiv \| I_{\lambda,m} \|_t = t_0 + \left[\sum_{k=1}^{m} \tau_k \theta_{k-1} + \frac{\theta_m \tau_{m+1}}{1-\gamma_{m+1}} \right] \omega i_0 . \tag{36b}$$

Here i_0 and t_0 are zero-order canopy interceptance and transmittance, respectively [cf. Eq. (6)]; and θ_k is defined by Eq. (30). Errors in the m-th approximation of canopy reflectance and transmittance are given by [Huang et al., 2007]

$$\left|\delta r_m\right| = \left| r(\lambda) - r_m(\lambda)\right| \le (\varepsilon_{r,m+1} + \varepsilon_{\gamma,m+1}) \frac{\theta_m \rho_{m+1}}{1-\gamma_{m+1}} s_{r,m} \omega i_0 , \tag{37a}$$

$$\left|\delta t_m\right| = \left| t(\lambda) - t_m(\lambda)\right| \le (\varepsilon_{t,m+1} + \varepsilon_{\gamma,m+1}) \frac{\theta_m \tau_{m+1}}{1-\gamma_{m+1}} s_{t,m} \omega i_0 . \tag{37b}$$

Here $\varepsilon_{\gamma,m}$ is defined by Eq. (32) and

$$\varepsilon_{\kappa,m+1} = \max_{k\ge 1} \frac{\left| \kappa_{m+1+k} - \kappa_{m+k} \right|}{\kappa_{m+k}}, \quad s_{\kappa,m} = \sum_{k=1}^{\infty} \frac{\theta_{m+k}}{\theta_m} \frac{\kappa_{m+k}}{\kappa_{m+1}} , \tag{37c}$$

where κ and κ_m represent either canopy reflectance ($\kappa = r$, $\kappa_m = \rho_m$) or canopy transmittance ($\kappa = t$, $\kappa_m = \tau_m$).

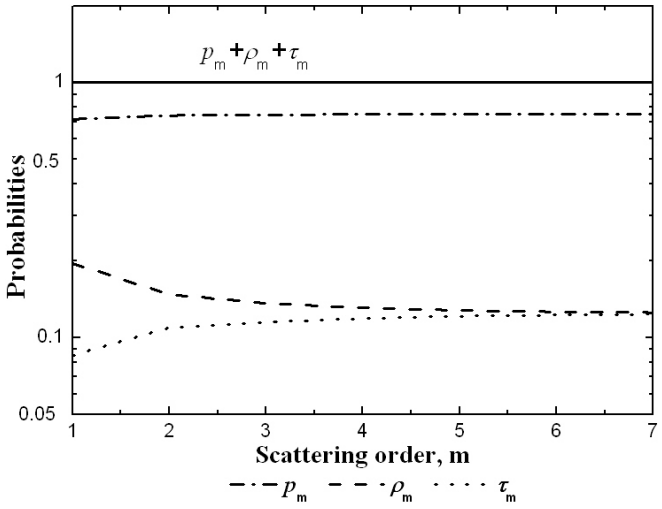

Figure 14. Recollision probability, p_m, and escape probabilities, τ_m and ρ_m, as a function of the scattering order m. Their limits are p_∞=0.75, τ_∞=0.125 and ρ_∞=0.125. The relative difference $\varepsilon_{\gamma,m+1}$ in the recollision probability is 3% for m=0 and 0.8% for m=1. Parameters of the RT simulations are the same as for Fig. 12, except ground cover=0.16.

In addition to two factors that determine the accuracy in the m-th approximation of the canopy interceptance [cf. Eq. (31)], δr_m and δt_m also depend on the convergence of two successive approximations κ_{m+k} and κ_{m+k+1} to ρ_∞ or τ_∞. Thus, the errors in the m-th approximations to the canopy reflectance and transmittance result from the errors in the recollision and escape probabilities, and from a contribution of photon multiple scattering to the canopy radiation regime. The m-th approximation to the canopy reflectance and transmittance, therefore, is less accurate compared to that to the canopy interceptance. This is illustrated in Fig. 14. In this example, the relative difference $\left|\gamma_{m+1+k} - \gamma_{m+1}\right| / \gamma_{m+1+k}$ is 3% for $m = 0$ and becomes negligible for $m \geq 1$. The zero and first order approximations provide accurate spectral invariant relationships for the canopy interceptance. The corresponding differences in the escape probabilities do not exceed 4% for $m \geq 2$, indicating that two scattering orders are required to evaluate spectral invariants for canopy transmittance and reflectance with accuracy comparable to that given by zero approximation to the canopy interceptance.

Spectral Invariant for Canopy BRF: The m-th approximation, $BRF \equiv I_{\lambda,m}(z = 0, \underline{\Omega})$, $\mu(\underline{\Omega}) > 0$ to the canopy bidirectional reflectance factor (BRF), is given by Eq. (28). Its error, $\left|\delta BRF_m\right| \equiv \left|\delta I_m(z = 0, \underline{\Omega})\right|$ is given by [Huang et al., 2007]

$$|\delta BRF_m| \leq i_0 \frac{\theta_{m+1}}{1-\gamma_{m+1}} S_{BRF,m+1} \times$$

$$\times \left[\max_{k \geq 1, \Omega \in 2\pi^+} \frac{|e_{m+1+k}(z = 0, \underline{\Omega}) - e_{m+k}(z = 0, \underline{\Omega})|}{e_{m+k}(z = 0, \underline{\Omega})} + \max_{k \geq 1} \frac{|\gamma_{m+k+1} - \gamma_{m+1}|}{\gamma_{m+k+1}} \right], \qquad (38)$$

where

$$S_{BRF,m+1}(z = 0, \underline{\Omega}) = \sum_{k=1}^{\infty} \frac{\theta_{m+1+k}}{\theta_{m+1}} e_{m+k}(z = 0, \underline{\Omega}).$$

If m is large enough, i.e., $\sqrt[m+1]{\theta_{m+1}} \approx \gamma_\infty$ and $e_{m+1} \approx e_\infty$, the term $S_{BRF,m+1}$ can be approximated as $S_{BRF,m+1} \approx e_\infty \gamma_\infty / (1-\gamma_\infty)$. Its values, therefore, are mainly determined by the contribution of photons scattered m+1 and more times to the canopy radiation regime.

According to Eq. (38), the accuracy in the m-th approximation to the canopy BRF depends on the convergence of γ_{m+k} and e_{m+k} to the eigenvalue, γ_∞, and corresponding eigenvector, e_∞, of the operator T. Convergence of the former is illustrated in Fig. 15. This figure shows variations in $\max_{\Omega \in 2\pi+}\{e_{m+1}(\underline{r},\underline{\Omega})/e_m(\underline{r},\underline{\Omega})\}$ and $\min_{\Omega \in 2\pi+}\{e_{m+1}(\underline{r},\underline{\Omega})/e_m(\underline{r},\underline{\Omega})\}$ with the scattering order m. In this example, the difference $e_{m+1+k} - e_{m+k}$ is negligible for $m \geq 4$, indicating that the forth approximation provides an accurate spectral invariant relationship for the canopy BRF. Variation in the probability e_m with the scattering order m should be accounted to evaluate the contribution of low order scattered photons.

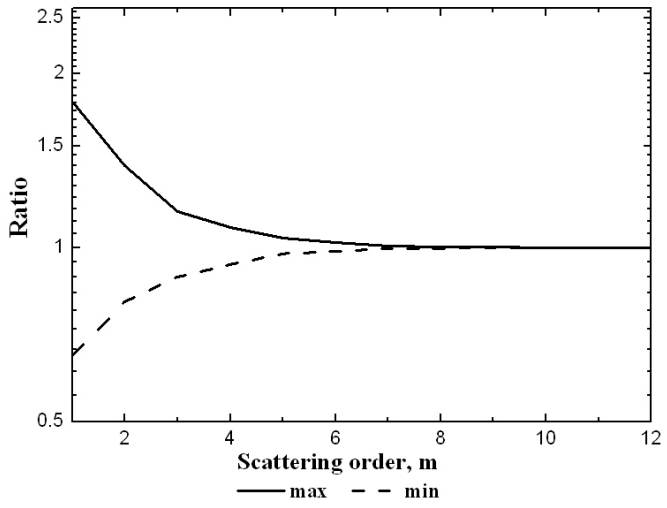

Figure 15. Convergence of e_m to the positive eigenvector, e_∞, of the operator T. The upper boundary of variations of the ratio e_{m+1}/e_m, $\max_{\Omega \in 2\pi}\{e_{m+1}/e_m\}$ (solid line) and corresponding lower boundary $\min_{\Omega \in 2\pi}\{e_{m+1}/e_m\}$ (dashed line) are shown with respect to the scattering order m. For $m \geq 5$, their values fall in the interval between 0.98 and 1.04. Parameters of the RT simulations are the same as for Fig. 13.

Inverse Linear Approximation to the Canopy Reflectance and Transmittance: The empirical and theoretical analysis indicates that the zero-order approximation provides an accurate spectral invariant relationship for the canopy interceptance; however more iterations are required to achieve comparable accuracy for the canopy transmittance and reflectance. The empirical analysis also suggests that zero-order approximation may result in a good accuracy in

case of reflectance and transmittance, if the recollision probability is replaced with its effective values.

In the following we derive effective recollision probabilities for canopy reflectance and transmittance in the zero-order approximation from the first-order approximation. According to Eqs. (36a), (37a) and (30), the first-order approximation (m=1) to the canopy spectral reflectance is

$$r(\lambda) = r_1(\lambda) + \delta r_1 = \left[\rho_1 + \frac{\omega p_1 \rho_2}{1 - p_2 \omega} + \frac{\omega p_1 \rho_2}{1 - p_2 \omega} S_{r,1} \right] \omega i_0 = \frac{1 - p_2 \omega \Delta_{r,1}}{1 - p_2 \omega} \omega \rho_1 i_0 . \qquad (39a)$$

Here $S_{r,1}$ [cf. Eq. (37c)] and $\Delta_{r,1}$ characterize the accuracy of the first approximation,

$$\Delta_{r,1} = 1 - \frac{\rho_2}{\rho_1} \frac{p_1}{p_2} [1 + S_{r,1}], . \quad S_{r,1} = \sum_{k=1}^{\infty} \frac{\theta_{k+1}}{\theta_1} \frac{\rho_{k+1}}{\rho_2} \left(\frac{\rho_{k+2} - \rho_{k+1}}{\rho_{k+1}} + \frac{\gamma_{k+1} - \gamma_2}{\gamma_{k+1}} \right). \qquad (39b)$$

Note, according to zero-order approximation [cf. Eq. (14a)] the reciprocal of the canopy spectral reflectance normalized by the leaf albedo, ω, varies linearly with ω. Based on this observation, we replace the relationship between the reciprocal of $r/(\omega i_0 \rho_1)$ and the leaf albedo ω given by first-order approximation [Eq. (39a)] with its zero-order form, given by a linear regression, $Y = \alpha_r - \beta_r p_2 \omega$. The coefficients R_1, R_2 and p_r in the zero-order approximation (14a), can be specified from the slope β_r and intercept α_r, namely

$$r(\lambda) = \omega(\lambda) R_1 + \frac{\omega(\lambda)^2 R_2}{1 - p_r \omega(\lambda)}, \quad R_1 = \frac{i_0 \rho_1}{\alpha_r}, \quad p_r = p_2 \frac{\beta_r}{\alpha_r}, \qquad (40a)$$

$$\alpha_r = 1 - 2 p_2 \int_0^1 \frac{1 - \Delta_{r,1}}{1 - p_2 \Delta_{r,1} \omega} \omega(2 - 3\omega) d\omega, \quad \beta_r = 6 \int_0^1 \frac{1 - \Delta_{r,1}}{1 - p_2 \Delta_{r,1} \omega} \omega(2\omega - 1) d\omega . \qquad (40b)$$

Similarly, the canopy transmittance is

$$t(\lambda) - t_0 = \frac{T_1\omega}{1 - p_t\omega}, \quad T_1 = \frac{i_0\tau_1}{\alpha_t}, \quad p_t = p_2\frac{\beta_t}{\alpha_t}. \tag{41}$$

Here α_t and β_t are given by Eq. (40b) but for $\Delta_{t,1}$ and $S_{t,1}$ which are calculated with τ_1, τ_2. We term this approach an *inverse linear approximation*. Note that if the escape probabilities do not vary with the scattering order ($\Delta_{r,1} = \Delta_{t,1} = 0$), the slope $\beta_r = \beta_t = p_2$ and intercept $\alpha_r = \alpha_t = 1$, and the inverse linear approximation coincides with the zero-order approximation. If variations in the escape probabilities become negligible for $m \geq 2$, ($\varepsilon_{\kappa,2} \approx 0, \kappa = r, t$), the effective probabilities p_r and p_t are functions of p_1, p_2, ρ_1, ρ_2 and, p_1, p_2, τ_1, τ_2 respectively.

Figure 16 demonstrates the energy conservation [Eq. (35a)] for $m = 1$. The escape probabilities are calculated from Eqs. (40) and (41) as R_1/i_0 and T_1/i_0. It follows from Fig. 15 that the impact of the regression coefficients α_r and α_t on the escape probabilities is minimal; that is, deviation of $R_1/i_0 + T_1/i_0 + p_1$ from unity does not exceed 5%. This is not surprising because values of $(1 - \Delta_{\kappa,1})/(1 - \Delta_{\kappa,1}p_2\omega)$ in Eq. (40b) for α_r ($\kappa = r$) and α_t ($\kappa = t$) are multiplied by the function $\omega(2 - 3\omega)$, integral of which is zero. The effective values of the recollision probabilities, p_r and p_t, however, depend on β_r and β_t.

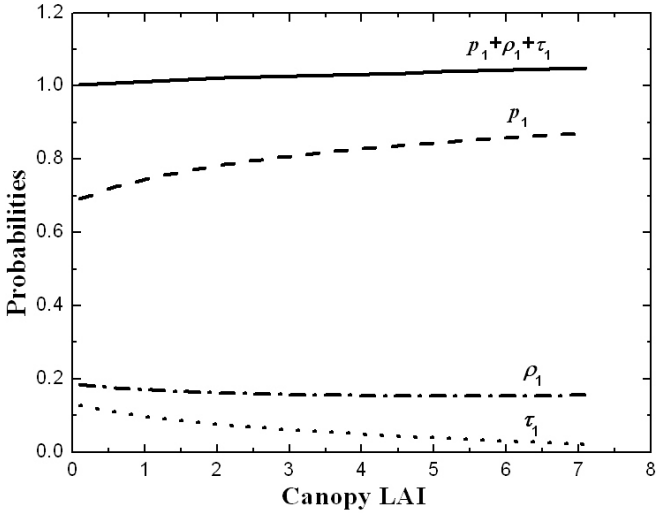

Figure 16. Energy conservation relationship $\rho_1 + \tau_1 + p_1 = 1$ as function of LAI. The escape probabilities ρ_1 and τ_1 were calculated as the ratios of coefficients R_1 and T_1 in the inverse linear approximations to i_0, i.e., $\rho_1 = R_1/i_0$ and $\tau_1 = T_1/i_0$. The deviation of $\rho_1 + \tau_1 + p_1$ from unity does not exceed 5%. Parameters of the RT simulations are the same as for Fig. 13.

Since eigenvalues and eigenvectors of the operator T are independent from the incident radiation, the limits p_∞, ρ_∞ and τ_∞ of the recollision and escape probabilities do not vary with the incident beam. Smolander and Stenberg [2005] showed that the first and higher orders of approximations to the recollision probability are insensitive to rather large changes in the solar zenith angle. Although the first approximations to the escape probabilities exhibit a higher sensitivity (Fig. 17) to the solar zenith angle, their sum, $\rho_1 + \tau_1 = 1 - p_1$, remains almost constant. This is consistent with the above theoretical results, suggesting that the canopy interaction coefficient requires less iterations to reach a plateau compared to the canopy reflectance and transmittance. The sensitivity of the effective recollision probabilities to the solar zenith angle is much smaller compared to the canopy interceptance.

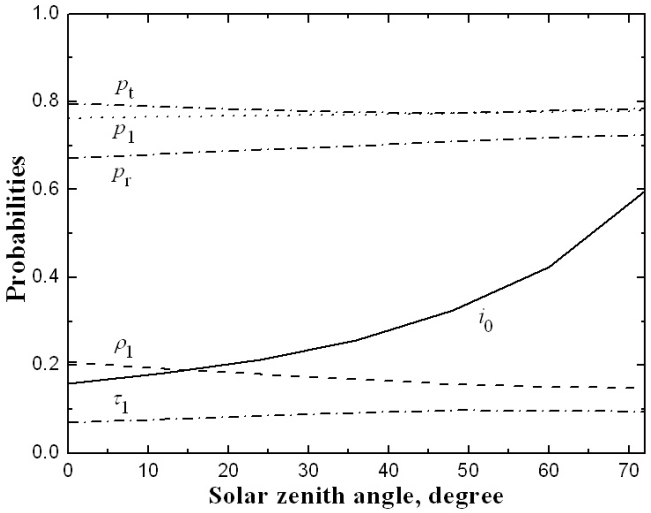

Figure 17. Recollision probability, p_1, its effective values, p_r and p_t, escape probabilities, ρ_1 and τ_1, and the canopy interceptance, i_0, as functions of SZA. Equation (40) was used to specify ρ_1 and τ_1. Parameters of the RT simulations are the same as for Fig. 13.

Figure 18 shows relative errors in the inverse linear approximation and the m-th approximations, m = 1, 2 and 3, to the canopy reflectance as a function of ω and LAI. The error decreases with the scattering order. For a fixed m, it increases with ω and LAI. This is consistent with the theoretical results stating that the convergence depends on the maximum eigenvalue $\gamma_\infty = p_\infty \omega$; that is, the higher its value is , the higher order of approximation is needed to estimate the canopy reflectance. In this example, the third and inverse linear approximations have the same accuracy level, i.e., they are accurate to within 5% if $\omega \le 0.9$. The relative error in the canopy transmittance (not shown here) exhibits similar behavior.

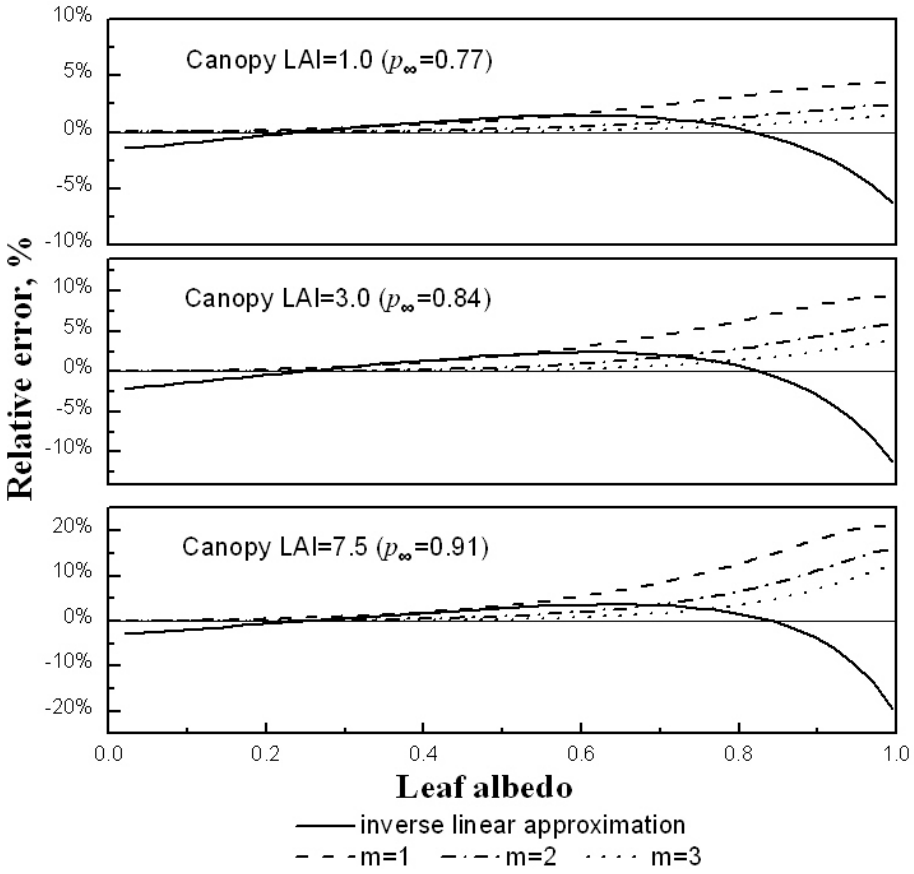

Figure 18. Relative error in the canopy reflectance as a function of ω and LAI. Parameters of the RT simulations are the same as for Fig. 13.

4. Scaling Properties of Spectral Invariants

The scaling effect, or scale dependence of RT parameters, arises due to phenomena of spatial heterogeneity (discontinuity) of canopy optical properties. For instance, single scattering albedo, $\omega(\lambda, V)$, is a function of the scale (volume, V) where it is defined. Consider sequence of *nested scales* represented by corresponding volumes: needle leaf tree stand (V_0), tree crowns (V_1), needle leaf shoots (V_2), and needles (V_3) (Fig. 19). Select a couple of scattering albedos, $\omega(\lambda, V_1)$ and $\omega(\lambda, V_2)$, which quantify the scattering properties at the scale of tree crown of volume V_1 and constituent objects (shoots) of volume V_2. By definition, single scattering of volume V_1 is the ratio of energy scattered by that volume to the amount of the energy intercepted

by the same volume. According to Eq. (8b) the tree crown single scattering albedo, $\omega(\lambda, V_1)$, can be expressed as

$$\omega(\lambda, V_1) \equiv \frac{s(\lambda, V_1)}{i_0(V_1)} = \omega(\lambda, V_2) \frac{1 - p(V_2 \to V_1)}{1 - \omega(\lambda, V_2)\, p(V_2 \to V_1)}. \qquad (44a)$$

Here $i_0(V_1)$ and $s(V_1)$ are the portion of photons intercepted and scattered by the volume V_1, and $p(V_2 \to V_1)$ is the recollision probability defined as the probability that a photon scattered by a volume V_2 (shoot) resided in the volume V_1 (tree crown) will hit again another volume V_2 (another shoot) in V_1. Its value is determined by the distribution of volumes V_2 (e.g., shoots) within V_1 (crowns). Thus, Eq. (44a) can be interpreted as one that provides a link between vegetation RT properties at different scales.

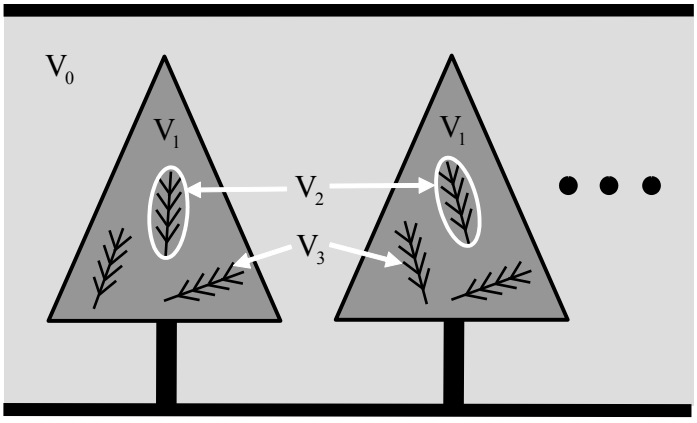

Figure 19. Schematic plot of nesting of scales. Tree stand occupies volume V_0, which consist of individual trees crowns of volume V_1, which, in turn, consist of shoots of volume V_2, which in turn consist of needles of volume V_3. The tree volumes are nested: $V_0 \supset V_1 \supset V_2 \supset V_3$.

Both $\omega(\lambda, V_1)$ and $p(V_2 \to V_1)$ vary with the scale V_1. However since the left-hand side of Eq. (44a) does not depend on V_2, the algebraic expression on the right-hand side of this equation should also be independent on the scale of V_2. Based on this property, variation in the leaf single scattering albedo and the recollision probability with the scale V can be specified as follows. Let us rewrite Eq. (44a) for needles (V_3) and shoot (V_2),

$$\omega(\lambda, V_2) = \omega(\lambda, V_3)\frac{1 - p(V_3 \to V_2)}{1 - \omega(\lambda, V_3)p(V_3 \to V_2)}. \quad (44b)$$

Substituting $\omega(\lambda, V_2)$ from Eq. (44b) into Eq. (44a) preserves the structure of Eq. (44a):

$$\omega(\lambda, V_1) = \omega(\lambda, V_3)\frac{1 - p(V_3 \to V_1)}{1 - \omega(\lambda, V_3)\, p(V_3 \to V_1)}, \quad (44c)$$

where

$$p(V_3 \to V_1) = p(V_3 \to V_2) + \left[1 - p(V_3 \to V_2)\right]p(V_2 \to V_1). \quad (45)$$

One can see that the probability $p(V_3 \to V_1)$ that a photon scattered by a volume V_3 (e.g., needles) will interact within volume V_1 (e.g., crown) again follows the *Bayes' formula*. Accordingly, Eq. (45) is called *nesting of scales*. The single scattering albedo and p-parameter exhibit the following scaling properties. Referring to Fig. 19 and taking into account Eqs. (44)-(45), provided $\omega, p \le 1$, one can derive that,

$$\omega(\lambda, V_2) \le \omega(\lambda, V_3) \text{ and } p(V_3 \to V_1) \ge p(V_2 \to V_1), \text{ if } V_3 \subset V_2;$$

$$p(V_3 \to V_1) \ge p(V_3 \to V_2), \text{ if } V_2 \subset V_1. \quad (46)$$

Consider the second property shown in Eq. (46), which conveys a fundamental law. It implies that the recollision probability increases with increasing complexity of canopy architecture (cf. Fig. 20). Namely, according to its definition, p=0 for the "Big Leaf" model, as there are no multiple scattering. As we add more hierarchical levels of structure, if photon reached particular structure elements it get trapped on structural sublevels, which increases probability of rescattering and thus value of p-parameter. The recollision probability, therefore, is a scaling parameter that accounts for a cumulative effect of the landscape's multi-level hierarchy.

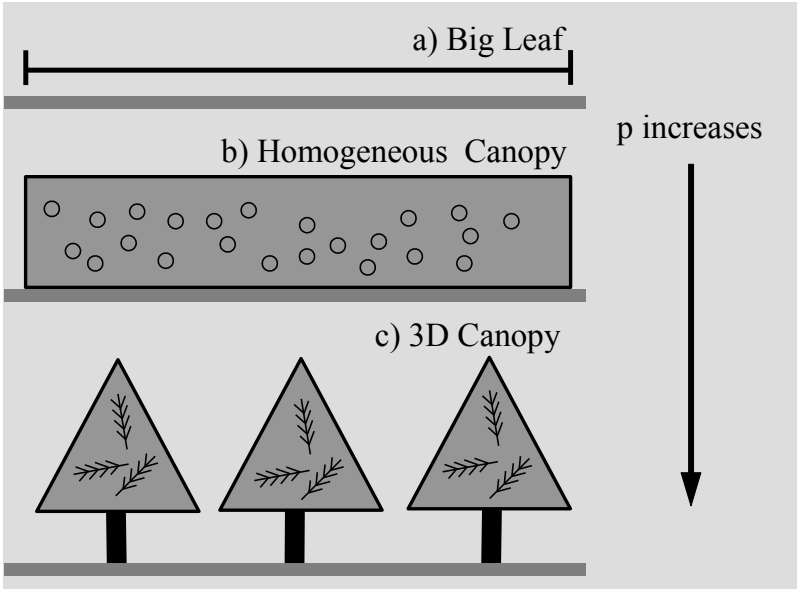

Figure 20. Recolision probability, p, as function of canopy structural hierarchy: (a) "Big Leaf" Canopy; (b) Turbid Medium; (c) 3D Canopy with nested scales of structure.

Case Study - Scaling from Needles to Shoots: The scaling properties of the p-parameter were first demonstrated by Smolander and Stenberg [2003; 2005] in the application for coniferous canopies. The 3D structure of the coniferous canopies exhibits foliage clumping at multiple scales, including clumping of needles into shoots and clumping of shoots into tree crowns; both give rise to the scaling effect. In particular, small-scale clumping of needles into shoots results in mutual shading and multiple scattering of light between needles of a shoot (Fig. 21), which ultimately leads to the known RT effect of coniferous canopies to appear darker than broadleaved canopies.

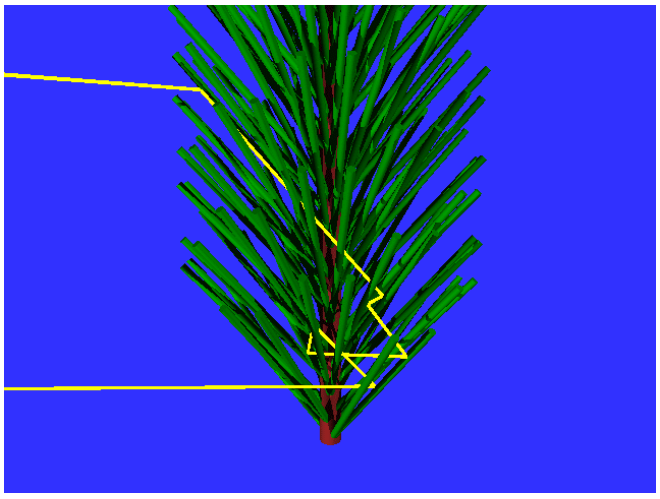

Figure 21. Scattering of photons on individual needles within shoot. The scattering is associated with loss of energy and thus shoot albedo is lower than albedo of individual needles (from Smolander and Stenberg, 2003].

The canopy clumping is described in the RT approach with spatially varying foliage volume density. However, the scale of variation of foliage density is limited by the size of canopy elementary volume. The elementary volume must be large enough to contain sufficient number of statistically independent foliage elements for the foliage volume density to be defined. Therefore, the approach is typically implemented at the large (landscape) scale, identifies individual tree crowns and space between them and defines the elementary volume to contain multiple leafs or needle shoots. The small-scale clumping of needles into shoots requires complex statistical description of distribution of needles. To overcome this problem, shot itself is typically used as the basic structural element in place of leaf for broadleaved canopies. The deviation of optical properties of elementary volume from those of individual needles, caused by shoot structure, is typically accounted for in the RT equation by adjusting extinction coefficient with empirically estimated clumping index (cf. Chapter 2). This *ad hook* approach is deficient in describing physical process of light scattering inside of a shoot, as it ignores wavelength dependence of the process and artificially couples shoot structure and needle optics.

Smolander and Stenberg [2003; 2005] developed p-parameter based RT framework to describe the effect of the small-scale clumping of needles into shoots to explain the difference in RT regimes in broadleaved and coniferous canopies. This study was focused only on small-scale clumping and large scale clumping was ignored. To support the theory, ray tracing simulations were performed for the model of canopy structure satisfying minimal requirements needed to meet the objectives of the study: a) realistic 3D model of shoots to represent small-scale structure; b) simple homogeneous turbid medium model for Poisson canopy to represent macroscopic structure. Foliage elements (shoots or leaves) were randomly distributed and spherically oriented (G-function and phase-function for spherically oriented leaves, cf. Chapter 3). Needle reflectances and transmittance were assumed to be similar to those of leaves, thus the difference between the two canopies reflectances caused solely by shoot structure. Geometrical model of Scots Pine (*Pinus Sylvestris L.*) shots was implemented referencing field measurements [Stenberg et al., 2002]. Three types of canopies were simulated: 1) *flat leaves*, 2) *shoots*, 3) *shoot-like leaves*, composed of leaves with the same G function and similar scattering properties

as shoots. Simulations were performed to generate reflectance of these canopies, assumed to be bounded below by black soil.

Recall (Chapter 3), shoot scale scattering in the needle leaf canopies is parameterized in terms shoot silhouette to total area ratio (STAR). Spherically averaged STAR is typically utilized,

$$\overline{\mathrm{STAR}} = \frac{1}{\mathrm{TNA}} \frac{1}{4\pi} \int_{4\pi} \mathrm{SSA}(\underline{\Omega}) \mathrm{d}\underline{\Omega}, \tag{47}$$

where $\underline{\mathrm{SSA}(\Omega)}$ is the shoot silhouette area in direction $\underline{\Omega}$ and TNA denotes the total needle area of the shoot. The $\overline{\mathrm{STAR}}$ parameter is analogous to G-function for leaves (cf. Chapter 3). In the case of spherically oriented scattering elements, the following holds:

$$\mathrm{G} = \begin{cases} 0.5, & \text{for leaves,} \\ 2\,\overline{\mathrm{STAR}}, & \text{for shoots.} \end{cases}$$

Note, the $\overline{\mathrm{STAR}}$ parameter is related to shoot structural parameter, $\mathrm{p}(\mathrm{L} \to \mathrm{Sh})$, which can be shown as follows. It follows from Cauchy's theorem for of convex, non self-shadowing objects that the ratio of silhouette to total area is ¼,. In contrast, needle leaf canopy shoot is a self-shadowing object due to self-shadowing of needles, and this ratio, the $\overline{\mathrm{STAR}}$ parameter, is smaller. Therefore, $(1/4 - \overline{\mathrm{STAR}}) \div 1/4 \equiv 1 - 4\,\overline{\mathrm{STAR}}$ quantifies the degree of self-shadowing, or the portion energy trapped inside of object due to self-shadowing. From another side, shoot structural parameter, $\mathrm{p}(\mathrm{L} \to \mathrm{Sh})$, is defined as the probability that a photon scattered by needle of the shoot will interact again with another needle of the same shoot. Comparing the above two definitions, we infer that

$$\mathrm{p}(\mathrm{L} \to \mathrm{Sh}) \approx 1 - 4\,\overline{\mathrm{STAR}}\,. \tag{48}$$

Note the following features of Eq. (48). First, the reason for the lack of exact equality is that $1 - 4\,\overline{\mathrm{STAR}}$ is defined as the mean over points on the surface, while $\mathrm{p}(\mathrm{L} \to \mathrm{Sh})$ is defined as

spatially averaged over points of interaction. Second, in contrast to $\overline{\mathrm{STAR}}$, $p(L \to Sh)$ is not just a function of shoot geometry but has some dependency on needle optical properties since they affect the directional distribution of scattered photons. Third, $p(L \to Sh)$ is defined based on the assumption that the probability of interactions stays constant with successive interactions. Equation (48) was verified with ray-tracing simulations for nine pine shoots and results are presented in Fig. 22.

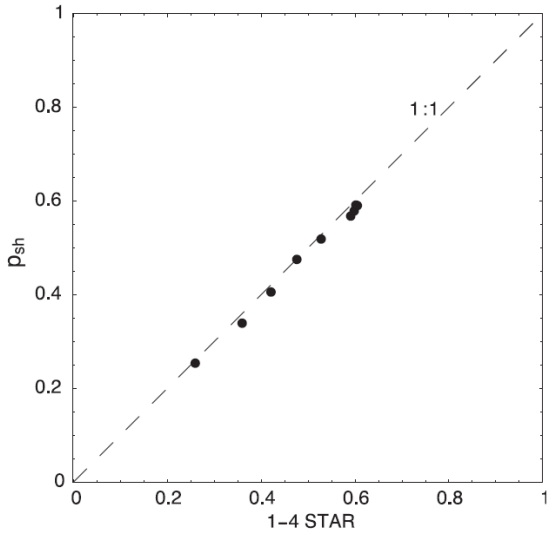

Figure 22. Relationship between p_{sh} and 1-4 $\overline{\mathrm{STAR}}$ for nine pine shoots. Shoot structural data from Stenberg et al. [2001] is used (from Smolander and Stenberg, [2003]).

In the shoot canopies shoot albedo varies with the direction of incoming beam (cf. results of simulations below). Average (over directions) shoot albedo, $\omega_{sh}(\lambda)$, is defined as fraction of scattered photons to photons intercepted by the shoot in an isotropic radiation field. Given $\mathrm{SSA}(\underline{\Omega})$ and $\omega_{sh}(\underline{\Omega})$, shoot silhouette area and shoot scattering coefficient in direction $\underline{\Omega}$, and taking into account that the number of intercepted photons is proportional to $\mathrm{SSA}(\underline{\Omega})$,

$$\omega_{sh}(\lambda) \equiv \frac{1}{4\pi\overline{\mathrm{SSA}}} \int_{4\pi} \omega_{sh}(\underline{\Omega})\mathrm{SSA}(\underline{\Omega})\mathrm{d}\underline{\Omega}\,. \tag{49}$$

The interaction of photon with the shoot occurred with probability $\mathrm{SSA}(\underline{\Omega})/S$, and thus the total fraction of intercepted photons N_i/N was proportional to $\overline{\mathrm{SSA}}$. The shoot albedo is equal to the fraction of photons escaped canopy to intercepted photons, N_e/N_i.

The shoot scattering phase-function and shoot albedo were generated with the 3D ray tracing. At each individual photon-needle interaction, a photon was scattered according to inform distribution with probability $\omega_L(\lambda)$, and absorbed with probability $1-\omega_L(\lambda)$, respectively,. Needle (or leaf) transmittance, $\tau_L(\lambda)$, and reflectance, $\rho_L(\lambda)$, were chosen as follows: $\rho_L(\lambda) = \tau_L(\lambda) = 0.5 \cdot \omega_L(\lambda)$; $\omega_L(\mathrm{Red}) = 0.1$, and $\omega_L(\mathrm{NIR}) = 0.9$. According to simulations for the NIR wavelength ($\omega_L(\mathrm{NIR}) = 0.9$), the shoot albedo was $\omega_{sh}(\mathrm{NIR}) = 0.81$, with reflectance $\rho_{sh}(\mathrm{NIR}) = 0.47$ and transmittance $\tau_{sh}(\mathrm{NIR}) = 0.34$. For the Red wavelength ($\omega_L(\mathrm{Red}) = 0.1$), the shoot albedo was $\omega_{sh}(\mathrm{Red}) = 0.059$, with $\rho_{sh}(\mathrm{Red}) = 0.034$ and $\tau_{sh}(\mathrm{Red}) = 0.025$. According to simulations, shoot albedo depends on shoot structural parameter, $p(\mathrm{L} \rightarrow \mathrm{Sh})$, and needle albedo, $\omega_L(\lambda)$, but is not sensitive to the ratio of needle transmittance to reflectance, $\tau_L(\lambda)/\rho_L(\lambda)$. Namely, ratio $\tau_L(\lambda)/\rho_L(\lambda)$ controls the shape of scattering phase function (forward vs. backward scattering), but does not change total needle albedo, and consequently has minor impact on canopy reflectance.

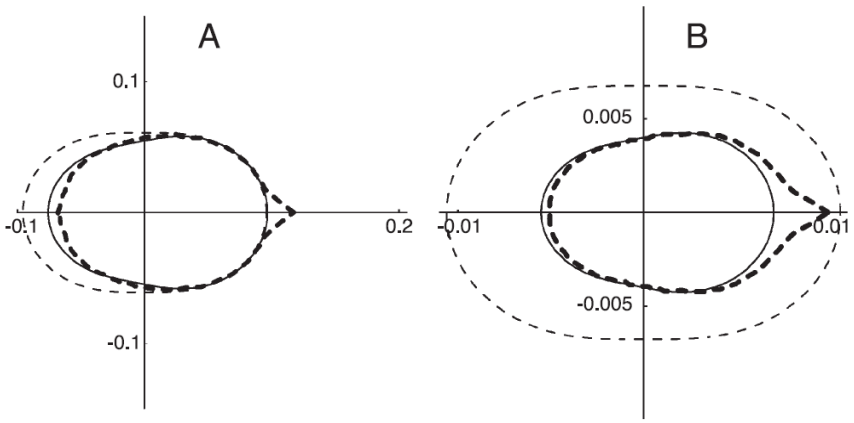

Figure 23. Cross-sectional views of scattering phase functions for (A) leaf with $\rho_L = 0.45$, $\tau_L = 0.45$ (thin dashed line), shoot (thick dashed line) with values $\rho_L = 0.45$ and $\tau_L = 0.45$ for its needles, and leaf with $\rho_L = 0.47$ and $\tau_L = 0.34$ (thin line), (B) leaf with $\rho_L = 0.05$, $\tau_L = 0.05$ (thin dashed line), shoot (thick dashed line) with values $\rho_L = 0.05$ and $\tau_L = 0.05$ for its needles, and leaf with $\rho_L = 0.034$ and $\tau_L = 0.025$ (thin line). The radiation is assumed to come from the direction of positive x-axis and to meet the object in origin (from Smolander and Stenberg, [2003]).

The scattering phase function of the spherically oriented shoots can be closely approximated by the scattering phase function of the shoot-like leaf, for which transmittance $\tau_L(\lambda)$ was 42% of $\omega_L(\lambda)$ at both wavelengths. Thus, the shoot scattering phase functions had more weight in the backscattering directions than the corresponding leaf scattering phase functions. Figure 23 shows the scattering phase function for the three types of foliage elements (flat leaves, shoots and shoot-like leaves). Note also the within-shoot hot spot effect in the backscattering direction in the shoot scattering phase-function, which can not be described by the bi-Lambertian distribution for flat leaves. However hot-spot effect can not be included for the shoot-like leaves. Overall, the effect of needle clumping and mutual shadowing in a shoot (compared to flat Lambertian leaf) is to decrease the radiation interception efficiency (G-function) and the shoot albedo, and to change the shape of the scattering phase function to weight it more towards the backscattering directions.

The relationship between shoot albedo, $\omega_{sh}(\lambda)$, and needle albedo, $\omega_L(\lambda)$, can be established as follows (cf. Section 2). At each interaction of photon and needle, photon is absorbed with probability $\omega_L(\lambda)$ and scattered with probability $1-\omega_L(\lambda)$ and can interact with shoot again. Assuming that the probability that scattered photon will interact with shoot again remains constant in successive interactions ($p(L \to Sh) = const$), shoot absorptance is obtained with infinite series,

$$A_{sh}(\lambda) \equiv [1-\omega_L(\lambda)] + [1-\omega_L(\lambda)]p(L \to Sh)\omega_L(\lambda) + [1-\omega_L(\lambda)]p^2(L \to Sh)\omega_L^2(\lambda) + ...$$
$$= \frac{1-\omega_L(\lambda)}{1-p(L \to Sh)\omega_L(\lambda)}.$$

Taking into account that $A_{sh}(\lambda) \equiv 1-\omega_{sh}(\lambda)$ the relationship between $\omega_{sh}(\lambda)$ and $\omega_L(\lambda)$ can be established,

$$\omega_{sh}(\lambda) = \omega_L(\lambda)\frac{1-p(L \to Sh)}{1-p(L \to Sh)\,\omega_L(\lambda)}. \qquad (50a)$$

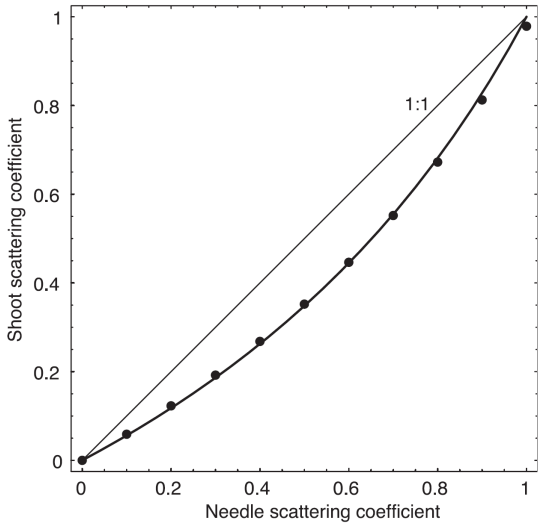

Figure 24. Predicted and simulated shoot albedo, $\omega_{sh}(\lambda)$, for different needle albedos, $\omega_L(\lambda)$ (from Smolander and Stenberg, [2003]).

Thus, if $p(L \to Sh)$ and needle albedo are known, the shoot albedo for any given wavelength can be calculated. Note, in case of $p(L \to Sh)=0$, corresponding to no within-shoot shading, than $\omega_{sh}(\lambda) = \omega_L(\lambda)$. At fixed $p(L \to Sh)$ the ratio $\omega_{sh}(\lambda) / \omega_L(\lambda)$ increases with $\omega_L(\lambda)$, i.e., the decrease in the shoot scattering from mutual shading is relatively less at wavelengths with high needle scattering. Equation (50a) was verified with ray-tracing simulations and results are presented in Fig. 24. The value of $p(L \to Sh)$ calculated according to ray tracing simulations (directly counting photons interactions) was 0.474, while $p(L \to Sh)$ estimated by fitting Eq. (50a) to the data points in Fig. 24 by the least squares method yields an estimate of 0.467 (1.5% difference). The difference is due to approximations in estimation of $p(L \to Sh)$, as it was assumed constant with respect to scattering order. In the simulations, the density of photons where scattering occurs varies with the scattering order, and it is not possible to analytically define the weight on the area over which $p(L \to Sh)$ is averaged.

Equation (50a) demonstrates effect of scaling between needles and shoot. Similar equation can be formulated for scaling at one level higher in the hierarchy, i.e. between shoot and canopy scales,

$$\omega_C(\lambda) = \omega_{sh}(\lambda) \frac{1 - p(Sh \to C)}{1 - p(Sh \to C)\, \omega_L(\lambda)}, \qquad (50b)$$

where $\omega_C(\lambda)$ is the canopy albedo, and $p(Sh \to C)$ is the recollision probability that photon scattered by shoot will interact again with another shoot with the canopy. Combining Eqs (50a) and (50b) we have:

$$\omega_C(\lambda) = \omega_L(\lambda)\frac{1 - p(L \to C)}{1 - p(L \to C)\,\omega_L(\lambda)}, \tag{51a}$$

where

$$p(L \to C) = p(L \to Sh) + [1 - p(L \to Sh)]p(Sh \to C). \tag{51b}$$

In words, the scattering between needles inside of whole canopy ($p(L \to C)$) can be decomposed into scattering between individual needles inside of a shoot ($p(L \to Sh)$) and scattering between shots inside of whole canopy ($p(Sh \to C)$). The relationship between $p(L \to C)$ and $p(Sh \to C)$ was verified with ray-tracing simulations for a range of LAI and results are shown in Fig. 23. In this simulations $\overline{STAR}$=0.133, $p(L \to Sh) = 1 - 4\overline{STAR}$=0.47 for *Pinus sylvestris* L. The parameter $p(Sh \to C)$ as function of LAI was well approximated by the relationship,

$$p(Sh \to C) = p(Sh \to C)_{max}[1 - \exp(-kLAI^b)], \tag{52}$$

where $p(Sh \to C)_{max}$=0.88, k=0.7, and b=0.75. In turn, $p(L \to C)$ was well predicted by the decomposition formula (Eq. 51), evaluated using $p(Sh \to C)$ and $p(L \to Sh)$. Note that there is a systematic offset between $p(L \to C)$ and $p(Sh \to C)$ due to between-needles scattering inside shoot ($p(L \to Sh)$). Simulations as function of direction (zenith angle) of incoming photons demonstrated low sensitivity of $p(Sh \to C)$ to zenith angles variations in spite the fact that zenith angle controls the distribution of the points of the first interaction of photons within canopy. Namely, for zenith angles < 50^0, the variation in $p(Sh \to C)$ was less than 1.2%.

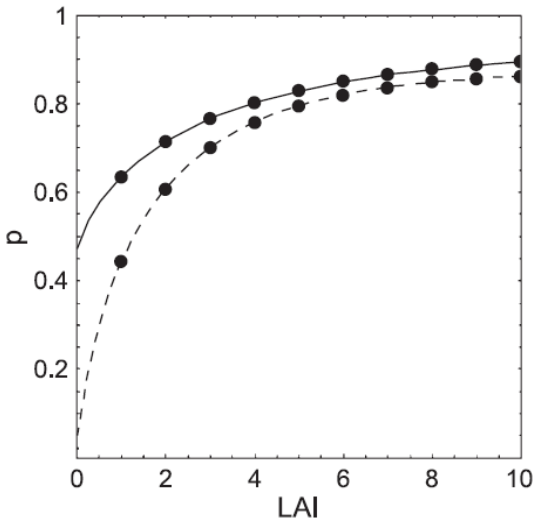

Figure 25. Recollision probabilities $p(Sh \to C)$ and $p(L \to Sh)$ as a function of LAI. Dots denote the p values derived from ray-tracing simulations. The dashed curve depicts $p(Sh \to C)$ according to fitting equation (Eq. (52)). The solid curve depicts $p(L \to C)$ according to the decomposition formula (Eq. (51)) (from Smolander and Stenberg, [2005]).

Finally consider Fig. 26 which compares ray-tracing simulated canopy BRF at Red and NIR wavelengths for the three canopy types (shoot, leaf and shoot-like leaf) bounded by a black surface. Clumping of needles into shoots produces a wavelength dependent reduction in canopy reflectance of need leaf canopy compared to that of broadleaf canopy with similar LAI. The reason for this effect is that the mutual shading of needle in a shoot leads to reduction of G-function and canopy interceptance for needle leaf compared to broadleaf canopies. Notice that the reflectance of the needle leaf canopy was well approximated by the shoot-like leaf canopy. Thus, integrating small-scale shoot structure in large-scale canopy RT models provides means to account for the observed difference between radiation regimes in coniferous and broadleaved canopies. Taking into account crown mutual shading will, presumably, further enhance this effect.

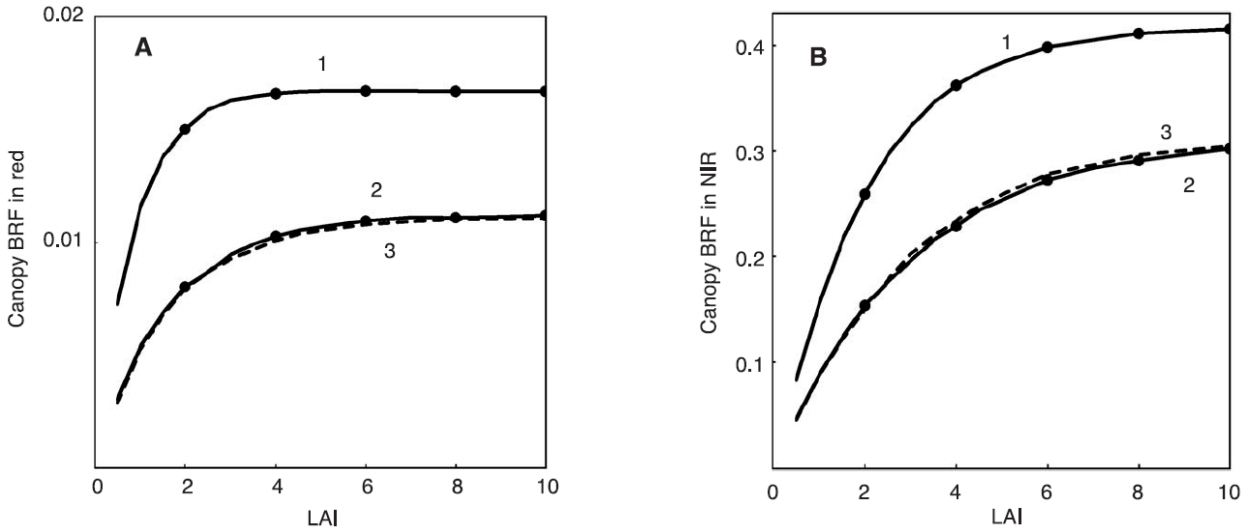

Figure 26. Predicted Canopy bidirectional reflectance factor (BRF) at Red and NIR wavelengths as a function of LAI for canopies bounded underneath by black soil. Curve (1) is for leaf canopy, curve (2) for shoot canopy and the dashed curve (3) for shoot-like leaf canopy. The black dots denote LAI values of 2, 4, 6, 8 and 10. The solar zenith angle is 45^0 and the view zenith angle is 0^0 (from Smolander and Stenberg, [2003]).

Case Study- Scaling from Leafs to Leaf Internals: Lewis and Disney [2007] further investigated the hypothesis that the scaling equations are applicable (in a consistent manner) across full range of scales from within leaf to canopy level scattering. The study utilized the PROSPECT leaf scattering model (Chapter 3). PROSPECT is a solar spectrum plate model of radiative transfer within a leaf. Leaf albedo, $\omega_L(\lambda)$, is calculated as function of leaf cell- air interface *refractive index* (n), the number of leaf layers, N and *absorption coefficient*, $A(\lambda)$. The absorption coefficient is a linear function of the concentration C_i [units of mass/unit LAI] of m biochemical constituents,

$$A(\lambda) = \sum_{i=1,m} C_i k_i(\lambda), \tag{53}$$

where $k_i(\lambda)$ is the *specific absorption coefficient* of the i-th constituent, a function of wavelength λ. Figure 27 shows $k_i(\lambda)$ as a function of wavelength for chlorophyll, water and dry leaf matter.

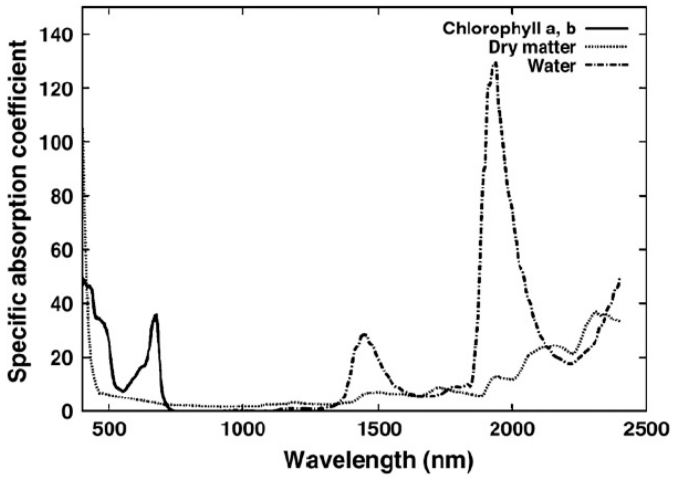

Figure 27. Specific absorption coefficients for chlorophyll, dry matter and water according to the PROSPECT model (from Disney and Lewis, [2007]).

The PROSPECT model identifies two components of leaf albedo, which corresponds to scattering (1) by leaf surface and (2) by leaf internals. Let $\omega_\infty(\lambda)$ be albedo of scattering from leaf surface, where the subscript accounts for the fact that scattering form leaf surface is equivalent to scattering from infinite leaf internals. Albedo $\omega_\infty(\lambda)$ is a function of a refractive index, which can be approximated by a quadratic $\omega_\infty(\lambda)$=-0.0492-0.00618n+0.04836n^2 (RMSE=2.37x10^{-3}, r^2=0.998). Let $\omega'_L(\lambda)$ be adjusted leaf albedo, which quantifies total scattering on leaf internals only and excludes scattering on leaf surface,

$$\omega'_L(\lambda) \equiv \frac{\omega_L(\lambda) - \omega_\infty(\lambda)}{1 - \omega_\infty(\lambda)}. \tag{54}$$

Note that denominator in Eq. (54) is introduced to ensure the standard range of variation of albedo, [0-1]. Lewis and Disney [2007] hypothesized that the general scaling relationship (cf. Eq. (44a)) should hold between adjusted leaf albedo, $\omega'_L(\lambda)$, and albedo of leaf internals, $\omega_{LI}(\lambda)$,

$$\omega'_{L}(\lambda) = \omega_{LI}(\lambda)\frac{1 - p(LI \to L)}{1 - \omega_{LI}(\lambda)\, p(LI \to L)}, \tag{55}$$

where albedo of leaf internals can be expressed as

$$\omega_{LI}(\lambda) \equiv \exp[-a(\lambda)\, A(\lambda)], \tag{56}$$

where, in turn, absorption coefficient, $A(\lambda)$, is given by Eq. (53) and coefficient $a(\lambda)$ is a function of refractive index, which can be approximated by quadratic, $a=1.3168-0.02294n + 0.01299n^2$ (RMSE= 5.06×10^{-5}, $r^2=0.9999$). Term $p(LI \to L)$ is the *equivalent recollision probability* for leaf internals, analogous to the *effective recollision probability*, $p(L \to Sh)$, defined by Smolander and Stenberg [2003] for the needles scattering inside a shoot . The leaf internals recollision probability extends set of similar terms, $p(L \to Sh)$ and $p(L \to C)$, recollision probabilities for shoot and canopy introduced by Smolander and Stenberg [2003]. The dependence of $p(LI \to L)$ on the refractive index, n, can be represented with quadratic, $p(LI \to L) = -1.2523+2.2307n-0.6094n^2$ (RMSE=8.95×10^{-4}, $r^2=0.9999$). The dependence of $\omega_{\infty}(\lambda)$, a, and $p(LI \to L)$ on refractive index is summarized in Fig. 28.

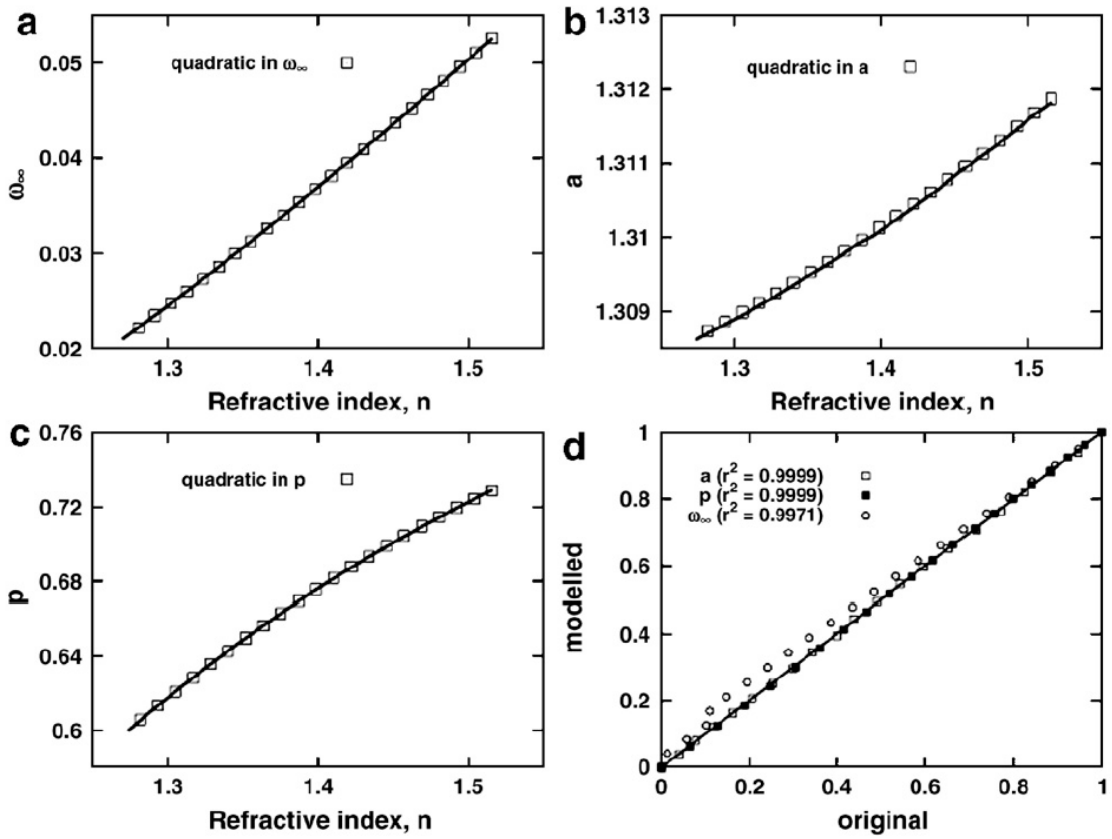

Figure 28. Variation of ω_∞ (Panel a), a (Panel b); and p_{leaf} (Panel c) with refractive index n as predicted with in PROSPECT (solid line) and quadratic approximation (symbols). Panel (d) shows scatter in each case against 1:1 line (from Lewis and Disney, [2007]).

While $p(LI \to L)$ varies significantly between 0.60 and 0.73 over the refractive index range across the solar spectrum (Fig. 28c), it appears that the assumption $p(LI \to L)$=const has negligible impact on simulated spectra of leaf albedo. Lewis and Disney [2007] set n=1.39, which corresponds to mid-range of solar spectrum and simultaneously minimizes errors in simulations of $\omega_L(\lambda)$. In this case according to quadratic approximation, $p(LI \to L)$=0.6708 and $\omega_\infty(\lambda)$=0.03566 and error in $\omega_L(\lambda)$ (difference between PROSPECT and approximation) is 0.010. Figure 29 compares $\omega_L(\lambda)$ retrievals based on spectral invariants approximation (Eq. (55)) and PROSPECT model for a range of concentrations of absorbing constituents. Two cases of spectral invariant model were tested: (1) variable and (2) fixed refractive index. In the first case r^2>0.9997, RMSE<0.0042, max error<0.013 and in the second case r^2>0.995, RMSE<0.016,

max error<0.049. Overall, spectral invariant approximation even in the case of fixed refractive index delivers very accurate estimate of leaf albedo spectra.

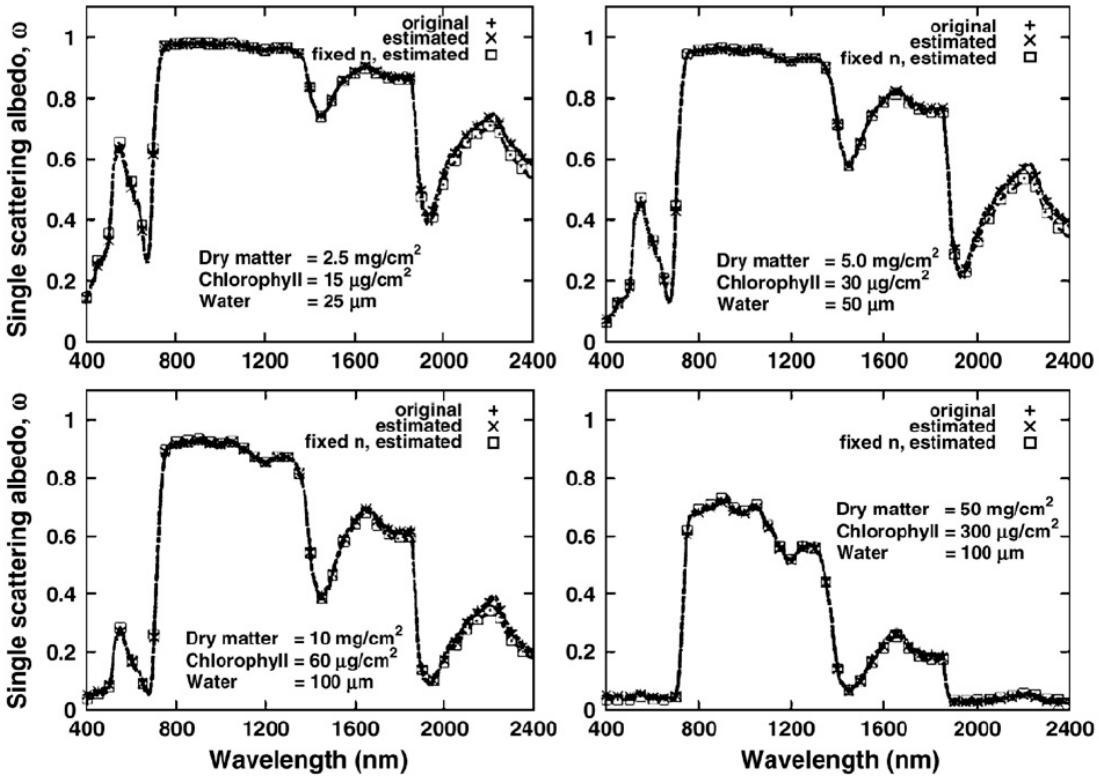

Figure 29. Accuracy of modeling of leaf spectra with spectral invariants approximation. Results shown for PROSPECT model ('original'); spectral invariant approximations with varying refractive index ('estimated'); and spectral invariant approximation with fixed refractive index ('fixed n, estimated') (from Lewis and Disney, [2007]).

The scaling approach, implemented by Smolander and Stenberg [2005] for "Canopy → Shoot → Leaf" scaling, was further extended by Lewis and Disney [2007] to incorporate one additional level down the hierarchy, Leaf Internals → Leaf. Combining Eqs. (51) and (55) and neglecting $\omega_\infty(\lambda)$ (Fig. 28), one can derive scaling relationship "Canopy → Shoot → Leaf → Leaf Internals" as follows,

$$\omega_C(\lambda) = \omega_{LI}(\lambda)\frac{1-p(LI \to C)}{1-\omega_{LI}(\lambda)\,p(LI \to C)}, \qquad (57a)$$

where $\omega_C(\lambda)$ is the canopy single scattering albedo, $\omega_{LI}(\lambda)$ is the single scattering albedo of leaf internals [Eq. (56)]. The recollision probability from leaf internals to canopy scales, $p(LI \to C)$, is given by the following *nesting* rule:

$$p(LI \to C) = p(LI \to L) + \left[1 - p(LI \to L)\right]$$

$$\times \left\langle p(L \to Sh) \quad + [1 - p(L \to Sh)]\, p(Sh \to C) \right\rangle . \qquad (57b)$$

Specifically, note the nesting of "leaf to shoot scattering" term (term in angular brackets, cf. Eq. (51b)) inside of "leaf internals to canopy scattering equation", which confirms the *Bayes' formula*. Overall, the scaling approach [Eq. (57)] is a powerful theoretical implementation of the shortwave radiation block in terms of few key parameters (canopy albedo, leaf biochemistry, and structural information). Nevertheless, practical implementation of the approach with multi-spectral remote sensing measurements may encounter challenges. P-parameter is an effective value, it can not be directly measured; rather it should be inferred from radiometric measurements, assuming knowledge of leaf biochemistry or leaf albedo. Leaf albedo can vary significantly over the canopy volume. For instance, coniferous forests exhibit vertical gradients of leaf biochemistry due to variations in needle and stand age, density of plants, etc. Therefore there is an internal difficulty in defining a (weighted) mean needle scattering spectra for use in the scaling applications to derive structural parameters. Further, there is a relatively strong coupling between leaf biochemistry and canopy structural parameters. Namely, the same spectra of leaf albedo can be derived from different combinations of structural information and leaf biochemistry [Lewis and Disney, 2007]. Consequently, the absolute concentration (per unit leaf area) of any biochemical constituents can not be derived from hyperspectral observations of total scattering.

References

Disney, M., P. Lewis, T. Quaife, and C. Nichol (2005). A spectral invariant approach to modeling canopy and leaf scattering. *Proc. The 9th International Symposium on Physical*

Measurements and Signatures in Remote Sensing (ISPMSRS), 17-19 October 2005, Beijing, China, Part 1, 318-320.

Huang, D., Y. Knyazikhin, R.E. Dikinson, M. Rautiainen, P. Stenberg, M. Disney, P. Lewis, A. Cescatti, Y. Tian, W. Verhoef, J.V. Martonchik, R.B. Myneni (2007). Canopy spectral invariants for remote sensing and model applications. *Remote Sens. Environ.,* **105**, 106-122.

Knyazikhin, Y., J.V. Martonchik, R.B. Myneni, D.J. Diner, S.W. and Running (1998). Synergistic algorithm for estimating vegetation canopy leaf area index and fraction of absorbed photosynthetically active radiation from MODIS and MISR data. *J. Geophys. Res*., **103**, 32257–32274.

Lewis, P., and M. Disney (2007). Spectral invariants and scattering across multiple scales from within-leaf to canopy. *Remote Sens. Environ.,* **xx**, xx-xx..

Marchuk, G.I., G.A. Mikhailov, M.A. Nazaraliev, R.A. Darbinjan, B.A. Kargin, and B.A. Elepov (1980). *The Monte Carlo Methods in Atmospheric Optics*, 208 pp., Springer-Verlag, New York.

Panferov, O., Y. Knyazikhin, R.B. Myneni, J. Szarzynski, S. Engwald, K.G. Schnitzler, and G. Gravenhorst (2001). The role of canopy structure in the spectral variation of transmission and absorption of solar radiation in vegetation canopies. *IEEE Trans. on Geosci. and Remote Sens.,* **39**, 241–253.

Riesz, F., and B. Sz.-Nagy (1990). *Functional Analysis*, Dover Publication, Inc., New York, 504 pp.

Ross, J. (1981). *The Radiation Regime and Architecture of Plant Stands*, Norwell, MA: Dr. W. Junk, pp. 391.

Smolander, S., and P. Stenberg (2003). A method to account for shoot scale clumping in coniferous canopy reflectance models. *Remote Sens. Environ.,* **88,** 363–373.

Smolander, S., and P. Stenberg (2005). Simple parameterizations of the radiation budget of uniform broadleaved and coniferous canopies. *Remote Sens. Environ.,* **94,** 355–363.

Vladimirov, V.S. (1963). Mathematical problems in the one-velocity theory of particle transport. *Tech. Rep. AECL-1661*, At. Energy of Can. Ltd., Chalk River, Ontario, 302 pp.

Remote Sensing of Environment 183 (2016) 98–108

Contents lists available at ScienceDirect

Remote Sensing of Environment

journal homepage: www.elsevier.com/locate/rse

Review

Photon recollision probability in modelling the radiation regime of canopies — A review

P. Stenberg [a,*], M. Mõttus [b], M. Rautiainen [c,d]

[a] University of Helsinki, Department of Forest Sciences, PO Box 27, FI-00014 Helsinki, Finland
[b] University of Helsinki, Department of Geosciences and Geography, PO Box 68, FI-00014, Finland
[c] Aalto University, School of Engineering, Department of Built Environment, PO Box 15800, FI-00076, Finland
[d] Aalto University, School of Electrical Engineering, Department of Radio Science and Engineering, PO BOX 13000, FI-00076, Finland

ARTICLE INFO

Article history:
Received 15 January 2016
Received in revised form 6 May 2016
Accepted 22 May 2016
Available online xxxx

Keywords:
Spectral invariants
Photon recollision probability
Radiative transfer
Conifer
DASF
PARAS model
Albedo
fPAR

ABSTRACT

Nearly two decades ago, the idea of the 'spectral invariants theory' was put forth as a new tool to model the shortwave radiation absorbed or scattered by vegetation. The theory states that the amount of radiation absorbed by a canopy should to a great accuracy depend only on the wavelength and a wavelength-independent parameter describing canopy structure. The revolutionary idea behind this theory was that it would be possible to approximate vegetation canopy absorptance, transmittance and reflectance based on only the optical properties of foliage elements and the spectrally invariant parameter(s). This paper explains how this so-called spectral invariant is related to photon recollision probability and to canopy structural variables. Other spectral invariants were later introduced to quantify the directionality of canopy scattering. Moreover, the paper reviews the advances in the theoretical development of the photon recollision probability (p) concept and demonstrates some of its applications in global and local monitoring of vegetation using remote sensing data.

Contents

* Corresponding author.
E-mail address: pauline.stenberg@helsinki.fi (P. Stenberg).

http://dx.doi.org/10.1016/j.rse.2016.05.013
0034-4257/

1. Introduction

Physically-based remote sensing of vegetation relies upon accurate models of the canopy shortwave radiation budget, which quantitatively describe how the fractions of solar radiation absorbed, transmitted and reflected by the canopy are related to the optical and structural properties of the canopy and background. Optical properties comprise the scattering and absorption spectra of the vegetation elements, which vary with the wavelength, whereas the structural canopy descriptors are independent of wavelength, or *spectrally invariant*. The variable focused on in this review — the *photon recollision probability*, is not one of the input parameters to the classical three-dimensional radiative transfer (RT) equation for vegetation (Ross, 1981), but is closely related to the solution of this equation (Knyazikhin, Martonchik, Myneni, Diner, & Running, 1998).

The concept of recollision probability can be pictured by thinking of the radiative transfer as a stochastic process: When a photon interacts with an element in the canopy, the probability that it will be absorbed or scattered varies with the wavelength. However, once the photon has been scattered, the probability that it will collide with the canopy again depends only on the location of the scattering event and the direction it was scattered into. This recollision probability is a geometric quantity which, in geometric optics approximation, does not depend on the wavelength. One may define a canopy averaged mean photon recollision probability, which was shown to link together the optical properties at canopy and leaf level by a set of simple algebraic relationships (Smolander & Stenberg, 2005). The existence of a spectrally invariant '*p*-parameter' satisfying similar relationships was, however, first discovered and theoretically established by Knyazikhin et al. (1998). Only a clear interpretation of this parameter was still lacking at the time. The fact that the somewhat heuristic 'photon recollision probability'-approach was found to be coherent with physically-based radiative transfer started a new era in the application of the 'spectral invariants theory': the single parameter representing canopy structure had now been defined and thus could also be quantified.

Knyazikhin et al. (1998) put forth the idea of the 'spectral invariants theory' when developing the theoretical grounds of the MODIS algorithm for retrieval of the leaf area index (LAI) and the fraction of photosynthetically active radiation (fPAR). They proposed a revolutionary idea that it would be possible to approximate vegetation canopy absorptance, transmittance and reflectance using only the optical properties of foliage elements and one spectrally invariant parameter for each approximated canopy characteristic. The theory states that, knowing the leaf albedo (1-absorptance), canopy absorptance at any wavelength can be estimated with high accuracy from canopy absorptance at a reference wavelength. This property laid the foundation for the synergistic look-up-table (LUT) based algorithm developed by Knyazikhin et al. (1998), which has been successfully implemented in the retrieval of global leaf area index (LAI) from canopy reflectance data measured by the MODIS instrument.

This approach was contrary to many other lines of development where more complexity was favored in canopy radiation models. A couple of years later, several independent research lines in Boston University, University of Helsinki and University College London were investigating the spectral invariants theory and its applications. This paper reviews the advances in the theoretical concepts behind the spectral invariants and shows examples of various applications of the concept in global and local monitoring of vegetation using remote sensing data.

2. *p*-Theory

2.1. The concept of recollision probability

Knyazikhin et al. (1998) proposed that the unique positive eigenvalue of the radiative transfer equation can be expressed as the product of the leaf albedo and a wavelength independent parameter, and the name '*p*-theory' originates from the symbol they used for this canopy structural parameter. Empirical evidence for the spectral invariant behavior of the *p* parameter was provided later by Panferov et al. (2001) and Wang et al. (2003) based on the measured spectral reflectance and transmittance data of forest canopies. However, a clear interpretation of how *p* is related to the canopy structure, allowing it to be estimated from canopy structural measurements, was still missing. A step towards this goal was taken by Smolander and Stenberg (2005), who defined *p* as a conditional probability — the recollision probability, and in their simulation study derived tight relationships between *p* and LAI in model canopies. It was shown that, in addition to LAI, *p* is linked to the clumping of foliage.

Smolander and Stenberg (2005) were thus first to introduce the term recollision probability for *p*, which they defined as the probability by which a photon scattered from a phytoelement (leaf or needle) in a vegetation canopy will interact within the canopy again. The escape probability $(1 - p)$ correspondingly is the probability by which a scattered photon will escape the canopy. These probabilities are defined conditional to the photon having survived an interaction inside the canopy. The fraction of photons that enter the vegetation from above and are intercepted by elements in the canopy is called the *canopy interceptance* (i_0). The zero order (or *uncollided*) transmittance (t_0) in turn is the fraction of photons that are transmitted directly through gaps in the canopy: $t_0 = 1 - i_0$. In a canopy bounded underneath by a non-reflecting ('black') surface (Fig. 1), the transmitted photons will not interact within the canopy again. Under this condition, and assuming further that the *p* remains constant in successive interactions, canopy absorptance (a) at a specific wavelength (λ) is obtained as the sum of a geometric series:

$$a(\lambda) = i_0\left[(1-\omega_L(\lambda)) + \omega_L(\lambda)p(1-\omega_L(\lambda)) + \omega_L(\lambda)^2p^2(1-\omega_L(\lambda)) + \ldots\right] = i_0\frac{1-\omega_L(\lambda)}{1-p\omega_L(\lambda)}. \quad (1)$$

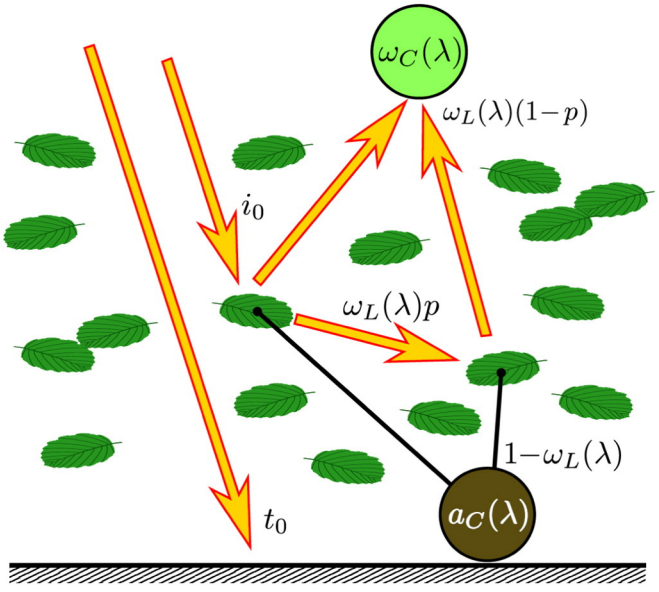

Fig. 1. Photons entering a canopy bounded below by black soil are first intercepted by leaves (i_0) or directly transmitted to and absorbed by the ground (t_0). The intercepted part is eventually absorbed (α_C) or scattered out from the canopy (ω_C) after one or multiple interaction and recollision events.

In Eq. (1), ω_L denotes the leaf scattering coefficient (single scattering albedo) and the common ratio ($p\omega_L$) of the series corresponds to the joint probability of recollision and a new scattering event.

Canopy scattering (s) under the black soil assumption is similarly obtained as:

$$s(\lambda) = i_0 \frac{\omega_L(\lambda) - p\omega_L(\lambda)}{1 - p\omega_L(\lambda)}. \quad (2)$$

Canopy absorptance and scattering sum up to the canopy interceptance: $a(\lambda) + s(\lambda) = i_0$. These wavelength dependent components normalized by i_0 thus define the *canopy spectral absorption and scattering coefficients*, α_C and ω_C:

$$\alpha_C(\lambda) = \frac{a(\lambda)}{i_0} = \frac{1 - \omega_L(\lambda)}{1 - p\omega_L(\lambda)} \quad (3)$$

and

$$\omega_C(\lambda) = \frac{s(\lambda)}{i_0} = \frac{\omega_L(\lambda) - p\omega_L(\lambda)}{1 - p\omega_L(\lambda)}. \quad (4)$$

We note that the derivation of Eqs. (1)–(4) rely on the assumptions of black soil and a constant p. Canopy absorption by Eq. (1) represents the solution to the so called 'black soil problem' (Knyazikhin et al. 1998; Wang et al. 2003), which in the case of a dark soil (background) and/or a dense canopy may be a good approximation. Whenever this is not true, another component, the solution to the 'soil problem', must be added. Similarly, the fact that p in reality is not constant must be carefully considered. The degree to which these issues limit the applicability of the recollision probability concept, and how to overcome the problems, will be addressed in subsequent sections.

2.2. Links to the radiative transfer equation

The link between the photon recollision probability p and the unique positive eigenvalue γ_0 of the radiative transfer equation is described by Huang et al. (2007) and Knyazikhin, Schull, Liang, Myneni, and Samanta (2011). In the successive orders of scattering approach, canopy scattering is calculated as the sum of contributions by different scattering orders, i.e. photons scattered 1, 2, …, n times before exiting the canopy. In this approach, we may define the operator $\mathbf{T}$ such that the radiation field I_λ of order $i + 1$ equals:

$$I_\lambda(i+1) = \mathbf{T} I_\lambda(i), \quad i = 1, 2, \ldots. \quad (5)$$

The largest (and the only positive) eigenvalue of operator $\mathbf{T}$, γ_0, is a linear function of the leaf albedo $\omega_L(\lambda)$: $\gamma_0 = p_{\text{inf}}\omega_L(\lambda)$. The spectrally invariant parameter p_{inf} is the limiting recollision probability as the order of scattering reaches infinity ($i \to \infty$).

Knyazikhin et al. (1998) used the largest eigenvalue of operator $\mathbf{T}$ to demonstrate the existence of the spectral invariants for canopy absorptance, although without introducing the concept of photon recollision probability. They derived the spectral invariant relationship for the norm $||I_\lambda||_1$ of the solution to the radiative transfer equation, or the product of the monochromatic radiance I_λ and the interaction cross-section σ integrated over the canopy volume and all directions. $||I_\lambda||_1$ is the mean spectral irradiance on all sides of a leaf and is thus a key component of the energy conservation law. For vegetation bounded underneath by a black surface and irradiated with unit irradiance, it corresponds to the mean number of photon interactions with phytoelements at wavelength λ in the canopy, and is called the interaction coefficient, i.e. $i(\lambda) = ||I_\lambda||_1$. The interaction coefficient multiplied by the leaf absorptance gives canopy absorptance: $a(\lambda) = i(\lambda)[1 - \omega_L(\lambda)]$. Knyazikhin et al. (1998) showed that, if the interaction cross-section (σ) does not depend on wavelength, then for the first eigenvector $e_0(\lambda)$ of Eq. (5), the norms $||I_\lambda e_0||_1$ at two arbitrary wavelengths, λ and λ_0, are linked together as:

$$||I_\lambda e_0||_1 = \frac{1 - \gamma_0(\lambda_0)}{1 - \gamma_0(\lambda)} ||I_{\lambda_0} e_0||_1 = \frac{1 - p_{inf}\omega_L(\lambda_0)}{1 - p_{inf}\omega_L(\lambda)} ||I_{\lambda_0} e_0||_1. \quad (6)$$

Next, based on the demonstrated proximity between the spectral dependencies of $e_0 I_{\lambda 1}$ and $I_{\lambda 1}$, Knyazikhin et al. (1998) derived the relationship for $i(\lambda) = ||I_\lambda||_1$:

$$i(\lambda) \approx \frac{1 - p\omega_L(\lambda_0)}{1 - p\omega_L(\lambda)} i(\lambda_0). \quad (7)$$

The recollision probability p is an approximation to p_{inf}. The goodness of this approximation depends on two factors: the contributions of the different scattering orders on total scattering, and how fast (in terms of scattering orders) the recollision probability approaches the diffuse limit p_{inf}. The speed of convergence depends, in turn, on the recollision probability and the leaf albedo: the higher the value of $p_{\text{inf}}\omega_L$, the slower the convergence. A detailed analysis of the accuracy of the approximation is given by Huang et al. (2007).

The conditions under which the spectral invariant relationships can be derived from the three-dimensional radiative transfer (RT) equation for vegetation are described in detail by Knyazikhin et al. (1998, 2011) and Huang et al. (2007). Some of the central assumptions and concepts are briefly summarized here. First of all, the interaction cross-section σ can be considered wavelength independent due to the large size of scattering elements relative to the wavelength of solar radiation (Ross, 1981). Another assumption used in the derivation is that the single scattering albedo (ω) inside the canopy volume does not depend on the location inside the canopy and the direction (Ω), and that it coincides with the leaf single scattering albedo (ω_L), i.e. the canopy consists of leaves only. The ratio $p = \gamma_0/\omega_L(\lambda)$ is then wavelength independent.

Substituting $i(\lambda) = a(\lambda) / [1 - \omega_L(\lambda)]$ in Eq. (7), the corresponding equation for canopy absorptance takes the form:

$$a(\lambda) = \frac{1 - p\omega_L(\lambda_0)}{1 - p\omega_L(\lambda)} \frac{1 - \omega_L(\lambda)}{1 - \omega_L(\lambda_0)} a(\lambda_0). \quad (8)$$

Evaluating Eq. (8) at $\omega_L(\lambda_0) = 0$ and $a(\lambda_0) = i_0$ gives

$$a(\lambda) = i_0 \frac{1 - \omega_L(\lambda)}{1 - p\omega_L(\lambda)} \quad (9)$$

which is seen to be identical to Eq. (1).

Similar relationships as Eq. (7) for the canopy interaction coefficient (i) can be formulated for canopy diffuse transmittance (t) and reflectance (r) (Smolander & Stenberg, 2005). Empirical evidence for the spectrally invariant behavior of the corresponding parameters (p, p_t and p_r) was derived from forest spectral reflectance and transmittance measurements by Panferov et al. (2001). It was found that specific combinations of the canopy spectral reflectance values r calculated as

$$\xi_r(\lambda_0, \lambda_1) = \frac{r(\lambda_0) - r(\lambda_1)}{\omega_L(\lambda_0) r(\lambda_0) - \omega_L(\lambda_1) r(\lambda_1)} \quad (10)$$

were concentrated around a certain canopy-specific value p_r, the mathematical expectation of ξ_r. Eq. (10) can be easily rearranged so that the dependence of the canopy reflectance r on the leaf albedo ω_L becomes similar to that of the canopy scattering ω_C in Eq. (4). An equation similar to Eq. (10) can be written for the transmittance t and the spectral invariant p_t.

The empirically-derived invariants p_r and p_t are approximate combinations of the spectrally invariant factors of the eigenvalues γ_i. More recently, Mõttus and Stenberg (2008) proposed a different

parameterization of canopy spectral reflectance using the reflectance ratio $r_C(\lambda)/\omega_C(\lambda)$ parameterized as:

$$\frac{r_C}{\omega_C} = \frac{1}{2} + \frac{q}{2}\frac{1-p\omega_L}{(1-p)\omega_L}. \quad (11)$$

The parameter q in Eq. (11) can be shown to be an approximation of the ratio of the two largest eigenvalues of $\mathbf{T}$, $q = \gamma_1/\gamma_0$ (Mõttus, 2010).

2.3. Scaling of p from leaf (needle) to canopy

The recollision probability can be defined at different hierarchical levels of the canopy and links the scattering properties at any two consecutive levels. For example, in their first simulation study with application of the p-theory, Smolander and Stenberg (2003) derived Eq. (4) at shoot level to model the effect of clumping of needles into shoots on the shoot scattering coefficient (ω_{sh}):

$$\omega_{sh}(\lambda) = \frac{\omega_L(\lambda) - p_{sh}\omega_L(\lambda)}{1 - p_{sh}\omega_L(\lambda)} \quad (12)$$

In Eq. (12), the 'shoot structural parameter' p_{sh} is the recollision probability within the shoot: it is the conditional probability that a photon which has survived an interaction within a shoot will interact again with a needle from the same shoot.

More generally, Eq. (4) can obviously be used at any level of the structural hierarchy to link the scattering coefficient of a unit (ω_{unit}) to that of its elements ($\omega_{element}$). Furthermore, letting $n(\lambda)$ denote the average number of interactions within the unit (shoot, canopy) for photons of wavelength λ, the ratio of these coefficients can be expressed as:

$$\frac{\omega_{unit}(\lambda)}{\omega_{element}(\lambda)} = n(\lambda)(1 - p_{unit}). \quad (13)$$

Eq. (13) states that the scattering coefficient of any unit normalized by that of its elements equals the (wavelength dependent) number of interactions multiplied by the spectrally invariant probability of escape ($1 - p$).

The total canopy *recollision and escape probabilities* in turn can be decomposed as

$$p(canopy) = p_1 + (1-p_1)p_2 + \ldots + (1-p_1)\ldots(1-p_{n-1})p_n \quad (14)$$

and

$$1 - p(canopy) = (1-p_1)(1-p_2)\ldots(1-p_n) \quad (15)$$

where n is the number of levels and p_i is the probability that a photon leaving a "clump" at the hierarchical level $i - 1$ will collide with a clump at level i (Fig. 2). The albedos at any two consecutive levels are linked by the equation (see Eq. (4)):

$$\omega_{i+1}(\lambda) = \frac{\omega_i(\lambda) - p_i\omega_i(\lambda)}{1 - p_i\omega_i(\lambda)}. \quad (16)$$

The goodness of the scaling depends on how well the p-theory approximates the radiation field inside the vegetation canopy. Theoretically, this is linked to the speed of convergence of the recollision probability with scattering order to its limiting value. As discussed in the following sections, in structurally complex extremely dense canopies, the connection between the photon recollision probability p and the eigenvalue γ_0 is lost, although the approximating equation (Eq. (9)) can still be used to describe total canopy absorption.

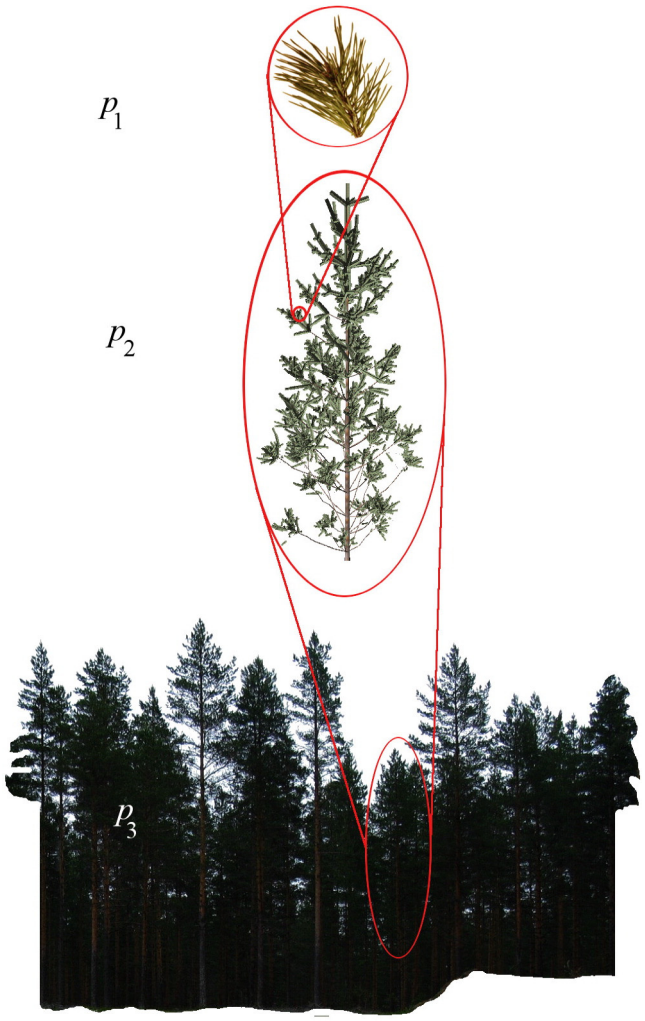

Fig. 2. In the forest depicted here, p_1 would be the recollision probability within a shoot, p_2 the recollision probability of a shoot-leaving photon within the crown, and p_3 the recollision probability of a crown-leaving photon with another, different crown.

2.4. Link between p and STAR

Smolander and Stenberg (2003) calculated the mean probability of escape ($1 - p_{sh}$) within modelled Scots pine shoots using Monte Carlo ray tracing (see Section 3.2.). They found that, to a very close approximation, $1 - p_{sh} = 4\text{STAR}$, where STAR is the spherically averaged silhouette to total needle area ratio of a shoot (Oker-Blom & Smolander, 1988) and 4STAR is analogous to the shoot shading factor β (Stenberg, 1996). As shown by Smolander and Stenberg (2003), 4STAR can be interpreted as the mean probability that a photon emitted from a random point on the needle surface of the shoot will not hit another needle of the shoot. Assuming Lambertian reflectance, it follows that the only difference between the escape probability and 4STAR comes from the spatial averaging: if the points of interaction were uniformly distributed over the total needle area of the shoot then the two quantities would coincide.

Based on the same assumption at canopy level, i.e. that the points of interaction are uniformly distributed over the total canopy leaf (needle) surface area, Stenberg (2007) later derived a simple analytical expression for the relationship between the total escape probability $1 - p$,

the leaf area index (LAI) and the canopy interceptance in diffuse (isotropic) radiation (i_D) (Eq. (A1) in Appendix A):

$$1-p=\frac{i_D}{\mathrm{LAI}}. \tag{17}$$

In deriving Eq. (17), Stenberg (2007) first defined the escape probability (P_{esc}) of a single photon scattered from a point r on a leaf (or needle) assumed to scatter as a Lambertian surface, i.e. reradiating photons following a cosine distribution around the direction Ω_r of the leaf normal, as:

$$P_{esc}(r)=\frac{1}{\pi}\int_{2\pi(\Omega_r)}\chi(r,\Omega)\cos(\Omega,\Omega_r)\mathrm{d}\Omega. \tag{18}$$

In Eq. (18), the function χ is defined such that it takes the value 1 if there is a free line of sight through the canopy from r to the direction Ω, and 0 otherwise, and integration is performed over the hemisphere $2\pi(\Omega_r)$ facing the leaf surface at r. The mean escape probability, $1-p$ (Eq. (17)), was then defined as P_{esc} averaged over (all the points r on) the total leaf (needle) surface area of the canopy, which was shown to equal the ratio of canopy diffuse interceptance (i_D) to the hemisurface LAI. In complete analogy to the shoot level p, the canopy level p (Eq. (17)) can be interpreted as the mean probability that a photon emitted from a random point on a Lambertian leaf (or needle) surface of the canopy will not hit another leaf of the canopy.

At a fixed LAI, the ratio i_D/LAI is smaller (and p larger) the more aggregated is the distribution of leaves in the canopy, or the smaller is the *canopy clumping index*. The clumping index (Γ), as defined by Eqs. (A2)–(A3) in the Appendix A, furthermore provides the link between the true LAI and the *effective leaf area index* (L_e) as $L_e = \Gamma\mathrm{LAI}$ (Eq. (A4) in Appendix A). Using these definitions, Eq. (17) can be written in the form

$$1-p=\Gamma\frac{i_D}{L_e}. \tag{19}$$

Rautiainen, Mõttus, and Stenberg (2009) studied the relationship between p, LAI and L_e based on empirical data (provided by measurements with the LAI-2000 Plant Canopy Analyzer) from five coniferous dominated test sites in Finland, containing in total 1032 pure or mixed plots with Norway spruce, Scots pine, Silver birch and Downy birch. They observed a tight relationship between i_D and L_e (Fig. 3), as could be expected based on their definitions (Eqs. (A1) and (A4)). This means that, at a fixed L_e, the ratio i_D/L_e has a near constant value and the escape probability (Eq. (19)) becomes proportional to the clumping index Γ.

2.5. Empirical proof of the p-theory

The first empirical proof of the p-theory was obtained in a joint laboratory experiment carried out by the University of Helsinki and University of Zurich in spring 2011 (Rautiainen et al., 2012). The aim of the experiment was to test if it was possible to upscale needle albedo to shoot albedo using only one parameter describing the shoots, i.e. the spherically averaged shoot silhouette to total needle area ratio (STAR). In other words, to test empirically the validity of Eq. (16).

First, using a spectroradiometer attached to the LAGOS goniometer located in the Remote Sensing Laboratories (University of Zurich), the upper and lower hemispherical bidirectional reflectance distribution functions (BRDF) for the study shoots were measured. The measured data were further processed to shoot spectral albedos. Simultaneously, the reflectance and transmittance values of single needles were measured. After the spectral measurements, the structure of the studied Scots pine shoots, including needle dimensions and shoot silhouette to total area ratios (STAR), were carefully measured in order to calculate the STAR values for the shoots.

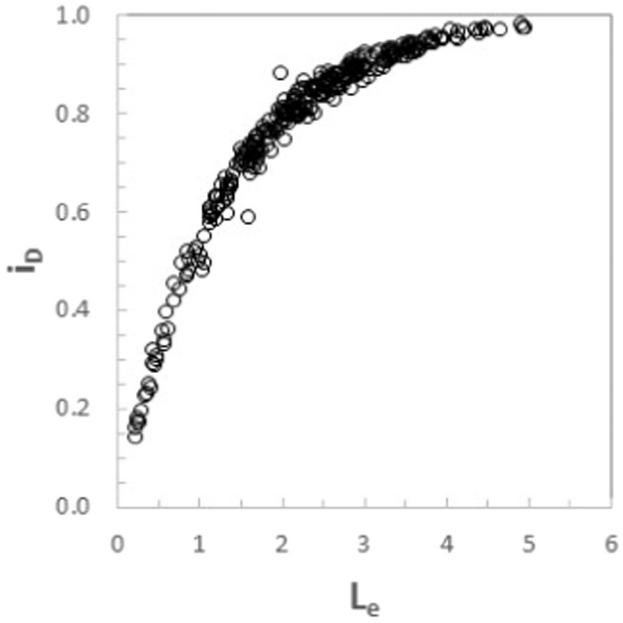

Fig. 3. The relationship between effective LAI (L_e) and canopy diffuse interceptance (i_D) can be easily measured with, for example, LAI-2000 Plant Canopy Analyzer or obtained from hemispherical photographs. This figure is based on 307 forest stands measured in Hyytiälä, Finland in 2013 (Majasalmi, Rautiainen, Stenberg and Manninen, 2015).

The empirical results confirmed the theory: STAR (which is linearly related to p) could indeed be used to scale between needle and shoot spectral albedos at these two hierarchical levels (Fig. 4). In an empirical follow-up study, Mõttus and Rautiainen (2013) also showed that common spectral vegetation indices, such as the normalized difference vegetation indices (NDVI) or photochemical reflectance index (PRI),

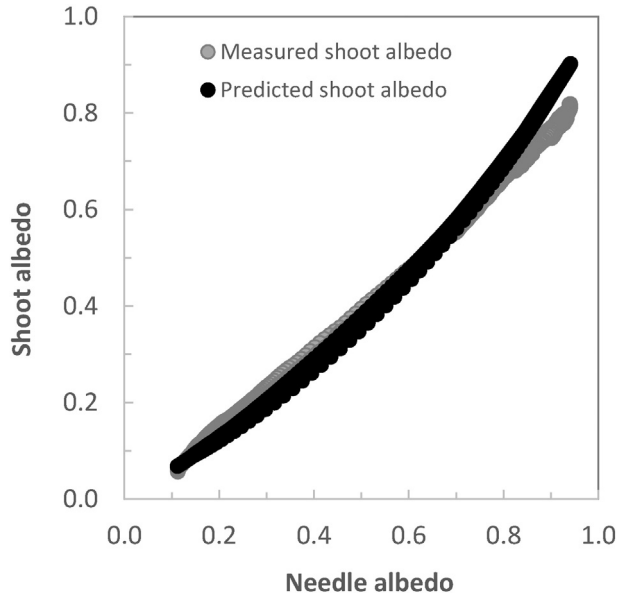

Fig. 4. The relationship between needle and shoot spectral albedos (400–1800 nm) averaged for ten Scots pine shoots. The needle albedos were measured, and the shoot albedos were both measured and predicted by STAR (which is linearly related to p) (see Section 2.4 and Eq. (16)).
The measurements and data are described in detail by Rautiainen et al. (2012).

can be scaled between needle and shoot levels using p. What still remains empirically unexplored, due to technical challenges in the measurement set-ups, is whether the same method could be used to scale between shoot and crown levels.

3. Simulation studies

3.1. Ray tracing to track collision and escape events

Tracking of individual photons inside a vegetation canopy, and thus directly determining the escape and recollision probabilities, is not possible. The closest alternative to measurement is Monte Carlo modelling using physically realistic representations of canopies. Such models sample the radiation field inside and above the canopy by tracing single photons drawn randomly from the incident radiation field. For the models used in the studies of photon recollision probability, a detailed 3D description of the canopy had been given as model input. As the photons are traced in the canopy, the fractions of photons which are scattered out after each scattering provide the recollision probabilities $p(1)$, $p(2)$, …, $p(i)$, …, where i is the scattering order. The recollision probability p is calculated as the average $p(i)$ weighted by the contribution of each order to the total canopy scattering.

The first simulation results were reported for a fractal-based three-dimensional barley canopy already in 1998 (Lewis & Disney, 1998). The geometric expansion (Eq. (1)) was found to be a useful way of representing canopy scattering as the rate of decay (i.e. photon recollision probability in modern terms) was found to be nearly constant for scattering orders of two and above. A more detailed simulation study in a canopy with randomly located, non-overlapping circular leaves with a spherical leaf angle distribution confirmed the monotonic increase of $p(i)$ with the scattering order i. The value of i after which $p(i)$ remained almost constant approximately equaled LAI (Lewis & Disney, 2007). Nevertheless, assuming a constant p for $i > 1$ gives reasonable accuracy for modelling total canopy scattering. The modelling exercises in these relatively simple canopies confirmed the quick convergence of $p(i)$ to p_{inf} mentioned above (Fig. 5).

Disney, Lewis, Quaife, and Nichol (2005) proposed an approximation of canopy reflectance where $p(1)$ is calculated separately from the recollision probability for $i > 1$, $p(i>1)$. Total canopy scattering now becomes

$$\omega_C(\lambda) = a\omega_L(\lambda) + \frac{b\omega_L^2(\lambda)}{1-p(i>1)\omega_L(\lambda)} \quad (20)$$

where a and b are the geometric (spectrally invariant) parts of the first- and multiple-order scattering, respectively. Disney et al. (2005) also suggest a simpler, but less accurate approximation assuming $b = a^2$. Later, the second-order recollision probability has been found to be a good substitute for the average p (Mõttus, 2007) or even the diffuse limit p_{inf} (Huang et al., 2007; Lewis & Disney, 2007). The first-order recollision probability, on the other hand, is markedly smaller than both p and p_{inf}.

Disney et al. (2005) validated the suitability of Eq. (20) for approximating the reflectance of five Sitka spruce stands of various ages. The stand-level reflectance, assumed proportional to ω_C was measured with a helicopter-mounted spectroradiometer in the visible and near infrared spectral regions. Needle spectral albedo was sampled with a contact probe. Eq. (20) was found to fit the data extremely well ($R^2 > 0.997$) even assuming $b = a^2$.

The situation was found to be more complicated for highly structured needleleaf forest canopies (Disney & Lewis, 2007). In some dense and complex pine canopies, $p(i)$ did not reach the diffuse limit even at $i = 100$. The authors also noted a marked impact of non-green material, i.e. tree trunks, on the distribution of exiting photons with scattering order. While the p-theory (Eq. (4)) was still a good approximation of the relationship between needle and canopy scattering, the fitted p-value became decoupled from its physical interpretation.

3.2. Deriving relationships between p and canopy structure

Smolander and Stenberg (2005) calculated the average p values (p_{LC} and p_{CC}) for two model canopies of varying LAI: a 'leaf canopy' (LC) and a coniferous 'shoot canopy' (CC), which were composed of randomly distributed single leaves or coniferous shoots, respectively. In both canopies, values of p were estimated in two different ways, which turned out to be in close to perfect agreement. First, p was obtained by fitting

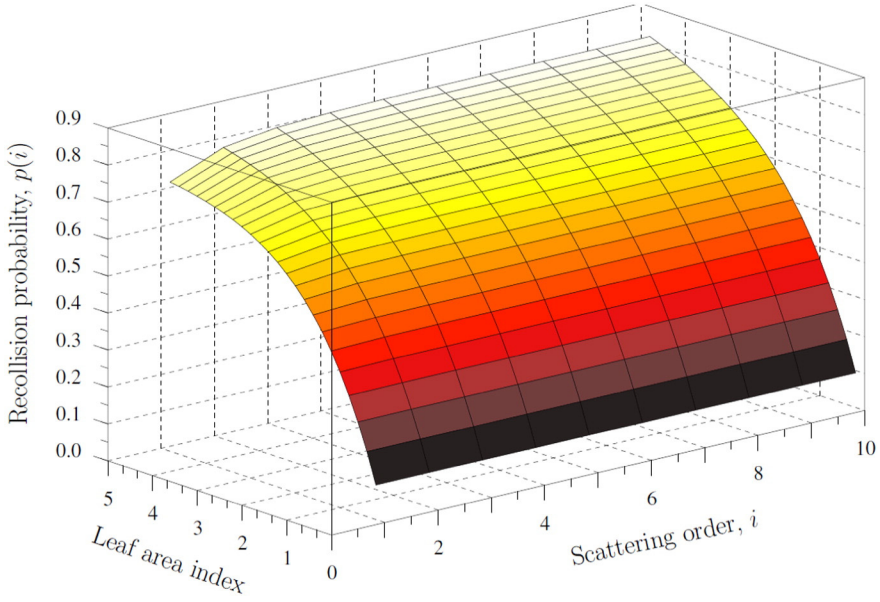

Fig. 5. Variation in p with scattering order for different values of LAI.
From Mõttus (2007).

Eq. (4) to simulated canopy scattering (ω_C) at different wavelengths (values of leaf albedo, ω_L). Secondly, p was calculated using the above described single photon ray tracing method with $\omega_L = 1$.

From simulations performed assuming a solar zenith angle (SZA) of 45°, a tight relationship of the form $p = a(1 - \exp(-b\text{LAI}))$ was found between p_{LC} and LAI for the leaf canopy. The dependence between p of the coniferous shoot canopy (p_{cc}) and LAI, in turn, was accurately predicted from the shoot level p value (p_{sh}) and p_{LC} of the leaf canopy with similar effective LAI (L_e) by the decomposition formula (see Eq. (14)):

$$p_{CC} = p_{sh} + (1-p_{sh})p_{LC}(L_e). \tag{21}$$

The effect on p_{LC} of different incidence angles of the incoming photons was studied separately. It was found that p_{LC} was practically insensitive to the solar zenith angle in the range commonly used in satellite remote sensing (less than 1.2% at solar zenith angles <50°). Finally, simulated values of the ratio of upward to total scattering (r_C/ω_C) at different wavelengths showed an increase with LAI and a slight decrease with increasing ω_L (as would be predicted by Eq. (11)). At similar values of LAI, the ratio r_C/ω_C was larger for the leaf canopy than for the shoot canopy.

Later, Stenberg (2007) applied Eq. (17) to estimate p of the same model canopies ('leaf canopy' and 'shoot canopy') as in Smolander and Stenberg (2005) and found very good agreement between the analytically derived and the Monte Carlo simulated values of p. The fit was the best at low to moderate values of LAI and, at similar LAI, was better for the shoot canopy than for the leaf canopy. This can be explained by that the assumption behind Eq. (17), that the points of interaction are evenly distributed over the total leaf (needle) area, is closer to the truth the more 'transparent' is the canopy, i.e. the smaller is the effective LAI (L_e).

Mõttus, Stenberg, and Rautiainen (2007) derived the relationships between p and LAI for forest stands of more complicated structures using simulations by the Kuusk–Nilson FRT model (Kuusk & Nilson, 2000) and assessed the effect on canopy structure on p by comparing the results to those obtained for 'structureless' (homogeneous) canopies of the same LAI by a two-stream model. Simulations by both models produced tight relationships between LAI and p but, as expected, for a fixed LAI p was larger when canopy structure was accounted for. More generally, results from the study confirmed that the concept of recollision probability is coherent with physically based canopy reflectance models.

The concept of spectral invariants was tested on multiple scales from within leaf to a horizontally homogeneous canopy by Lewis and Disney (2007). They demonstrated that the p-theory can very accurately approximate the leaf scattering computed with the widely-used PROSPECT model (Jacquemoud et al., 1996). Inside the leaf, the role of ω is taken by the exponent of the product of pigment concentration and its spectral absorption coefficient. The "within-leaf recollision probability" p_{leaf} (note that at within-leaf scale, no physical connection has been established between the collision events and p_{leaf}) was found to vary with the refractive index of the leaf wax layer between 0.60 and 0.73. For a wide range of leaf properties, the p-theory approximated PROSPECT with $R^2 > 0.9997$ and RMSE < 0.0042. Using the (de)composition formula, leaf- and canopy level p-values can be combined thus linking canopy spectral reflectance to the pigment concentration with a single parameter. Based on their results, Lewis and Disney (2007) concluded that "without knowledge of either p, or the leaf biochemical constituents, independent retrieval of either from total scattering measurements is not possible."

In a simulation study, Stenberg and Manninen (2015) used the approach proposed by Disney et al. (2005) to separate the first order and multiple order recollision probabilities and calculated canopy scattering by Eq. (20), where parameters a and b were derived as: $a = 1 - p(1)$ and $b = p(1)(1 - p)$. For the modelled canopies, the first order $p(1)$ was calculated analytically and the multiple order mean p was calculated using Eq. (17). Results confirmed that $p(1)$ indeed differs more from the mean p the denser is the canopy but that the difference decreases with clumping. In dense but clumped canopies, thus, the difference between $p(1)$ and mean p had only minor effect on total canopy scattering (ω_C). However, the reflectance ratio (r_C/ω_C) was found to decrease with clumping because it reduces the relative contribution of first order scattering (with higher reflectance ratio) to the total scattering.

4. Use of *p* in modelling canopy reflectance and radiation regime

4.1. Canopy BRF using PARAS model

A family of models, called 'PARAS', where canopy structure is parameterized purely based on the recollision probability, has been developed to simulate different components of the canopy radiation budget, e.g., canopy reflectance (BRF, albedo) and absorption (fPAR). The first version of the PARAS model was formulated for the canopy BRF by Rautiainen and Stenberg (2005) as:

$$\text{BRF} = cgf(\theta_1)\rho_G cgf(\theta_2) + f(\theta_1,\theta_2)i_0(\theta_2)\frac{\omega_L - p\omega_L}{1 - p\omega_L}. \tag{22}$$

Here, the assumption of 'black soil' was relaxed so that the contribution from photons arriving through gaps in the illumination direction (θ_2), reflected at the ground (ρ_G), and escaping through gaps in the view direction (θ_1) was added to the canopy-only reflectance. Multiple scattering between canopy and soil was not accounted for. The second term on the right hand of Eq. (22) is simply canopy scattering for the black soil problem (Eq. (2)) weighted by the function f, which describes the directional distribution of escaped photons normalized so that integrated over all view directions (Ω_1) it yields unity:

$$\frac{1}{\pi}\int_{4\pi} f(\theta_1,\theta_2)|\cos\theta_1|\mathrm{d}\Omega_1 = 1. \tag{23}$$

Integration over the upper hemisphere, in turn, gives the total upwards (or backwards) scattered fraction of the radiation intercepted by the canopy:

$$\frac{1}{\pi}\int_{2\pi^+} f(\theta_1,\theta_2)|\cos\theta_1|\mathrm{d}\Omega_1 = Q. \tag{24}$$

The incoming direction of radiation (θ_2) has an impact on the canopy interceptance (i_0), but its possible influence on p (through its effect on where the first interactions occur) is not explicitly taken into account in the model formulation. Originally, the value of p for input to the model (Eq. (22)) was calculated using the relationships between p and LAI for leaf and shoot canopies derived by Smolander and Stenberg (2005) in their simulation study. (Recall that in that study the dependence of p on the solar zenith angle was found to be insignificant.) In later applications of the PARAS models, Eq. (17) has generally been used to produce the input value of p. Note that using Eq. (17) for the estimation of p requires that the LAI is measured (or estimated) independent of the canopy diffuse interceptance (i_D), or alternatively, using some known or assumed value of the clumping index (Γ). Also, although the variation in f with view angle is represented in the model formulation, it has (so far) not been a subject of study in the applications. If the canopy reflectance is assumed to be Lambertian (i.e. f is constant), then it follows from Eq. (23) that $f(\theta_1,\theta_2) = Q$ for all view

directions. While the PARAS BRF model does not rely upon such a (false) assumption, in the first model applications the value of f for a nadir view ($\theta_1 = 0$) was approximated using simulated data on Q ($= r_C/\omega_C$) by Smolander and Stenberg (2005). The first analytical approach to separate canopy scattering into reflectance and transmittance, i.e. to estimate Q (Eq. (11)), was presented by Mõttus and Stenberg (2008). They also derived values of Q by simulation for a set of (measured) forest stands of varying LAI, and these simulation based dependencies of Q on LAI have later been used in the PARAS BRF model. Note that the reflectance ratio as predicted by Eq. (11) is not strictly spectrally invariant.

The model (Eq. (22)) was applied to show improved agreement between modelled and measured BRF for coniferous stands when within-shoot scattering accounted for (in calculating the p) (Rautiainen & Stenberg, 2005), and later Rautiainen et al. (2007) successfully applied the model to subarctic forests to demonstrate the role of understory vegetation in forming stand reflectance. Stenberg, Rautiainen, Manninen, Voipio, and Mõttus (2008) used the model to investigate which spectral vegetation indices would perform well in mapping LAI of boreal forests. More recently, the PARAS model has also been used to estimate chlorophyll content of spruce needles from CHRIS PROBA data (Yanez-Rausell et al., 2015).

4.2. Canopy albedo and absorption using PARAS model

Manninen and Stenberg (2009) extended the original PARAS model to include multiple scattering between canopy and ground with the motivation to make it applicable also in the case of a highly reflective background such as snow. They used it to simulate the effect of snow covered forest floor on the black- and white-sky albedos. Two components were thus added to the right hand side of Eq. (22): 1) photons first scattered downwards from the canopy, then reflected from the forest floor and transmitted without interaction through the canopy upwards, and 2) photons reflected from the forest floor and scattered upwards through the canopy. In addition, hemispherical integration over all view angles (for black-sky albedo) or integration over both incident and view angles (for white-sky albedo) was performed to convert BRF to black sky and white sky albedo, respectively. Simulation results showed that for snow covered forest floors the added multiple scattered component increased the total canopy albedo in NIR by up to 0.2 units. In summer conditions, on the other hand, the contribution to the albedo from the added components was negligible in the red band and not larger than about 0.05 in NIR. Evaluation of the albedo model against measured forest albedo data from the Arctic Research Centre of the Finnish Meteorological Institute (FMI-ARC) in Sodankylä (northern Finland) showed that it successfully simulated the main features of measured albedo values.

The PARAS albedo model developed later by Stenberg, Lukeš, Rautiainen, and Manninen (2013) is a simplified version of the Manninen and Stenberg (2009) model, but provides separately the three different components of the total radiation budget. The total canopy spectral absorption (A_C) and ground absorption (A_G) are defined as the fractions of the incoming photons at a specific wavelength which will finally be absorbed by the canopy or be transmitted to and absorbed by the ground. The spectral *albedo* (R_C), or the fraction of the incoming photons that escapes the canopy upwards, is then obtained as:

$$R_C(\lambda) = 1 - A_C(\lambda) - A_G(\lambda). \tag{25}$$

In the model two simplifying assumptions were made allowing A_C and A_G to be derived with help of geometric series. First, it was assumed that the fractions of backward scattering (Q) and forward scattering ($1 - Q$) do not depend on whether the canopy is irradiated from above or below. Secondly, the ground reflectance (ρ_G) was assumed to be purely Lambertian. (The first assumption was used also in the simulations by Manninen and Stenberg (2009), but the snow albedo was modelled as combination of completely forward/backward and Lambertian scattering.) The equations for canopy (A_c) and ground spectral absorption (A_G) are:

$$A_C(\lambda) = i_0\alpha_C(\lambda) + \frac{[t_0 + i_0(1-Q)\omega_C(\lambda)]\rho_G(\lambda)i_D\alpha_C(\lambda)}{1 - Q\omega_C(\lambda)i_D\rho_G(\lambda)} \tag{26}$$

and

$$A_G(\lambda) = [t_0 + i_0(1-Q)\omega_C(\lambda)](1-\rho_G(\lambda)) + \frac{[t_0 + i_0(1-Q)\omega_C(\lambda)]\rho_G(\lambda)i_D Q\omega_C(\lambda)(1-\rho_G(\lambda))}{1 - Q\omega_C(\lambda)i_D\rho_G(\lambda)}. \tag{27}$$

Derivation of the model actually followed the same principle as presented in Knyazikhin et al. (1998) and further outlined in Wang et al. (2003) so that, in Eqs. (26) and (27), the first term represents the solution to the 'black soil problem', and the second term is the additional contribution due to interactions between the canopy and underlying surface. Note that Eqs. (26) and (27) above are formulated for radiation incident from a specific angle (e.g. the sun zenith angle), at which t_0 and i_0 correspond to the uncollided transmittance and the interceptance, respectively, but they can easily be applied also to diffuse radiation by integrating over the respective distribution of sky radiation.

The model by Stenberg et al. (2013) was used to produce the black-sky albedos of 644 boreal forest stands in Finland composed of Scots pine, Norway spruce and Silver birch. Results were compared to those simulated using the detailed reflectance and transmittance model (FRT) by Kuusk and Nilson (2000) with input from an extensive forest inventory database and locally measured spectral data on leaf and needle albedos, and ground (understory) reflectance. Results showed that the albedos of the stands simulated by PARAS and FRT had approximately the same range and strong positive correlation. Inclusion of branch area index (BAI) in calculating the p value (by adding the BAI to LAI in Eq. (17)) further improved the agreement, so that the overall root mean square error (RMSE) between the PARAS and FRT simulated albedos was 0.011, and the ranges of albedo values were almost identical. It was concluded that although complex 3D models using detailed input on the structure of stands may be required to realistically describe the angular variation in reflectance (BRDF) for a forest, the spectrally invariant parameters are an efficient means to couple forest canopy structure and albedo.

The model was also adapted for calculating the fraction of absorbed photosynthetically active radiation (fPAR) (canopy spectral absorptance by Eq. (26) integrated over PAR wavelengths) of a forest by Majasalmi et al. (2014) and Majasalmi, Rautiainen and Stenberg (2015). First, the simulated fPAR values were validated against measurements in differently structured boreal coniferous and broadleaved stands, which was followed by simulations of diurnal and seasonal fPAR dynamics. Overall, the model performed well in fPAR calculations: the RMSE between the simulated and measured fPAR values ranged from 0.03 to 0.06, depending on the time of the day and sky conditions. As ground reference measurements of fPAR are tedious and slow, a physically-based model could be used to produce the in situ estimates of fPAR for validating satellite-based products for a larger area. For boreal forests, Majasalmi, Rautiainen, Stenberg and Manninen (2015) explored the potential of using this fPAR model to produce the ground reference values for the validation of MODIS (MOD15A2) and GEOV1 fPAR (g2_BIOPAR_FAPAR) products. Application of the model also allowed separating the contributions of understory and tree layer fPAR, and analysing their role in the performance of the satellite-based products. Thus, Majasalmi, Rautiainen, Stenberg and Manninen (2015) were able to report, for example, that the MODIS fPAR represented the fPAR of the tree canopy layer whereas the GEOV1 fPAR product was more similar to the total fPAR of both the understory and tree layers. Similarly for agricultural areas, Fan, Liu, and Xiru (2014) also applied a photon recollision based model to generate fPAR values comparable to

satellite products (MOD15A2). These studies on forest albedo, fPAR and satellite product validation are examples of how the *p*-theory can be used as a tool to estimate canopy radiation budget in different types of vegetation canopies. A strength of the *p*-theory based model approach is its simple parameterization, as described in the following section.

4.3. Measurements of PARAS model input parameters

A key property of any canopy radiation model is that the input parameters have a physical interpretation and can be measured in the field or in a laboratory. The PARAS family of models is based on a small, measurable set of input parameters describing the structure and optical properties of forest elements. Canopy structure is mainly parameterized through the recollision probability p which, knowing the clumping index (Γ), can be calculated by Eq. (17) or (19) using the effective LAI (L_e) and canopy diffuse interceptance (i_D) obtained from measurements with, for example, the LAI-2000 Plant Canopy Instrument (Li-Cor Inc.) or a camera with a hemispherical lens (Fig. 6A). The clumping index is not a directly measurable parameter, but the shoot level clumping can be estimated by STAR (Fig. 6B). In addition to p, the structural input data required by the model are canopy gap fractions to estimate bidirectional gap probabilities of the forest floor (or understory layer). These canopy gap fractions can also be obtained from LAI-2000 data or hemispherical photographs of the canopies. Besides the abovementioned canopy structural variables, the model requires spectral data on the foliage elements and forest floor. The spectral albedos of leaves or needles can be measured in laboratory (or field conditions) (e.g. Lukeš, Stenberg, Rautiainen, Mõttus, & Vanhatalo, 2013), and the BRF or BRDF of forest floor vegetation in the field (e.g. Peltoniemi et al., 2005; Rautiainen et al., 2011). The PARAS models do not require expert guesses for input parameters as they can be measured (Fig. 6).

5. Applications in monitoring vegetation

Operational monitoring of vegetation, such as producing LAI maps for extensive areas, requires an algorithm which is based on a simple set of input parameters. Therefore, the concept of spectral invariants (or photon recollision probability) has originally been applied in LAI/

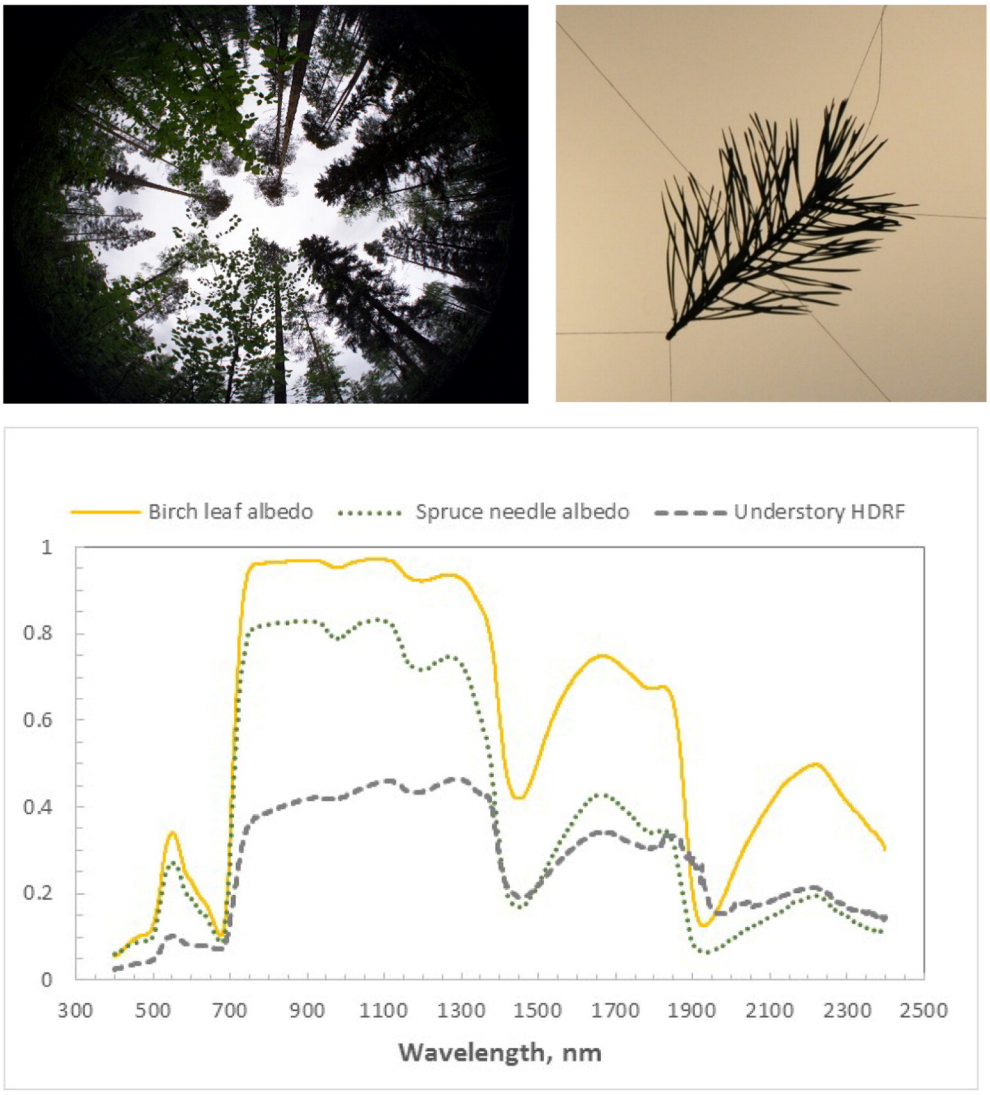

Fig. 6. Measurements of input variables needed for the PARAS models. A. Data on canopy gap fractions and diffuse interceptance, and leaf area index which are needed to calculate p (see Eq. (17)) and the contribution of understory (see Eq. (22)) can directly be obtained from LAI-2000 Plant Canopy Analyzer output files or hemispherical photographs. B. STAR values of coniferous shoots can be measured using photographic methods. STAR is linearly related to p (see Section 2.4). C. Data on the spectral properties of tree leaves and needles, and understory vegetation are also needed as input and can be measured with spectroradiometers. These examples are based on data measured in Hyytiälä, Finland.

fPAR retrieval algorithms utilizing MODIS (Knyazikhin et al., 1998; Shabanov et al., 2003) and Landsat or SPOT (Ganguly et al., 2008a,b, 2012; Heiskanen, Rautiainen, Korhonen, Mõttus, & Stenberg, 2011) data. In addition to LAI and fPAR, spectral invariants have been linked to other variables describing canopy structure. For example, Schull et al. (2007) showed that the spectral invariants theory can be applied to retrieve height of canopies from airborne multiangular remote sensing data. Furthermore, Schull et al. (2011) showed that, if leaf single scattering albedo is known, p (and related information on canopy structure) can be retrieved from hyperspectral remote sensing data using a simple linear regression method. Lukeš, Rautiainen, Stenberg, and Malenovský (2011) evaluated independently Schull's methods for retrieving the recollision probability and escape factor from multiangular CHRIS PROBA data for a spruce site. They were able to reproduce Schull et al.'s (2007) findings using completely different data sets from another biome, and concluded e.g. that in coniferous canopies the spectral invariants theory performs well in the near infrared spectral range.

The most recent development in the spectral invariants theory has been the introduction of the directional area scattering factor (DASF, Knyazikhin et al., 2012), formulated as an extension to the work by Schull et al. (2007, 2011). DASF is an estimate of the fraction of leaf area in a canopy that is visible from outside the canopy in a given direction. Formally, it is defined as the canopy BRF if the foliage does not absorb radiation ($\omega_L = 1$). For a canopy bounded underneath by black soil, DASF is identical to the product of i_0 and f (Eq. (22)), and the ratio of BRF to DASF equals the canopy scattering coefficient (ω_C). For dense canopies ($i_0 \sim 1$), furthermore, DASF approximately coincides with the function f which describes the proportion of photons scattered from a canopy into a particular direction (the view direction). In other words, DASF varies with view direction and is a function of geometric properties of the tree canopy (e.g. foliage grouping, crown shape, spatial distribution of trees). For closed canopies (i.e. canopies where the influence of forest floor is negligible), DASF can be directly estimated from air or satellite borne BRF data in the spectral range between 710 nm and 790 nm (Knyazikhin et al., 2012).

By now, the concept of DASF has been shown useful in mapping vegetation structure in both forest and agricultural vegetation. In a study based on reflectance data from CHRIS PROBA, Latorre-Carmona et al. (2014) reported that the DASF is directly related to crop type. Vanhatalo, Rautiainen, and Stenberg (2014), on the other hand, reported that DASF shows good potential in monitoring the broadleaf fraction of boreal forests when using hyperspectral satellite data (e.g. EO-1 Hyperion images). Furthermore, Stenberg and Manninen (2015) suggested that this might be linked to different degrees of clumping in broadleaved vs coniferous stands based on their result that, for a nadir view, DASF increases with the clumping index. The validity of the applications described above is, however, confined to dense canopies due to the underlying assumption of a vegetation bounded underneath by a non-reflecting black surface as shown in an empirical study by Vanhatalo et al. (2014). Alternatively, methods for removing the impact of background (e.g. forest floor) on total forest (or other vegetation canopy) reflectance need to be applied in sparse canopies.

Currently, the team led by Prof. Yuri Knyazikhin (Boston University) applies DASF in the development of new algorithms for retrieving global data records of fraction of photosynthetically active radiation absorbed by green leaves, leaf area and its sunlit fraction from Deep Space Climate Observatory (DSCOVR, launched in 2015) data. Future applications can also be expected to arise from the applications of spectral invariants in describing the radiation budget of vegetation in global radiation balance or climate models.

Acknowledgments

This study was partly funded by the Academy of Finland (grants 266152, 286390).

Appendix A

Canopy diffuse interceptance, or the interceptance of *isotropic* radiation, is obtained as:

$$i_D = 2\int_0^{\frac{\pi}{2}} [1 - t_0(\theta)] \cos\theta \sin\theta d\theta. \quad (A1)$$

The uncollided transmittance (or gap probability), t_0, can be expressed by the Beer's law equation as a function LAI, the mean projection of unit foliage area (G) and a clumping index (Γ) as (Nilson, 1971):

$$t_0(\theta) = \exp[-\Gamma(\theta) G(\theta) \mathrm{LAI} / \cos\theta]. \quad (A2)$$

Eq. (A2) with $\Gamma(\theta) = 1$ (for all θ) applies to a Poisson canopy composed of randomly distributed leaves and the clumping index consequently is defined as the parameter needed to correct for deviations in the relationship between t_0 and LAI caused by a non-random leaf dispersion.

As $\Gamma(\theta)$ varies with the direction, the total hemispherical clumping index Γ is defined as:

$$\Gamma = 2\int_0^{\pi/2} \Gamma(\theta) G(\theta) \sin\theta d\theta. \quad (A3)$$

With the clumping index defined by Eq. (A3), the effective leaf area index (L_e) now becomes equal to the product of and the true leaf area index:

$$L_e = -2\int_0^{\frac{\pi}{2}} \ln[t_0(\theta)] \cos\theta \sin\theta d\theta = 2\int_0^{\frac{\pi}{2}} \Gamma(\theta) G(\theta) L \sin\theta d\theta = \Gamma L. \quad (A4)$$

References

Disney, M., & Lewis, P. (2007). Spectral invariant behaviour of a complex 3D forest canopy. In M. Schaepman, S. Liang, N. Groot, & M. Kneubühler (Eds.), *Proc. 10th international symposium on physical measurements and signatures in remote sensing (ISPMSRS'07). The international archives of the ISPRS, Vol. XXXVI.* (pp. 102–107).

Disney, M., Lewis, P. T., Quaife, T., & Nichol, C. (2005). A spectral invariant approach to modelling canopy and leaf scattering. *Proc. 9th international symposium on physical measurements and signatures in remote sensing, Beijing, China, 17–19 Oct 2005* (pp. 318–320).

Fan, W., Liu, Y., & Xiru, X. (2014). A new FAPAR analytical model based on the law of energy conservation: A case study in China. *IEEE Journal of Selected Topics in Applied Earth Observations and Remote Sensing, 7*(9), 3945–3955.

Ganguly, S., Nemani, R., Zhang, G., Hashimoto, H., Milesi, C., Michaelis, A., ... Myneni, R. (2012). Generating global Leaf Area Index from Landsat: Algorithm formulation and demonstration. *Remote Sensing of Environment, 122*, 185–202.

Ganguly, S., Schull, M., Samanta, A., Shabanov, N., Milesi, C., Nemani, R., ... Myneni, R. (2008a). Generating vegetation leaf area index earth system data record from multiple sensors. Part 1: Theory. *Remote Sensing of Environment, 112*(12), 4333–4343.

Ganguly, S., Schull, M., Samanta, A., Shabanov, N., Milesi, C., Nemani, R., ... Myneni, R. (2008b). Generating vegetation leaf area index Earth system data record from multiple sensors. Part 2: Implementation, analysis and validation. *Remote Sensing of Environment, 112*(12), 4318–4332.

Heiskanen, J., Rautiainen, M., Korhonen, L., Mõttus, M., & Stenberg, P. (2011). Retrieval of boreal forest LAI using a forest reflectance model and empirical regressions. *International Journal of Applied Earth Observation and Geoinformation, 13*, 595–606.

Huang, D., Knyazikhin, Y., Dickinson, R. E., Rautiainen, M., Stenberg, P., Disney, M., ... Myneni, R. B. (2007). Canopy spectral invariants for remote sensing and model applications. *Remote Sensing of Environment, 106*, 106–122.

Jacquemoud, S., Ustin, S. L., Verdebout, J., Schmuck, G., Andreoli, G., & Hosgood, B. (1996). Estimating leaf biochemistry using the PROSPECT leaf optical properties model. *Remote Sensing of Environment, 56*, 194–202.

Knyazikhin, J., Martonchik, J. V., Myneni, R. B., Diner, D. J., & Running, S. W. (1998). Synergistic algorithm for estimating vegetation canopy leaf area index and fraction of absorbed photosynthetically active radiation from MODIS and MISR data. *Journal of Geophysical Research, 103*(D24), 32,257–32,275.

Knyazikhin, Y., Schull, M. A., Liang, X., Myneni, R. B., & Samanta, A. (2011). Canopy spectral invariants. Part 1: A new concept in remote sensing. *Journal of Quantitative Spectroscopy & Radiative Transfer, 112*, 727–735.

Knyazikhin, Y., Schull, M. A., Stenberg, P., Mõttus, M., Rautiainen, M., Yang, Y., ... Myneni, R. B. (2012). Hyperspectral remote sensing of foliar nitrogen content. *PNAS*. http://dx.doi.org/10.1073/pnas.1210196109.

Kuusk, A., & Nilson, T. (2000). A directional multispectral forest reflectance model. *Remote Sensing of Environment*, *72*, 244–252.
Latorre-Carmona, et al. (2014). On hyperspectral remote sensing of leaf biophysical constituents: Decoupling vegetation structure and leaf optics using CHRIS-PROBA data over crops in barrax. *IEEE Geoscience and Remote Sensing Letters*, *11*(9), 1579–1583.
Lewis, P., & Disney, M. (1998). *The Botanical Plant Modelling System (BPMS): A case study of multiple scattering in a barley canopy. Proc. geoscience and remote sensing symposium (IGARSS '98), Vol. 3.* (pp. 1481–1483), 1481–1483.
Lewis, P., & Disney, M. (2007). Spectral invariants and scattering across multiple scales from within-leaf to canopy. *Remote Sensing of Environment*, *109*, 196–206.
Lukeš, P., Rautiainen, M., Stenberg, P., & Malenovský, Z. (2011). Empirical test of the spectral invariants theory using imaging spectroscopy data from a coniferous forest. *International Journal of Applied Earth Observation and Geoinformation*, *13*, 668–675.
Lukeš, P., Stenberg, P., Rautiainen, M., Mõttus, M., & Vanhatalo, K. (2013). Optical properties of leaves and needles for boreal tree species in Europe. *Remote Sensing Letters*, *4*(7), 667–676.
Majasalmi, T., Rautiainen, M., & Stenberg, P. (2015a). Corrigendum to "modeled and measured fPAR in a boreal forest: Validation and application of a new model". *Agricultural and Forest Meteorology*, *204*, 46–47.
Majasalmi, T., Rautiainen, M., Stenberg, P., & Manninen, T. (2015b). Validation of MODIS and GEOV1 fPAR products in a boreal forest site in Finland. *Remote Sensing*, *7*(2), 1359–1379.
Majasalmi, T., Rautiainen, M., & Stenberg, P. (2014). Modeled and measured fPAR in a boreal forest: Validation and application of a new model. *Agricultural and Forest Meteorology*, *189*, 118–124.
Manninen, T., & Stenberg, P. (2009). Simulation of the effect of snow covered forest floor on the total forest albedo. *Agricultural and Forest Meteorology*, *149*, 303–319.
Mõttus, M. (2007). Photon recollision probability in discrete crown canopies. *Remote Sensing of Environment*, *110*, 176–185.
Mõttus, M. (2010). The physics of spectral invariants. *Proceedings of the 2nd Workshop on Hyperspectral Image and Signal Processing: Evolution in Remote Sensing (WHISPERS), Reykjavik, Iceland, June 14–16, 2010*. http://dx.doi.org/10.1109/WHISPERS.2010.5594910 (4 pp.).
Mõttus, M., & Rautiainen, M. (2013). Scaling PRI between coniferous canopy structures. *IEEE Journal of Selected Topics in Applied Earth Observations and Remote Sensing*, *6*(2), 708–714.
Mõttus, M., & Stenberg, P. (2008). A simple parameterization of canopy reflectance using photon recollision probability. *Remote Sensing of Environment*, *112*, 1545–1551.
Mõttus, M., Stenberg, P., & Rautiainen, M. (2007). Photon recollision probability in heterogeneous forest canopies: Compatibility with a hybrid GO model. *Journal of Geophysical Research — Atmospheres*, *112*, D103104. http://dx.doi.org/10.1029/2006JD007445.
Nilson, T. (1971). A theoretical analysis of the frequency of gaps in plant stands. *Agricultural Meteorology*, *8*, 25–38.
Oker-Blom, P., & Smolander, H. (1988). The ratio of shoot silhouette area to total needle area in Scots pine. *Forest Science*, *34*, 894–906.
Panferov, O., Knyazikhin, Y., Myneni, R. B., Szarzynski, J. E., Schnitzler, K. G., & Gravenhorst, G. (2001). The role of canopy structure in the spectral variation of transmission and absorption of solar radiation in vegetation canopies. *IEEE Transactions on Geoscience and Remote Sensing*, *39*, 241–253.
Peltoniemi, J. I., Kaasalainen, S., Näränen, J., Rautiainen, M., Stenberg, P., Smolander, H., ... Voipio, P. (2005). BRDF measurement of understorey vegetation in pine forests: Dwarf shrubs, lichen and moss. *Remote Sensing of Environment*, *94*, 343–354.
Rautiainen, M., & Stenberg, P. (2005). Application of photon recollision probability in coniferous canopy reflectance simulations. *Remote Sensing of Environment*, *96*, 98–107.
Rautiainen, M., Mõttus, M., Heiskanen, J., Akujärvi, A., Majasalmi, T., & Stenberg, P. (2011). Seasonal reflectance dynamics of common understory types in a Northern European boreal forest. *Remote Sensing of Environment*, *115*, 3020–3028.
Rautiainen, M., Mõttus, M., & Stenberg, P. (2009). On the relationship of canopy LAI and photon recollision probability in boreal forests. *Remote Sensing of Environment*, *113*, 458–461.
Rautiainen, M., Mõttus, M., Yanez-Rausell, L., Homolova, L., Malenovsky, Z., & Schaepman, M. E. (2012). A note on upscaling coniferous needle spectra to shoot spectral albedo. *Remote Sensing of Environment*, *117*, 469–474.
Rautiainen, M., Suomalainen, J., Mõttus, M., Stenberg, P., Voipio, P., Peltoniemi, J., & Manninen, T. (2007). Coupling forest canopy and understory reflectance in the Arctic latitudes of Finland. *Remote Sensing of Environment*, *110*, 332–343.
Ross, J. (1981). *The radiation regime and architecture of plant stands.* The Hague: Dr. W. Junk Publishers (391 pp.).
Schull, M. A., Ganguly, S., Samanta, A., Huang, D., Shabanov, N. V., Jenkins, J. P., ... Knyazikhin, Y. (2007). Physical interpretation of the correlation between multi-angle spectral data and canopy height. *Geophysical Research Letters*, *34*(18), L18405.
Schull, M. A., Knyazikhin, Y., Xu, L., Samanta, A., Carmona, P. L., Lepine, L., ... Myneni, R. B. (2011). Canopy spectral invariants. Part 2: Application to classification of forest types from hyperspectral data. *Journal of Quantitative Spectroscopy & Radiative Transfer*, *112*, 727–735.
Shabanov, et al. (2003). Effect of foliage spatial heterogeneity in the MODIS LAI and FPAR algorithm over broadleaf forests. *Remote Sensing of Environment*, *85*(4), 410–423.
Smolander, S., & Stenberg, P. (2003). A method to account for shoot scale clumping in coniferous canopy reflectance models. *Remote Sensing of Environment*, *88*, 363–373.
Smolander, S., & Stenberg, P. (2005). Simple parameterizations of the radiation budget of uniform broadleaved and coniferous canopies. *Remote Sensing of Environment*, *94*, 355–363.
Stenberg, P. (1996). Correcting LAI-2000 estimates for the clumping of needles in shoots of conifers. *Agricultural and Forest Meteorology*, *79*, 1–8.
Stenberg, P. (2007). Simple analytical formula for calculating average photon recollision probability in vegetation canopies. *Remote Sensing of Environment*, *109*, 221–224.
Stenberg, P., & Manninen, T. (2015). Effect of clumping on canopy scattering and its directional properties: A model simulation using spectral invariants. *International Journal of Remote Sensing*. http://dx.doi.org/10.1080/01431161.2015.1049383.
Stenberg, P., Lukeš, P., Rautiainen, M., & Manninen, T. (2013). A new approach for simulating forest albedo based on spectral invariants. *Remote Sensing of Environment*, *137*, 12–16.
Stenberg, P., Rautiainen, M., Manninen, T., Voipio, P., & Mõttus, M. (2008). Boreal forest leaf area index from optical satellite images: Model simulations and empirical analyses using data from central Finland. *Boreal Environment Research*, *13*, 433–443.
Vanhatalo, K. M., Rautiainen, M., & Stenberg, P. (2014). Monitoring the broadleaf fraction and canopy cover of boreal forests using spectral invariants. *Journal of Quantitative Spectroscopy and Radiative Transfer*. http://dx.doi.org/10.1016/j.jqsrt.2013.09.011.
Wang, Y., Buermann, W., Stenberg, P., Smolander, H., Häme, T., Tian, Y., ... Myneni, R. B. (2003). A new parameterization of canopy spectral response to incident solar radiation: Case study with hyperspectral data from pine dominant forest. *Remote Sensing of Environment*, *85*(3), 304–315.
Yanez-Rausell, L., Malenovsky, Z., Rautiainen, M., Clevers, J., Lukeš, P., Hanuš, J., & Schaepman, M. (2015). Estimation of spruce needle-leaf chlorophyll content based on DART and PARAS canopy reflectance models. *Journal of Selected Topics in Applied Earth Observations and Remote Sensing*. http://dx.doi.org/10.1109/JSTARS.2015.2400418.

remote sensing

MDPI

Review

An Interplay between Photons, Canopy Structure, and Recollision Probability: A Review of the Spectral Invariants Theory of 3D Canopy Radiative Transfer Processes

Weile Wang [1,2,*], Ramakrishna Nemani [1], Hirofumi Hashimoto [1,2], Sangram Ganguly [1,3], Dong Huang [4], Yuri Knyazikhin [5], Ranga Myneni [5] and Govindasamy Bala [6]

1 NASA Ames Research Center, Moffett Field, CA 94035, USA; rama.nemani@nasa.gov (R.N.); hirofumi.hashimoto@gmail.com (H.H.); sangram.ganguly@gmail.com (S.G.)
2 School of Natural Sciences, California State University Monterey Bay, Seaside, CA 93955, USA
3 Bay Area Environmental Research Institute, Moffett Field, CA 94035, USA
4 NASA Goddard Space Flight Center, Greenbelt, MD 20771, USA; hdtown@gmail.com
5 Department of Earth and Environment, Boston University, Boston, MA 02215, USA; jknjazi@bu.edu (Y.K.); rmyneni@bu.edu (R.M.)
6 Center for Atmospheric and Oceanic Sciences, Indian Institute of Science, Bangalore 560012, India; bala.gov@gmail.com
* Correspondence: weile.wang@nasa.gov; Tel.: +1-650-604-3916

Received: 1 October 2018; Accepted: 12 November 2018; Published: 14 November 2018

Abstract: Earth observations collected by remote sensors provide unique information to our ever-growing knowledge of the terrestrial biosphere. Yet, retrieving information from remote sensing data requires sophisticated processing and demands a better understanding of the underlying physics. This paper reviews research efforts that lead to the developments of the stochastic radiative transfer equation (RTE) and the spectral invariants theory. The former simplifies the characteristics of canopy structures with a pair-correlation function so that the 3D information can be succinctly packed into a 1D equation. The latter indicates that the interactions between photons and canopy elements converge to certain invariant patterns quantifiable by a few wavelength independent parameters, which satisfy the law of energy conservation. By revealing the connections between plant structural characteristics and photon recollision probability, these developments significantly advance our understanding of the transportation of radiation within vegetation canopies. They enable a novel physically-based algorithm to simulate the "hot-spot" phenomenon of canopy bidirectional reflectance while conserving energy, a challenge known to the classic radiative transfer models. Therefore, these theoretical developments have a far-reaching influence in optical remote sensing of the biosphere.

Keywords: vegetation remote sensing; stochastic radiative transfer equation; spectral invariants theory

1. Introduction

The past a few decades have seen rapid development in scientific research and applications that monitor and/or simulate terrestrial ecosystems with the help of remote sensing data [1]. Thanks to advances in technology, we have sensors that operate across a broad spectral range, at high spatial, temporal, and spectral resolutions, and with passive or active modes. For instance, on sun-synchronous orbits the classic MODIS (Moderate Resolution Imaging Spectroradiometer) and SUOMI NPP (National Polar-Orbiting Partnership) VIIRS (Visible Infrared Imaging Radiometer Suite) are now joined by

Landsat 8/OLI (Operational Land Imager) [2,3], Copernicus Sentinel-2 [4], and JPSS (Joint Polar Satellite System) VIIRS [5]. On geostationary orbits we now have advanced multi-band imagers on Himawari-8/9 [6], GOES-16/17 [7,8], FengYun-4 [9] and the forthcoming sensors from Korea Meteorological Administration and European Organization for the Exploitation of Meteorological Satellites (EUMETSAT). On the International Space Station there is ECOSTRESS (Ecosystem Spaceborne Thermal Radiometer Experiment on Space Station), which will be soon joined by GEDI (Global Ecosystem Dynamics Investigation) [10]. A plethora of remote sensing products have been derived that reflect various characteristics of the terrestrial biosphere, including vegetation spectral indices, land cover types, canopy structural parameters, and many others. As remote sensing data uniquely provide consistent coverage over large spatial scales, it is rare nowadays that a global change study does not use such information.

Remote sensing data are not uncertainty-free but come with caveats. In optical remote sensing, for example, photons that reach the sensor have gone through complicated interactions with the atmosphere-vegetation-soil medium [11]. A series of processing must be conducted to calibrate and correct the top-of-atmosphere signals before information about the surface can be extracted from them. As remote sensors cannot directly measure the surface biophysical characteristics of interest, models are used to transform the measurements into estimates of the desirable vegetation canopy variables (e.g., Leaf Area Index), a process methodologically called "inversion." The inverse problems encountered in remote sensing are often under-determined and "ill-posed" [12], thus *a priori* information, additional constraints on potential solution space, and regularization techniques are often applied to make the problem solvable [13–17]. Given these challenges, a better understanding of the methodological backgrounds of remote sensing products can be beneficial for users of these datasets.

Interactions between photons and the atmosphere-vegetation-soil medium are succinctly quantified by the radiative transfer equation (RTE) and the associated boundary conditions [18]. The theory of radiative transfer was originally developed to study the scattering and absorption of sunlight in the atmosphere and later to simulate the transport of neutrons in nuclear reactors [19]. The theory was applied to model the radiation regime in vegetation canopy in the second half of the last century [20–22]. A range of models have been developed to describe the radiation regime in vegetation canopies as well as their interactions with the atmosphere and the soil. Some of the representative models, for instance, include Raytran [23], DART (Discrete Anisotropic Radiative Transfer) [24,25], SAIL (Scattering by Arbitrary Inclined Leaves) [26–28], PROSPECT [29], GORT (Geometric Optical-Radiative Transfer) [30,31], and PARAS [32]. A recent review of the canopy radiative transfer models can be found in Reference [18].

Compared with turbid media or nuclear reactors, vegetation canopy has its own structural and optical characteristics. On one hand, leaves have finite sizes and therefore cast shadows [33], which violates the assumptions of Beer's law [34,35]. For instance, the mutual shadowing effects of the canopy elements are mainly responsive for a sharp peak of the canopy reflectance in the retro-illumination direction. This phenomenon is often called the "hot-spot" effect, which is difficult to simulate with the classic RTE [33,36]. On the other side, the sizes of leaves (and twigs, branches, etc.) are often much larger than the spectral wavelengths considered in optical remote sensing. The total extinction coefficient (or cross-section) of photons in vegetation canopies is thus determined by the structural distribution of the leaves (and other phytoelements) rather than the wavelengths of photons [37]. Such characteristics of the vegetation medium present both challenges and opportunities to research efforts on the radiative transfer theory in vegetation canopies.

This paper intends to contribute a review of the theoretical advancements in modeling radiative transfer processes in 3D vegetation canopies. It particularly focuses on the developments of the stochastic radiative equation and the spectral invariant theory, which have been widely applied in retrieving vegetation structural information from remote sensors like MODIS and MISR (Multi-Angle Imaging Spectroradiometer) to the recent EPIC (Earth Polychromatic Imaging Camera) on the DSCOVR (Deep Space Climate Observatory) platform and the latest geostationary sensors like AHI (Advanced

Himawari Imager; on Himawari-8/9) and ABI (Advanced Baseline Imager; on GOES-16/17). However, a detailed account of such theoretical progresses is somewhat scarce in recent review papers [38–45] or textbooks [46] on remote sensing sciences and applications, which becomes a main motivation for this paper.

A question may rise: Why should we care so much about the theoretical properties of the radiative transfer processes in a time of big data, artificial intelligence and machine learning? It is true that in general the RTE has to be solved numerically [47]. In many applications we rely on statistical or empirical methods to solve the problem at hand [43]. Artificial intelligence and machine learning tools have also been introduced into remote sensing applications since their early stages and are gaining increasing popularity with rapid developments in the technology [48]. However, as mentioned earlier, the task of remote sensing is essentially ill-posed. The solution to the inverse problem often is not unique [43] and may not even be physical [35]. For instance, though the spectroscopy of a single leaf may be accurately measured in a laboratory, those measured for a forest stand by remote sensors convolute signals from the phytoelements (e.g., leaves, twigs, branches, trunks), the land surface, the atmosphere in between, as well as the interactions among them [22]. It is far from straightforward to establish a robust quantitative link between satellite measurements and leaf-level biogeochemical or biogeophysical traits. Without a clear understanding of the underlying processes, we may misinterpret empirically identified correlations from the data [49]. Furthermore, physically-based radiative transfer models (RTM) usually assume many parameters, which make them difficult to invert in practice [43]. The success of an RTM in remote sensing applications thus requires a balance between the simplicity of the model formulation and the fidelity of physics it preserves. Such a task can only be achieved with a deep understanding of the radiative transfer processes. As we will discuss later, the stochastic RTE and the spectral invariant theory represent elegant advancements with this modeling aspect regarded.

The rest of the paper is organized as follows. We begin by introducing the radiative transfer equation formulated for 3D vegetation canopies. We then focus on four particular topics in the main text, including the decomposition of RTE into the black-soil ("BS") and the soil ("S") problems, the development of the stochastic RTE that efficiently packs 3D canopy features into a 1D form, the spectral invariants theory that links the solutions of the RTE at different wavelengths by a few key canopy structural parameters, and the latest effort to address the "hot-spot" problem in vegetation remote sensing. We conclude the paper with a brief summary of the key ideas reviewed in these topics.

We would like to emphasize that, although the concepts of the spectral invariants and stochastic canopy geometrical properties may appear abstract, they have concrete physical interpretations and are measurable from ground and remote observations. Additionally, the basic ideas behind these theoretical developments are actually simple. Their derivations repeatedly make use of the ideas of decomposition and superposition, convergence and invariants, and the law of energy conservation. Therefore, we invite the readers to pay more attention to these ideas rather than the mathematical details of the theory, if the latter appears to be a bit complicated at the first look.

2. Radiative Transfer Equation for Vegetation Canopy

The classic RTE theory assumes that the radiative transfer properties of a vegetation canopy are largely determined by how the leaves are distributed in space, how they are oriented, and the fashions in which photons interact with the leaves [11,22,37,50]. These three aspects are mathematically described by the leaf area density distribution function $u_L(x)$, the leaf normal distribution function $g_L(x, \Omega_L)/2\pi$, and the leaf element scattering phase function $\gamma_L(\lambda, x, \Omega \to \Omega\prime, \Omega_L)$, respectively (Figure 1). Here, Ω_L represents the direction of the leaf normal, Ω is the incident direction, and $\Omega\prime$ is the direction in which photons are scattered into. Note that the scattering phase function γ_L explicitly depends on both Ω and $\Omega\prime$ but not only the scattering angle $\cos^{-1}\left(\Omega \cdot \Omega^{-1}\right)$, which is a key difference between vegetation canopies and gaseous media [37].

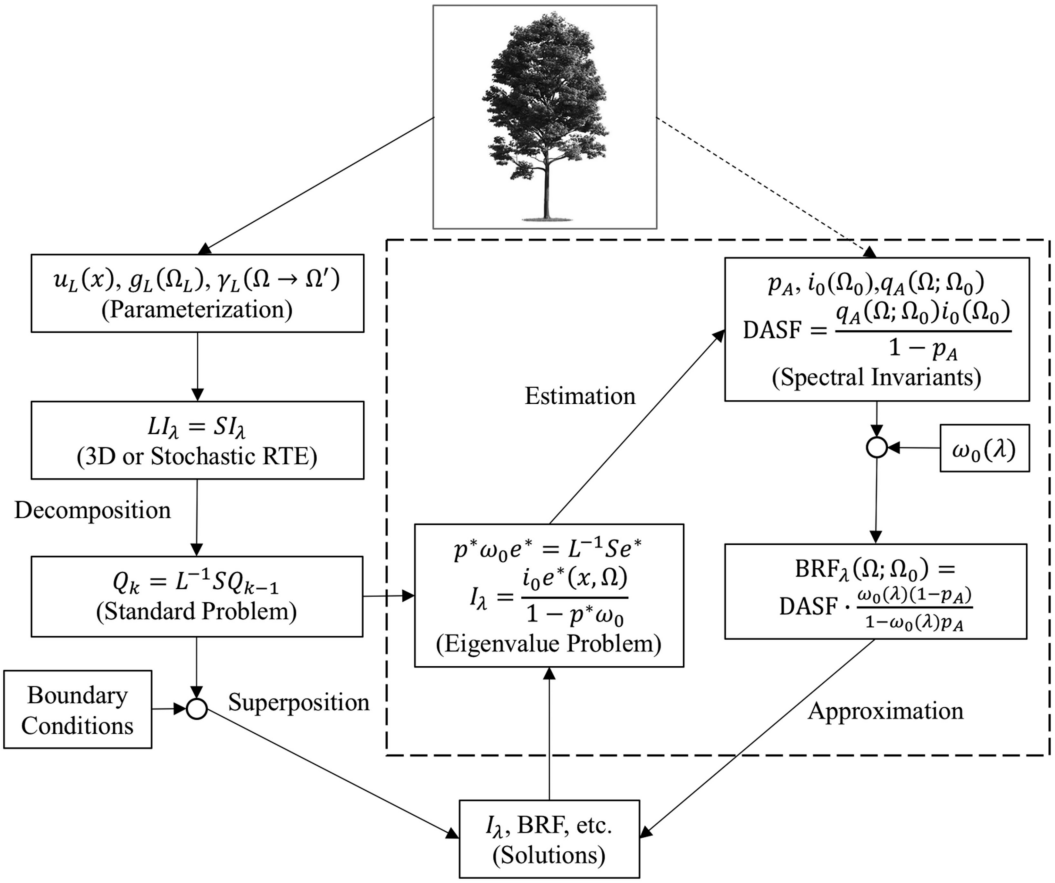

Figure 1. Schematic diagram of the Radiative Transfer Equation (RTE) and the Spectral Invariants theory. The left side of the flowchart (outside the dashed box) describes the successive-order scattering approximation (SOSA) scheme to solve the RTE. The right side of the diagram (inside the dashed box) indicates the logic flow of the spectral invariants theory. The symmetric arrangement of the diagram is to emphasizes that the canopy spectral invariants provide an equivalent set of parameters (other than the traditional ones) to succinctly characterize the canopy structural properties.

From these functions we can derive a few key parameters to be used in RTE, including the single scattering albedo $\omega_0(\lambda)$, the total extinction cross-section $\sigma(\Omega)$, and the differential scattering cross-section $\sigma_S(\Omega \to \Omega\prime)$. Here we have assumed that ω_0 is a variable of only spectral wavelength and that $\sigma(\Omega)$ and $\sigma_S(\Omega \to \Omega\prime)$ do not depend on locations (x) or spectral wavelengths (x). The detailed definitions of these variables and their relationships are given in the Appendix A. Note that although the single scattering albedo is generally understood as the averaged leaf albedo, its definition actually depends on the spatial scales of the elementary scatters considered in the equation [51]. As will be discussed later, this parameter is related to the canopy scattering coefficients by the associated scaling rules [45].

Denoting $I_\lambda(x,\Omega)$ as the monochromatic radiation intensity (radiance), we use the operator notations [52] to describe the radiative transfer processes in vegetation canopies (for readers who are not familiar with linear differential/integral operators, you may think them as matrices with infinite dimensions). In particular, the streaming-collision operator (L) describes the spatial/directional change of the radiation intensity and the extinction of radiance due to collisions between photons and phytoelements (Reference [52]; the same for Equations (2)–(5)),

$$LI_\lambda \equiv \Omega \cdot \nabla I_\lambda(x,\Omega) + \sigma(x,\Omega) I_\lambda(x,\Omega) \quad (1)$$

The scattering operator (S_λ) describes the addition of radiance by photons scattered in from other directions,

$$S_\lambda I_\lambda \equiv \int_{4\pi} \omega_0(\lambda)\sigma_S(x, \Omega\prime \to \Omega) I_\lambda(x, \Omega\prime) d\Omega\prime \tag{2}$$

The steady state RTE is thus

$$LI_\lambda = S_\lambda I_\lambda, \tag{3}$$

with the boundary conditions specified by

$$I_\lambda(x_T, \Omega) = \delta(\Omega - \Omega_0), n_T \cdot \Omega < 0 \tag{4}$$

and

$$I_\lambda(x_B, \Omega) = \frac{1}{\pi} \int_{n_B \cdot \Omega\prime > 0} \rho_\lambda(x_B, \Omega\prime \to \Omega) I_\lambda(x_B, \Omega\prime) |n_B \cdot \Omega\prime| d\Omega\prime, n_B \cdot \Omega < 0 \tag{5}$$

where x_T and $x_B \in \partial V$, n_T and n_B and the outward normal of the boundary, ρ_λ is the bidirectional reflectance factor (BRF) of the lower boundary (i.e., soil surface). In remote sensing applications the influence of lateral boundaries is considered small and thus neglected [35,37]. For simplicity we also only consider the direct solar illumination but neglect the diffuse radiation. This corresponds to the case where the influences of path radiances are removed through atmospheric corrections.

The RTE of Equation (3) describes photon-canopy interactions in three spatial dimensions (i.e., x) and two directional dimensions (Ω and $\Omega\prime$). As the phase function γ_L is not rotational invariant, we cannot decompose the solution in spherical harmonics to simplify the calculation [37]. Direct numerical schemes to solve the equation thus have to perform 5-dimensional integration at every iteration, which is complicated and prone to numerical errors. Therefore, we seek to simplify the problem based on its mathematical/physical properties, which is discussed in the following sections.

3. Black-Soil and Soil Problems

A key property of the RTE is its linearity with regard to I_λ, which allows the problem to be decomposed into a set of sub-problems that are easier to solve. The classic MODIS algorithm [35] decomposes the RTE problem according to its boundary conditions. The easiest boundary condition is represented by the black-soil ("BS") problem, which is formulated for a vegetation canopy illuminated from above by a mono-directional sun beam and otherwise bounded by purely absorbing (i.e., "black") surface from below. In contrast, the soil ("S") problem is formulated for the same canopy but illuminated from below by anisotropic sources and bounded by absorbing surfaces everywhere else. Such a decomposition scheme separates the influence of illumination conditions from those of soils. The two sub-problems are solved independently but their solutions can be flexibly superposed to render the full solution of the original problem (Figure 1).

To solve the black-soil problem, we further decompose the radiation field into the un-collided component, Q_0,

$$Q_0(x_T, \Omega) = \delta(\Omega - \Omega_0),\ n_T \cdot \Omega < 0 \tag{6}$$

and the collided (or diffuse) components, I_{dif}, which satisfies the so-called standard problem with zero boundary conditions where no photon entering the canopy from above or below [53],

$$L_0 I_{dif} = S_\lambda I_{dif} + S_\lambda Q_0. \tag{7}$$

As L is an ordinary differential operator, the solution of Q_0 can be relatively easily obtained. By introducing the integral operator $T = L_0^{-1} S_\lambda$, we write the diffuse component, I_{dif}, symbolically as

$$I_{dif} = T I_{dif} + T Q_0. \tag{8}$$

We should explain the physical meaning of the T operator later in Section 5. For now, note that we can solve for I_{dif} as

$$I_{dif} = \frac{TQ_0}{E - T}, \tag{9}$$

where "E" is the identity operator (i.e., $EI_{dif} = I_{dif}$). Adding Q_0 to both sides, we obtain the solution of the black-soil problem as

$$\begin{aligned} I_{bs} = I_{dif} + Q_0 = \tfrac{Q_0}{E-T} \\ = \left(E + T + T^2 + \cdots + T^k + \cdots\right) Q_0. \end{aligned} \tag{10}$$

The last line of Equation (10) is the expansion of the operator $(E - T)^{-1}$ in Neumann series, which is analogous to geometrical series of numbers. Physically it indicates that I_{BS} is the superposition of photons that are un-collided, once-collided, twice-collided, and so on. The condition that the series converge is provided by the law of energy conservation because the system is dissipative. This superposition scheme, generally referred to as "successive-order scattering approximation" (SOSA; Reference [54]), also bridges the black-soil problem solution to a few key concepts in the radiative transfer theory in vegetation canopies.

The soil ("S") problem is formulated as follows:

$$\begin{aligned} LI_s = S_\lambda I_s, \\ I_s(x_B, \Omega) = d_B(x_B, \Omega), n_B \cdot \Omega < 0, \end{aligned} \tag{11}$$

where $d_B(x_B, \Omega)$ is an anisotropic source normalized to have its hemispherical integral (i.e., irradiance) to be unit. Note that the soil problem also assumes purely absorbing boundaries and the only difference is that the canopy is illuminated from below by a diffuse source. It can be solved with the same approach as the black-soil problem.

We now explain how to use the solutions of the black-soil and the soil problems to model interactions between the canopy and the underlying soil surface. First, the anisotropic source in the S-problem is initialized by radiation that passes through the canopy and reflected by the soil surface. If the spatial distribution pattern of the downward radiation (as which is regulated by the structure of the canopy) does not change significantly, we may assume that the anisotropy is determined by the soil surface but independent on the incoming radiation field [35].

Let the spatial mean effective ground bi-hemispherical reflectance (BHR) of the soil surface to be ρ_{eff} and the mean radiation flux (irradiance) from the downward radiance generated by the black-soil problem to be F_{bs}. As the system is linear, the radiation field that generated by the first interaction of the canopy and the soil surface is (approximately) $\rho_{eff} F_{bs} I_s$. A part of the photons will be scattered back by the canopy to interact with the soil surface again. Denote the mean BHR of the canopy illuminated by the anisotropic source $d_B(x_B, \Omega)$ to be $\overline{R}_s$, and the radiation field generated by the second interaction between the canopy and the soil surface is thus $\left(\rho_{eff}\right)^2 R_s F_{bs} I_s$. As this process iterates, we arrive at the total radiation generated by the interactions between the canopy and the soil surface

$$I_{rest}(x, \Omega) = \frac{\rho_{eff} F_{bs}}{1 - \rho_{eff} R_s} I_s(x, \Omega) \tag{12}$$

and the solution to the full RTE problem is therefore

$$I_\lambda(x, \Omega) = I_{bs}(x, \Omega) + \frac{\rho_{eff} F_{bs}}{1 - \rho_{eff} R_s} I_s(x, \Omega). \tag{13}$$

The above derivation of Equation (13) is slightly different from Reference [35] but shares the same the idea. Ultimately, these decomposition schemes can be derived from the concept of Green's function of the RTE [53]. The assumption about the constancy of canopy BHR (R_s) and the anisotropy $d_B(x_B, \Omega)$ is reasonable. This is because the diffused radiation field within the canopy tend to converge toward certain spatial distributions that are independent on external illumination conditions (see below).

4. Stochastic Radiative Transfer Equation

In remote sensing applications we are generally more interested in the statistical mean of the radiation fields than individual solutions [35]. An apparent way to achieve this goal is to generate an ensemble of representative canopy realizations, solve the RTE for them separately, and then calculate the mean in the end. However, this approach costs time and computation resources. Alternatively, we can also calculate the statistical mean canopy first before solving for the RTE. The second approach is the main idea behind the development of the Stochastic RTE, which turns out to be more efficient in addressing the question [55]. As the ensemble mean is usually equivalent to the average of the 3D radiation field over the horizontal space (i.e., the ergodicity assumption), the central task of Stochastic RTE is the same as to efficiently pack a 3D radiative regime into a 1D form.

To illustrate, recall that $\Omega \cdot \nabla I(x, \Omega)$ is a directional derivative, i.e.,

$$\Omega \cdot \nabla I(x, \Omega) = \frac{\mathrm{d}I(x_B + \xi\Omega, \Omega)}{\mathrm{d}\xi} = \frac{\mathrm{d}I(x_B + (z - z_B)/\mu\Omega, \Omega)}{1/\mu \mathrm{d}z}. \tag{14}$$

Integrating the RTE over the vertical dimension from the top ($z = 0$) or the bottom ($z = 1$) of the canopy leads to

$$\begin{aligned} &I(x, \Omega) + \tfrac{1}{\mu} \textstyle\int_Z u_L(x')\sigma(\Omega) I(x', \Omega) dz' \\ &= \tfrac{1}{\mu} \textstyle\int_Z \omega_0 u_L(x') dz' \int\limits_{4\pi} \sigma_s(\Omega\prime \to \Omega) I(x', \Omega\prime) d\Omega\prime + I(x_B, \Omega) \end{aligned} \tag{15}$$

where $x' = x + (z' - z)/\mu\Omega$ and Z represents appropriate integration intervals. The subscript "B" denotes general boundaries, which may be "top" or "bottom" according to the direction of the integration [55]. Let $\langle \cdot \rangle$ denote the horizontal average. Apply the operator to both sides of the equation and we obtain,

$$\begin{aligned} &I(x, \Omega) + \tfrac{1}{\mu} \textstyle\int_Z \sigma(\Omega) \langle u_L(x') I(x', \Omega) \rangle dz' \\ &= \tfrac{1}{\mu} \textstyle\int_Z \omega_0 dz' \int\limits_{4\pi} \sigma_s(\Omega\prime \to \Omega) \langle u_L(x') I(x', \Omega\prime) \rangle d\Omega\prime + I(x_B, \Omega) \end{aligned} \tag{16}$$

where $I(x, \Omega) = \langle I(x, \Omega) \rangle$. Therefore, the original RTE becomes a 1D equation with regard to the vertical ("z") dimension.

Note that in Equation (16) $I(x, \Omega)$ is the mean radiation intensity (at the vertical level z) averaged over the whole horizontal domain while the "second-moment" variable $\langle u_L(x) I(x, \Omega) \rangle$ is the mean intensity averaged only at locations where a leaf element presents. These two variables are generally different from each other except for special cases. In order to evaluate $\langle u_L(x) I(x, \Omega \rangle)$, we multiply both sides of the RTE by $u_L(x)$ and integrate over the horizontal scale to get

$$\begin{aligned} &\langle u_L(x) I(x, \Omega) \rangle + \tfrac{1}{\mu} \sigma(\Omega) \textstyle\int_Z \langle u_L(x) u_L(x') I(x', \Omega) \rangle dz' \\ &= \tfrac{1}{\mu} \textstyle\int_Z \omega_0 dz' \int\limits_{4\pi} \sigma_s(\Omega\prime \to \Omega) \langle u_L(x) u_L(x') I(x', \Omega\prime) \rangle d\Omega\prime + \langle u_L(x_B) I(x, \Omega) \rangle \end{aligned} \tag{17}$$

Now another new (the "third-moment") variable, $\langle u_L(x) u_L(r') I(r', \Omega\prime) \rangle$, appears in the equation! The procedure can go on and on, but every time we try to solve for a lower-moment variable, we end up introducing a new higher-order unknown into the equation. The process is conceptually analogous

to the "Reynolds Averaging" technique in fluid dynamics. A parameterization scheme thus must be introduced to "close" the Stochastic RTE [56].

The scheme adopted in the current literature is derived based on the binary-medium assumption, under which the leaf density function $u_L(x)$ is represented by an indicator function $\chi(x)$ that specifies the presence ($\chi = 1$) or absence ($\chi = 0$) of a unit leaf element (d_L), i.e., $u_L(x) = d_L\chi(x)$. Note that for a random variable like $\chi(x)$ its spatial averaging ($\langle\cdot\rangle$) is essentially the same as its spatial expectation. As $\chi(x) = \chi(x)^2$, by the standard formula of statistical covariance of two variables, we see that

$$\begin{aligned}&\langle\chi(x)\chi(x')I(x',\Omega\prime)\rangle = \langle\chi(x)\chi(x')^2I(x',\Omega\prime)\rangle\\&= \langle\chi(x)\chi(x')\rangle\langle\chi(x')I(x',\Omega\prime)\rangle + \mathrm{cov}(\chi(x)\chi(x'),\chi(x')I(x',\Omega\prime)).\end{aligned} \tag{18}$$

The first term in Equation (18) represents the "global mean" of $\chi(x)\chi(x')$ and $\chi(x')I(x',\Omega\prime)$, respectively, whose meaning will be explained below. The second (the covariance) term represents their "local chaotisity", which is assumed negligible [57]. We thus arrive at

$$\langle\chi(x)\chi(x')I(x',\Omega\prime)\rangle \approx \langle\chi(x)\chi(x')\rangle\langle\chi(x')I(x',\Omega\prime)\rangle. \tag{19}$$

By the common notation of the literature [55,58], we define

$$\begin{aligned}p_c(z) &= \langle\chi(x)\rangle,\\ q_c(z,z',\Omega) &= \langle\chi(x)\chi(x')\rangle,\\ K(z,z',\Omega) &= q_c(z,z,\Omega)/p_c(z),\\ U(z,\Omega) &= \langle\chi(x)I(x,\Omega)\rangle/p_c(z),\end{aligned} \tag{20}$$

where $p_c(z)$ is the probability of finding leaf elements at locations z. $q_c(z,z',\Omega)$ and $K(z,z',\Omega)$ are the joint and the conditional probability (or pair correlation functions) of finding leaf elements at locations z and z' along the direction Ω simultaneously. $U(z,\Omega)$ is the mean radiation intensity averaged over vegetation occupied horizontal space (i.e., with gaps excluded). The stochastic RTE is then fully specified as [55,58]

$$\begin{aligned}&I(z,\Omega) + \tfrac{1}{\mu}\textstyle\int_Z \sigma(\Omega)p_c(z')U(z',\Omega)dz'\\&= \tfrac{1}{\mu}\textstyle\int_Z \omega_0 dz' \int\limits_{4\pi} p_c(z')U(z',\Omega\prime)\sigma_s(\Omega\prime\to\Omega)d\Omega\prime + I(z_B,\Omega)\end{aligned} \tag{21}$$

and

$$\begin{aligned}&U(z,\Omega) + \tfrac{1}{\mu}\sigma(\Omega)\textstyle\int_Z K(z,z',\Omega)U(z',\Omega)dz'\\&= \tfrac{1}{\mu}\textstyle\int_Z \omega_0 dz' \int\limits_{4\pi} \sigma_s(\Omega\prime\to\Omega)K(z,z',\Omega\prime)U(z',\Omega\prime)d\Omega\prime + U(x_B,\Omega)\end{aligned} \tag{22}$$

with corresponding boundary conditions adapted for $I(x_B,\Omega)$ and $U(x_B,\Omega)$, respectively. In general, we must evaluate $U(z,\Omega)$ first by Equation (22) before solving Equation (21) for $I(z,\Omega)$. Note that because $K(z,z',\Omega\prime)$ is a function of both z' and z, Equation (22) is a Volterra integral equation.

The stochastic RTE was initially developed to solve the mean radiation intensity in the medium of broken clouds [57,59,60]. It was first applied to the vegetation canopy by Reference [61]. The current form of the Stochastic RTE in vegetation canopy was introduced in Reference [55], who also detailed a SOSA procedure to solve the Volterra integral equation.

The most important feature of the Stochastic RTE is the incorporation of the pair correlation function $K(z,\ z',\Omega\prime)$. The function succinctly characterizes the structural and the spatial distribution properties such as heterogeneity and anisotropy of the 3D canopies. It encompasses information presented by traditional metrics like forest gap fractions and clumping indices. Indeed, the introduction of $K(z,\ z',\ \Omega\prime)$ allows the 1D RTE to resolve the differences between $U(x_B,\Omega)$ and $I(x_B,\Omega)$, which can be used to retrieve canopy gap fractions [62]. The first set of realistic pair-correlation functions was derived by Reference [58] using stochastic geometry models [63]. The approach is to idealize individual

tree crowns as regular geometrical objects (e.g., spheres, cylinders, cones, etc.) and assume their locations follow certain spatial patterns (e.g., Poisson's distribution). The pair-correlation functions then can be computed analytically or statistically. Reference [58] presents detailed examples of the pair correlation functions for different crown shapes and canopy distribution patterns. As a special case, when the leaf elements are spatially not correlated, $K(z,\ z',\Omega\prime)$ reduces to $p_c(z)$, Equation (22) reduces to a classic 1D RTE, and $U(z,\Omega)$ becomes the same as $I(z,\Omega)$. Reference [58] also systematically compared the simulation results of the stochastic RTE with those of the classic 1D RTE as well as field measurements, showing that the Stochastic RTE is able to capture the 3D radiation effects previously reported in the literature and therefore the pair-correlation function provides a "most natural and physically meaningful" [58] measure to 3D canopy structural properties over a range of scales.

There are a couple of more facts about the Stochastic RTE that need attention. First, the pair correlation function is not a merely theoretical concept but can be evaluated from observations for real-world applications. With the development of terrestrial lidar scanning (TLS) instruments, now we can measure the 3D structure of forest stands with relative ease and the pair correlation function of the canopy can be accurately computed with such measurements. The function can also be estimated from high-resolution satellite imageries and air-/space-born lidar data over larger spatial scales. Second, as the pair correlation function encapsulates purely the structural or geometrical characteristics of the canopy, it has a close connection with the school of geometrical optical (GO) models in remote sensing [30,31,64,65]. Indeed, the stochastic geometry models used in deriving the theoretical pair correlation functions in Reference [58] are essentially the same as those used in References [64,65]. However, the two schools are different in the specific approaches to use the canopy geometric information. In GO models, the information is used to derive "kernels" of the bidirectional reflectance distribution function (BRDF), which allow the model to fit with observations in a semi-empirical fashion. In contrast, the Stochastic RTE tries to preserve the law of energy conservation and rigorously follows the radiative transfer formulation. As a cost, the Stochastic RTE inherits the limitations of the 3D RTE and cannot resolve, at least to certain spatial scales, the "hot-spot" effects of the canopy radiation regime [33]. We shall return to this topic in Section 6.

5. Canopy Spectral Invariants

The preceding sections have described the traditional algorithms to solve the RTE at a specific wavelength (λ). In remote sensing applications we often need to obtain solutions at many wavelengths to sample the (multiple or hyperspectral) bandwidth of the sensors. Do we have to iterate the process for $I_\lambda(x,\Omega)$ at every wavelength? This question is the main concern of the spectral invariant theory (Figure 1).

The idea underlying the spectral invariant theory is simple: The single albedo $\omega_0(\lambda)$ is the only parameter in the RTE of Equation (1) that depends on wavelengths, while all the other parameters are determined by the structures of the canopy [52]. Therefore, we seek a formula to separate the influence of $\omega_0(\lambda)$ on the solutions of $I_\lambda(x,\Omega)$ at different wavelengths. There are multiple ways in the literature [35,52,66] to derive the spectral invariants theory. Below we follow the SOSA approach described in Reference [66], which represents the most general case and is the easiest to understand. We will use the black-soil problem as the example, though the same methods can be applied to the "S" problem as well [67].

Recall that the black-soil problem can be decomposed to successively collided problems, each of which satisfies the Law of Energy Conservation. For instance, integrating the first-collision problem over the spatial domain and the solid angles eventually leads to (Appendix A)

$$\int_{\delta V} \mathrm{d}x_B \int_{\Omega\cdot\mathrm{n}(x_B)>0} Q_1|\Omega\cdot\mathrm{n}(x_B)|\mathrm{d}\Omega + \int_{4\pi\times V} \sigma Q_1 \mathrm{d}\Omega\mathrm{d}x = \omega_0 \int_{4\pi\times V} \sigma Q_0 \mathrm{d}\Omega\mathrm{d}x \tag{23}$$

or, by the norm notation [66],

$$\| Q_1 \|_\rho + \| Q_1 \| = \omega_0 \| Q_0 \|, \tag{24}$$

where "$\| \cdot \|$" and "$\| \cdot \|_\rho$" indicate the intercepted and the escaped (either being reflected or transmitted) radiation energy, respectively. Equation (24) simply indicates that the portion (i.e., ω_0) of photons scattered from the first collision will either escape through the boundary or collide with the canopy again.

Note that the stream-collision operator (L or L_0) depends only on canopy structural parameters, and the un-collided radiation field Q_0 and the initial interceptance $\| Q_0 \|$ are therefore wavelength independent. The first-collided radiation field Q_1 (and thus $\| Q_1 \|$) is regulated by $\omega_0(\lambda)$, but the ratios

$$\begin{aligned} p_1 &= \frac{\|Q_1\|}{\omega_0 \|Q_0\|} \\ q_1 &= \frac{\|Q_1\|_r}{\omega_0 \|Q_0\|} \end{aligned} \tag{25}$$

are also wavelength independent. Physically p_1 represents the recollision probability that the scattered photons will re-collide with the canopy again and q_1 denotes the probability that the photos will escape the canopy. Clearly $p_1 + q_1 = 1$, satisfying the conservation of energy.

Following the same idea, we normalize the radiation fields as

$$e_k(x, \Omega) = \frac{Q_k(x, \Omega)}{\| Q_k \|}, k = 1, 2, \ldots \tag{26}$$

It is easy to see that $\| e_k(x, \Omega) \| = 1$ and they satisfy the standard RTE

$$p_k \omega_0 e_k = T e_{k-1}. \tag{27}$$

Equations (26) and (27) have clear physical interpretations: $e_k(x, \Omega)$ represents the probability density function that a photon scattered k times will arrive at x along the direction Ω. Therefore, the operator T transforms the probability distribution of photons between successive orders of scattering and evaluates their recollision probability [66]. Note that the factor ω_0 is separated from $e_k(x, \Omega)$ so that the normalized radiation fields are indeed wavelength-independent.

Based on the above definitions we can re-write the solution of the black-soil problem as:

$$I_\lambda(x, \Omega) = \| Q_0 \| \left(\sum_{k=0}^{\infty} T^k \right) \frac{Q_0}{\| Q_0 \|} = i_0 \sum_{k=0}^{\infty} \theta_k^k \omega_0^k e_k(x, \Omega) \tag{28}$$

where $i_0 = \| Q_0 \|, \theta_k = \sqrt{p_0 p_1 p_2 \cdots p_k k}$, and $p_0 = 1$. Note that i_0, θ_k, and $e_k(x, \Omega)$ are all wavelength independent.

In Equation (28) if the θ_k's and the e_k's change little (i.e., invariant) over the order of scattering, the equation can be significantly simplified. Fortunately, this is exactly what the spectral invariants theory suggests: Based on a fundamental property established for the eigenvalues/eigenvectors of the linear RTE operator T [68], the theory indicates that the RTE has a unique dominant eigenvalue γ^* (or $p^* \omega_0$) that corresponds to a positive (and physically feasible) eigenvector $e^*(x, \Omega)$, such that

$$p^* \omega_0 e^*(x, \Omega) = T e^*(x, \Omega). \tag{29}$$

Therefore, if $e_0 = e^*(x, \Omega)$, we will subsequently have $e_k = e^*(x, \Omega)$ and $\theta_k = p^*$, so that

$$I_\lambda = \frac{i_0 e^*(x, \Omega)}{1 - \gamma^*} = \frac{i_0 e^*(x, \Omega)}{1 - p^* \omega_0(\lambda)}. \tag{30}$$

Although the set ($p_k \omega_0$, e_k) derived by the SOSA method are generally different from the ideal eigenvalue-eigenvector pair ($p^* \omega_0$, e^*), analyses show that they converge rapidly so that we only

need a couple of (p_k, e_k) pairs to accurately represent the full solution of Equation (28). For instance, Reference [66] uses a zero-order approximation to satisfactorily estimate the recollision probability p^* and the initial interceptance i_0 from field measured $i(\lambda)$ and $\omega_0(\lambda)$. A detailed analysis of the SOSA approximation can be found in Reference [66] and earlier studies [69–72]. Consistent results are also supported by simulations from Monte Carlo Ray Tracing (MCRT) models [73–75]. The key message is that once we have estimated a few parameters and functions (p_k, e_k, and i_0), the solution $I_\lambda(x, \Omega)$ can be easily obtained with the knowledge of ω_0 at any other wavelength (Figure 1).

The interpretation of the parameter p^* as the recollision probability of photons by Reference [76] represents an important contribution to the spectral invariants theory. It helps us develop a physical intuition to the mathematical concept of the leading eigenvalue of the RTE and associate it with measurable structural properties of vegetation canopies. Once established, the interpretation sees immediate applications in scaling relevant canopy properties across different canopy hierarchies [32,74,76]. For instance, suppose p^*_{sh} and p^*_{cr} are the recollision probabilities of shoots and crowns, the overall p^* parameter for the two-level canopy, resulting from a finite-state Markov process [67], naturally follows

$$p^* = p^*_{sh} + (1 - p^*_{sh}) p^*_{cr}. \tag{31}$$

Similarly, the apparent single scattering albedos of two levels of canopy structures (e.g., shoots and crowns) are related by

$$\omega_{cr} = \frac{\omega_{sh}(1 - p^*_{sh})}{1 - p^*_{sh}\omega_{sh}}. \tag{32}$$

It can be easily verified that the canopy scattering albedo W can be represented by either ω_{cr} or ω_{sh} [76]:

$$W = \frac{\omega_{cr}(1 - p^*_{cr})}{1 - p^*_{cr}\omega_{cr}} = \frac{\omega_{sh}(1 - p^*)}{1 - p^*\omega_{sh}}. \tag{33}$$

Therefore, the single albedo of a higher level structure (e.g., ω_{cr}) totally encapsulates the scattering properties of the lower level structures (e.g., ω_{sh}). The overall scattering coefficients of the crown (or the canopy) will not change if we replace the shoots (needles) with broadleaves of the same (apparent) single albedo. This property suggests that we can use the same set of simulation results (i.e., Look-Up Tables) to retrieve effective structural parameters for both clumped and non-clumped canopies. Additionally, the scaling rules of the recollision coefficients and the scattering coefficients are often associated with changes in spatial scales. They can be used to generate consistent products from satellite sensors operating at different spatial resolutions [77,78]. A detailed review of the physical interpretation of the p^* parameter, its links with measurements, and the scaling rules can be found in a recent review by Reference [45].

In practice, the recollision probability (p^*) of a vegetation canopy can be estimated from field measurements of canopy reflectance, absorptance, transmittance, and single-scattering albedo [66,72]. In remote sensing applications, the common measurements of the surface after atmospheric corrections are the bidirectional reflectance factor (BRF). Therefore, it is desirable to derive a relationship between BRFs and the spectral invariant parameters. Note that under the assumption that the irradiance of the incoming solar radiation is unity, the BRF is just the averaged top-of-canopy radiance (Equation (28) or Equation (30) for the ideal case) multiplied by a constant factor (π). The desired relationship is thus [52]

$$\mathrm{BRF}_\lambda(\Omega; \Omega_0) = \frac{\pi p_A \langle e(x_B, \Omega) \rangle_{x_B} i_0}{1 - p_A} \cdot \frac{\omega_0(\lambda)(1 - p_A)}{1 - \omega_0(\lambda) p_A}, \tag{34}$$

where $\langle \cdot \rangle_{x_B}$ denotes spatial average over the canopy boundary x_B, and p_A denotes the effective recollision probability. In Equation (34) we have neglected the un-collided component of the radiance, as it does not contribute to the reflectance.

In Equation (34) the first term on the right side combines the recollision probability (p_A), the interceptance (i_0), and canopy escape probability ($q_A = \pi p_A \langle e(x_B, \Omega) \rangle_{x_B}$), all being spectral invariant. We define this term the Directional Area Scattering Factor (DASF) [52,79],

$$\mathrm{DASF}(\Omega; \Omega_0) = \frac{q_A(\Omega; \Omega_0) i_0(\Omega_0)}{1 - p_A}, \tag{35}$$

which can be understood as the BRF for a purely reflective canopy (e.g., $\omega_0 = 1$). The second term on the right side of Equation (34) is just the canopy scattering coefficient W in Equation (33). Therefore, BRF is succinctly represented by the product of DASF and the canopy single scattering albedo W.

An important feature of DASF is that it is measurable from both field observations and satellite remote sensing data. When $\omega_0(\lambda)$ is known, DASF can be easily estimated from ground measurements of spectral BRF using the inverse linear regression method [66]. In remote sensing applications where $\omega_0(\lambda)$ is difficult to obtain, Reference [49] developed an algorithm to retrieve DASF from BRF between 710 nm and 790 mm with an intrinsic leaf scattering spectrum $\varpi_0(\lambda)$, where $\varpi_0(\lambda)$ is computed with theoretical models. A key component of the algorithm is to use the scaling rule of Equation (33) to estimate $\omega_0(\lambda)$ from $\varpi_0(\lambda)$ with a within-leaf recollision probability p_L, an intermediate variable that is later cancelled from the calculation. The algorithm is recently used in Reference [80] to derive a global DASF map from the GOME-2 (Global Ozone Monitoring Experiment-2) data.

Of the above spectral invariant parameters, only p^* is an intrinsic property of the canopy while the others (i_0, p_A, q_A and DASF) are influenced by the external illumination conditions. The values of these parameters generally change with the direction of the incident beam (Ω_0). Indeed, the directional illumination has an important effect on the angular signature of canopy BRF (and DASF), which we review in the next section.

6. The "Hot-Spot" Problem

In optical remote sensing, the term "hot spot" refers to the phenomenon that the canopy reflectance has a sharp peak in the retro-illumination direction. The main physical mechanism of the phenomenon is the mutual shadowing of the canopy elements. This is because shadows are invisible from the backscattering direction but become increasingly visible when the view and the illumination angles deviate away from each other [33,36].

It is known that the classic RTE has difficulties simulating the hot-spot effects. This is because the stream-collision operator, which follows the Beer's law, is essentially formulated for gaseous media where the spatial distribution of the scatters is statistically independent at all spatial scales [34]. On the contrary, leaves have finite sizes and their spatial distributions are intrinsically correlated at a certain level. To illustrate the difference between the two cases, we consider a conceptual experiment that a purely absorptive ($\omega_0 = 0$) canopy bounded below by a perfect mirror ($\rho_\lambda = 1$) that is positioned to reflect the nadir incident photons back along the same paths they come from (i.e., the retro-illumination direction). Let the optical depth of the canopy be σ and the intensity of the radiation beam be 1. Under the gaseous media assumption, the intensity of the reflected radiation beam at the top of the canopy will be $\exp(-2\sigma)$, attenuated by the same fashion on the incident and the return paths. For finite-sized leaves, the intensity of the reflected radiation will be $\exp(-\sigma)$, for all the photons that reach the lower surface (i.e., mirror) are guaranteed a free path to travel through the canopy on the way back.

The above example suggests that, due to the effects of mutual shadowing, the canopy extinction cross section in the backscattering direction $\sigma(x, -\Omega_0)$ appears to be smaller than those of other directions. Therefore, previous efforts to model the hot-spot phenomenon focused on developing a function $H(x, \Omega, \Omega_0)$ to regulate the cross section $\sigma(x, \Omega)$, especially for the first collision component [33,81–83]. However, the incorporation of $H(x, \Omega, \Omega_0)$ in the RTE is equivalent to the introduction of an additional source term in the equation. As a result, the solution no longer satisfies the law of energy conservation [35].

Recently, Reference [79] developed a new algorithm that uses the spectral invariant theory to model the spectral BRF of vegetation canopies in the hot-spot region. A key idea of the algorithm is to decompose the canopy into sun-lit and sun-shaded leaf area, where the former is referred to as the "stochastic reflecting boundary" and the latter as the "interior" of the canopy. Photons escaping from the sun-shaded leaf area must have gone through multiple scattering. Thus, their escape probability approximately converges to a certain value, $q_{iso}(\Omega)$. Photons reflected from the sun-lit leaf area that is visible from the direction Ω can escape with a unit probability. Thus, their conditional escape probability, $q_{lit}(\Omega;\Omega_0)$, is expected to be higher than $q_{iso}(\Omega)$. Therefore, we need to evaluate their contribution to the canopy directional escape probability $q_A(\Omega;\Omega_0)$ separately. Let $h(\Omega_0,\Omega)$ represent the correlation between the sun-lit and the visible leaf areas. The probability $q_A(\Omega;\Omega_0)$ is therefore composed of two components that is weighted by $h(\Omega_0,\Omega)$ as

$$q_A(\Omega;\Omega_0) = [1 - h(\Omega_0;\Omega)]q_{iso}(\Omega) + h(\Omega_0;\Omega)q_{lit}(\Omega_0;\Omega). \tag{36}$$

Similarly, we can decompose DASF and BRF by contributions from the interior leaves and the stochastic boundary separately [79].

In the above equation $q_{lit}(\Omega_0;\Omega)$ can be evaluated from canopy structural properties and q_{iso} can be estimated with the classic RTE [79]. Therefore, if the correlation function h is known, we can estimate q_A. Conversely, if q_A is known, we can estimate the correlation function h as [79]

$$h(\Omega;\Omega_0) = \frac{q_A(\Omega;\Omega_0) - q_{iso}(\Omega)}{q_{lit}(\Omega;\Omega_0) - q_{iso}(\Omega)}. \tag{37}$$

The current algorithm of Reference [79] uses the latter approach to evaluate correlation coefficient $h(\Omega_0;\Omega)$ with a stochastic RTE (Section 3) that is modified to incorporate an additional hot-spot parameter c_{HS} [36]. The stochastic RTE needs to run twice, with an actual c_{HS} and with a zero value, respectively, in order to evaluate $q_A(\Omega;\Omega_0)$ and $q_{iso}(\Omega)$ [79].

The algorithm of Reference [79] has two main benefits. First, some of the intermediate results are easy to verify with field measurements. For instance, the visible fraction of leaf area (VFLA) can be estimated with below canopy measurements of transmittance $t_0(\Omega)$ as [79]

$$VFLA(\Omega) = \frac{1 - t_0(\Omega)}{|\ln(t_0(\Omega))|} = \frac{i_0(\Omega)}{|\ln(t_0(\Omega))|}, \tag{38}$$

and the canopy DASF under isotropic illumination conditions (an approximation for the interior canopy component) can be estimated as [79]

$$\frac{q_{iso}(\Omega)i_0(\Omega_0)}{1 - p_{iso}} \approx \frac{i_0(\Omega)i_0(\Omega_0)}{2{\cdot}i_{dif}}, \tag{39}$$

where i_{dif} is the canopy interceptance under the isotropic sky radiation [84]. These relationships provide a set of convenient tools to validate the solutions.

Second and more importantly, the spectral invariants relationships do not necessarily depend on the formulation of the classic RTE but are supported by both observations and the simulation results of MCRT models, whose formulation does not require Beer's law at all [85]. Therefore, the spectral invariants relationships may conserve energy and capture the hot-spot phenomenon at the same time. Reference [79] illustrates this potential with a simple stochastic Monte Carlo model. Though the algorithm is still subjected to further examinations and refinements in the future, it introduces a new and promising perspective to address the old challenge.

7. Summary

This paper reviews developments of the radiative transfer theory in optical remote sensing of terrestrial vegetation, including the decomposition of the black-soil (BS) and the soil (S) problems, the development of the stochastic RTE, the theory of spectral invariants, and the latest effort to address the "hot-spot" challenge. The first three topics are centered around the idea as how to simplify the solutions of the RTE under different boundary conditions (e.g., soil reflective properties), over full 3-dimensional spatial domains, and with regard to radiation at different wavelengths. The last topic is intended to highlight the advantage of the spectral invariants theory in remote sensing applications.

As the RTE is linear as regard to I_λ, a fundamental strategy to solve the equation is decomposition and superposition. The separation of the black-soil and the soil problems, the expansion of Neumann's series, and the method of successive orders of scattering approximation discussed in Section 3 are all demonstrations of this strategy. The concept of invariants, the convergence of the radiation field to a certain distribution that does not change (except for the magnitude) over subsequent scattering, is also a natural result that follows the line of thinking. The existence of such a unique intrinsic solution is backed by the mathematical theories of eigenvalues/eigenvectors of the RTE and the physical law of energy conservation.

Another important thread of developments in the Stochastic RTE and the spectral invariants theory is to efficiently represent the canopy structural or geometrical information in the equation. The stochastic RTE introduces a pair-correlation function $K(z,\ z', \Omega)$, which describes the probability of simultaneously finding leaves at two locations $(z,\ z')$ along the direction Ω. It characterizes the heterogeneity and anisotropy characteristics of the canopies and regulate the corresponding cross sections (σ and σ_s). Therefore, the function provides a natural and physically meaningful measure of 3D canopy structural properties over a range of scales.

The spectral invariants theory further simplifies the representation of canopy structural characteristics to a single wavelength-independent parameter p^*, which defines the recollision probability that a scattered photon will interact with the canopy again. Once p^* (and the corresponding escape probability function) is estimated, we can accurately approximate the solution (radiance or BRF) of the RTE at any other wavelength with the knowledge of $\omega_0(\lambda)$, which imbues the wavelength-dependent influence on the radiation field. As p^* represents recollision probability, it can be used to scale canopy properties (e.g., scattering coefficients) across various canopy hierarchies or spatial scales.

Although the pair-correlation function $K(z,\ z', \Omega)$, the photon recollision probability p^*, and the other spectral invariants functions/parameters such as DASF appear to be "abstract," they all can be estimated from field measurements or remote sensing data. For instance, the pair-correlation function can be derived from high-resolution satellite images and lidar data. The recollision probability of a vegetation canopy can be determined from field measurements of canopy reflectance, absorptance, transmittance, and single-scattering albedo with simple linear correlations. DASF can also be retrieved directly from ground measurements or hyperspectral remote sensing data between 710 nm and 790 mm for dense vegetation in a similar fashion. These concepts, backed by rigorous mathematical analysis and physical principles, thus represent our current best understanding of the empirical relationships identified from observations.

The spectral invariants theory also provides a promising approach to solve the "hot-spot" problem known to the classic RTE models. This challenge has its roots in the formulation of the equation based on the turbid medium assumption and Beer's law. On the contrary, leaves are finite sized and their spatial correlations cannot be neglected. Previous efforts to address this problem usually introduce a semi-empirical factor to regulate the extinction cross section in the equation, which however violate the law of energy conservation. A new algorithm was recently developed to address the challenge based on the spectral invariants theory. The algorithm decomposes the canopy into a reflective boundary and interior points and models the escape probability (and DASF) for the two components separately. The directional escape probability from the reflective boundary is assumed to be unity, a feature that

cannot be simulated by the classic RTE. As such, the new approach does not depend on the Beer's law formulation in the RTE but satisfies the law of energy conservation. This example further demonstrates the spectral invariants theory as a powerful tool in optical remote sensing applications.

Funding: W.W., R.N., H.H., and S.G. are supported by the National Aeronautics and Space Administration (NASA) under grants to NASA Earth Exchange (NEX). Y.K. is supported by NASA under grant NNX15AR03G.

Acknowledgments: The authors are grateful to four anonymous reviewers, whose constructive comments have helped significantly improve the quality of the paper. We are also thankful to Yujie Wang of NASA Goddard Space Flight Center and Bin Yang of Hunan University, China for insightful discussions on the spectral invariants theory.

Conflicts of Interest: The authors declare no conflict of interest.

Nomenclature

$\gamma_L(\lambda, x, \Omega \to \Omega\prime, \Omega_L)$	Leaf element scattering phase function
θ_k	Geometric mean of photon recollision probabilities, i.e., $\sqrt{p_0 p_1 \cdots p_k k}$
λ	Wavelength
μ	Cosine of zenith angle of direction Ω
$\sigma(x, \Omega)$	Total extinction coefficient (or cross section)
$\sigma_S(\lambda, x, \Omega \to \Omega\prime)$	Differential scattering coefficient (or cross section)
$\omega_0(\lambda)$	Single scattering albedo
Ω_L	Leaf normal direction vector
Ω, $\Omega\prime$	Incident and scattered radiation direction vectors, respectively
$g_L(x, \Omega_L)$	Leaf normal distribution function
$i_0(\Omega_0)$	Canopy interceptance
p^*, p_A	Theoretical and effective photon recollision probability, respectively
$q(\Omega; \Omega_0)$	Photon escape probability density function
$u_L(x)$	Leaf area density distribution function
BRF	Bidirectional reflectance factor
DASF	Directional area scattering factor
E	Identity operator
$I_\lambda(x, \Omega)$	Monochromatic radiation intensity (radiance)
$K(z, z', \Omega)$	Conditional pair correlation functions of finding leaf elements at locations z and z' along Ω simultaniously
L	Streaming-collision operator
Q_k	The k-th collided component of radiation field
S_λ	Scattering operator
T	Integral operator defined as $L_0^{-1} S_\lambda$
$U(z, \Omega)$	Horizontal mean radiation intensity averaged over vegetated area
$\langle \cdot \rangle$	Horizontal average operator
$\| \cdot \|$, $\| \cdot \|_\rho$	Integral norm operator that indicates the intercepted and the escaped radiation energy, respectively.

Appendix

Appendix A.1 Definitions of the Canopy Structural Parameters

The leaf albedo is mathematically defined as

$$\omega_L(\lambda, x, \Omega, \Omega_L) = \int_{4\pi} \gamma_L(\lambda, x, \Omega \to \Omega\prime, \Omega_L) d\Omega \tag{A1}$$

the total extinction coefficient (or cross-section) is

$$\sigma(x, \Omega) = \frac{u_L(x)}{2\pi} \int_{2\pi+} g_L(x, \Omega_L) |\Omega \cdot \Omega_L| d\Omega_L \tag{A2}$$

and the differential scattering cross-section is

$$\sigma_S(\lambda, x, \Omega \to \Omega\prime) = \frac{u_L(x)}{2\pi} \int\limits_{2\pi+} g_L(x, \Omega_L)|\Omega{\cdot}\Omega_L|\gamma_L(\lambda, x, \Omega \to \Omega\prime, \Omega_L)d\Omega_L \tag{A3}$$

As photons scattered from one direction provide sources for radiation in other directions, the two cross-section terms are closely related by

$$\int\limits_{4\pi} \sigma_S(\lambda, x, \Omega \to \Omega\prime)d\Omega\prime = \omega_0(\lambda, x, \Omega)\sigma(x, \Omega) \tag{A4}$$

where $\omega_0(\lambda, x, \Omega)$ is the single scattering albedo, which is usually defined as an average to the leaf albedo

$$\omega_0(\lambda, x, \Omega) = \frac{\int_{2\pi+} g_L(x, \Omega_L)|\Omega{\cdot}\Omega_L|\omega_L(\lambda, x, \Omega, \Omega_L)d\Omega_L}{\int_{2\pi+} g_L(x, \Omega_L)|\Omega{\cdot}\Omega_L|d\Omega_L} \tag{A5}$$

For simplicity, in the paper we further made the following assumptions

$$\begin{array}{c} \omega_0(\lambda, x, \Omega) = \omega_0(\lambda), \\ \sigma(x, \Omega) = u_L(x)\sigma(\Omega), \\ \sigma_S(\lambda, x, \Omega \to \Omega\prime) = \omega_0(\lambda)u_L(x)\sigma_S(\Omega \to \Omega\prime). \end{array} \tag{A6}$$

Note that ω_0 is only a variable of spectral wavelength while $\sigma(\Omega)$ and $\sigma_S(\Omega \to \Omega\prime)$ are spatially and spectrally independent.

Appendix A.2 Derivation of Equation (23)

Integrating the first-collision problem over the spatial domain and the solid angles leads to

$$\int\limits_{4\pi\times V} L_0 Q_1 \mathrm{d}\Omega\mathrm{d}x = \int\limits_{4\pi\times V} SQ_0 \mathrm{d}\Omega\mathrm{d}x \tag{A7}$$

By Stokes' Theorem,

$$\int\limits_{4\pi\times V} \Omega{\cdot}\nabla Q_1 \mathrm{d}\Omega\mathrm{d}x = \int\limits_{\delta V} \mathrm{d}x_B \int\limits_{4\pi} Q_1|\Omega{\cdot}\mathrm{n}(x_B)|\mathrm{d}\Omega \tag{A8}$$

where δV represents the boundary of the domain. As the incoming radiation (i.e., $\Omega{\cdot}\mathrm{n}(x_B) < 0$) in the standard problem is zero, Equation (A7) thus becomes

$$\int\limits_{\delta V} \mathrm{d}x_B \int\limits_{\Omega{\cdot}\mathrm{n}(x_B)>0} Q_1|\Omega{\cdot}\mathrm{n}(x_B)|\mathrm{d}\Omega + \int\limits_{4\pi\times V} \sigma Q_1 \mathrm{d}\Omega\mathrm{d}x = \int\limits_{4\pi\times V} SQ_0 \mathrm{d}\Omega\mathrm{d}x \tag{A9}$$

By the definition of the scattering operator (Equation (2)), we have

$$\begin{array}{l} \int\limits_{4\pi\times V} SQ_0 \mathrm{d}\Omega\mathrm{d}x = \int\limits_{4\pi\times V} \int\limits_{4\pi} \omega_0(\lambda)\sigma_S(x, \Omega\prime \to \Omega)Q_0(x, \Omega\prime)d\Omega\prime\, \mathrm{d}\Omega\mathrm{d}x \\ = \int\limits_{4\pi\times V} \int\limits_{4\pi} \omega_0(\lambda)\sigma_S(x, \Omega\prime \to \Omega)Q_0(x, \Omega\prime)\mathrm{d}\Omega\, \mathrm{d}\Omega\prime\, \mathrm{d}x \\ = \omega_0(\lambda) \int\limits_{4\pi\times V} \sigma Q_0\, \mathrm{d}\Omega\prime\, \mathrm{d}x \end{array} \tag{A10}$$

In the last step of Equation (A10) we used the relationship from Equation (A4). As the integration is performed over all solid angles (i.e., 4π), we can safely exchange $\Omega\prime$ with Ω and thus obtain Equation (23) in the main text.

Appendix A.3 Energy Conservation between p_A and q_A

Integrating the effective directional escape probability density function over all the out-scattering directions Ω, we have

$$\frac{1}{\pi}\int_{4\pi} q_A(\Omega;\Omega_0)|\mu|\mathrm{d}\Omega = (1-p_A)\sum_{k=1}^{\infty}\left(\frac{1}{\pi}\int_{4\pi} q_k(\Omega;\Omega_0)|\mu|\mathrm{d}\Omega\right)\theta_{k-1}^{k-1} \tag{A11}$$

By Equations (25) and (35),

$$\frac{1}{\pi}\int_{4\pi} q_k(\Omega;\Omega_0)|\mu|\mathrm{d}\Omega = q_k = 1-p_k \tag{A12}$$

where q_k on the right-hand-side of the equation is the k-th escape probability. Substituting it into Equation (A11), we have

$$\begin{aligned}&\tfrac{1}{\pi}\textstyle\int_{4\pi} q_A(\Omega;\Omega_0)|\mu|\mathrm{d}\Omega = (1-p_A)\sum_{k=1}^{\infty}(1-p_k)\theta_{k-1}^{k-1}\\ &= (1-p_A)\textstyle\sum_{k=1}^{\infty}\left(\theta_{k-1}^{k-1}-\theta_k^k\right)\\ &= 1-p_A\end{aligned} \tag{A13}$$

In the last step of Equation (A13) we used the fact that $\theta_0 = p_0 = 1$ (Equation (28)).

References

1. National Research Council (NRC). *Earth Observations from Space: The First 50 Years of Scientific Achievements*; The National Academies Press: Washington, DC, USA, 2008; p. 142.
2. Roy, D.P.; Wulder, M.A.; Loveland, T.R.; Woodcock, C.E.; Allen, R.G.; Anderson, M.C.; Helder, D.; Irons, J.R.; Johnson, D.M.; Kennedy, R.; et al. Landsat-8: Science and product vision for terrestrial global change research. *Remote Sens. Environ.* **2014**, *145*, 154–172. [CrossRef]
3. Loveland, T.R.; Irons, J.R. Landsat 8: The plans, the reality, and the legacy. *Remote Sens. Environ.* **2016**, *185*, 1–6. [CrossRef]
4. Drusch, M.; Del Bello, U.; Carlier, S.; Colin, O.; Fernandez, V.; Gascon, F.; Hoersch, B.; Isola, C.; Laberinti, P.; Martimort, P.; et al. Sentinel-2: ESA's optical high-resolution mission for GMES operational services. *Remote Sens. Environ.* **2012**, *120*, 25–36. [CrossRef]
5. Goldberg, M.D.; Kilcoyne, H.; Cikanek, H.; Mehta, A. Joint Polar Satellite System: The United States next generation civilian polar-orbiting environmental satellite system. *J. Geophys. Res. Atmos.* **2013**, *118*, 13463–13475. [CrossRef]
6. Bessho, K.; Date, K.; Hayashi, M.; Ikeda, A.; Imai, T.; Inoue, H.; Kumagai, Y.; Miyakawa, T.; Murata, H.; Ohno, T.; et al. An Introduction to Himawari-8/9—Japan's New-Generation Geostationary Meteorological Satellites. *J. Meteorol. Soc. Jpn.* **2016**, *94*, 151–183. [CrossRef]
7. Schmit, T.J.; Griffith, P.; Gunshor, M.M.; Daniels, J.M.; Goodman, S.J.; Lebair, W.J. *A Closer Look at the ABI on the GOES-R Series*; BAMS: Boston, MA, USA, 2017.
8. Kalluri, S.; Alcala, C.; Carr, J.; Griffith, P.; Lebair, W.; Lindsey, D.; Race, R.; Wu, X.; Zierk, S. From Photons to Pixels: Processing data from the Advanced Baseline Imager. *Remote Sens.* **2018**, *10*, 177. [CrossRef]
9. Yang, J.; Zhang, Z.; Wei, C.; Lu, F.; Guo, Q. *Introducing the New Generation of Chinese Geostationary Weather Satellites, Fengyun-4*; BAMS: Boston, MA, USA, 2017.
10. Starvros, E.N.; Schimel, D.; Pavlick, R.; Serbin, S.; Swann, A.; Duncanson, L.; Fisher, J.B.; Fassnacht, F.; Ustin, S.; Dubayah, R.; et al. ISS observations offer insights into plant function. *Nat. Ecol. Evol.* **2017**, *1*, 0194. [CrossRef] [PubMed]
11. Myneni, R.B.; Maggion, S.; Iaquinta, J.; Privette, J.L.; Gobron, N.; Pinty, B.; Kimes, D.S.; Verstraete, M.M.; Williams, D.L. Optical remote sensing of vegetation: Modeling, caveats, and algorithms. *Remote Sens. Environ.* **1995**, *51*, 169–188. [CrossRef]
12. Rodgers, C.D. *Inverse Methods for Atmospheric Sounding: Theory and Practice*; World Scientific Publishing Co. Pte. Ltd.: Singapore, 2000; p. 238.
13. Combal, B.; Baret, F.; Weiss, M.; Trubuil, A.; Macé, D.; Pragnére, A. Retrieval of canopy biophysical variables from bidirectional reflectance using prior information to solve the ill-posed inverse problem. *Remote Sens. Environ.* **2002**, *84*, 1–15. [CrossRef]
14. Baret, F.; Buis, S. Estimating Canopy Characteristics from Remote Sensing Observations: Review of Methods and Associated Problems. In *Advances in Land Remote Sensing*; Liang, S., Ed.; Springer: Dordrecht, The Netherlands, 2008.

15. Lauvernet, C.; Baret, F.; Hascoët, L.; Buis, S.; Le Dimet, F.-X. Multitemporal-patch ensemble inversion of coupled surface–atmosphere radiative transfer models for land surface characterization. *Remote Sens. Environ.* **2008**, *112*, 851–861. [CrossRef]
16. Dorigo, W.; Richter, R.; Baret, F.; Bamler, R.; Wagner, W. Enhanced automated canopy characterization from hyperspectral data by a novel two step radiative transfer model inversion approach. *Remote Sens.* **2009**, *1*, 1139–1170. [CrossRef]
17. Atzberger, C.; Richter, K. Spatially constrained inversion of radiative transfer models for improved LAI mapping from future Sentinel-2 imagery. *Remote Sens. Environ.* **2012**, *120*, 208–218. [CrossRef]
18. Kuusk, A. Canopy radiative transfer modeling. In *Comprehensive Remote Sensing: Remote Sensing of Terrestrial Ecosystem*; Liang, S., Ed.; Elsevier: Amsterdam, The Netherlands, 2018; Volume 3.
19. Shore, S.N. Blue sky and hot piles: The evolution of radiative transfer theory from atmosphere to nuclear reactors. *Hist. Math.* **2002**, *29*, 463–489. [CrossRef]
20. Ross, J.; Nilson, T. Concerning the theory of plant cover radiation regime. In *Investigations on Atmospheric Physics*; Inst. Phys. Astron. Acad. Sci. ESSR: Tartu, Estonia, 1963; pp. 42–64. (In Russian)
21. Ross, J.; Nilson, T. Radiation exchange in plant canopies. In *Heat and Mass Transfer in the Biosphere*; de Vries, D.A., Afgan, H.H., Eds.; Scripta: Washington, DC, USA, 1975; pp. 327–336.
22. Ross, J. *The Radiation Regime and Architecture of Plant Stands*; Dr. W. Junk: Norwell, MA, USA, 1981; p. 391.
23. Govaerts, Y.; Verstraete, M. Raytran: A Monte Carlo ray-tracing model to compute light scattering in three-dimensional heterogeneous media. *IEEE Trans. Geosci. Remote Sens.* **1998**, *36*, 493–505. [CrossRef]
24. Gastellu-Etchegorry, J.; Demarez, V.; Pinel, V.; Zagolski, F. Modeling radiative transfer in heterogeneous 3-D vegetation canopies. *Remote Sens. Environ.* **1996**, *58*, 131–156. [CrossRef]
25. Gastellu-Etchegorry, J.; Yin, T.; Lauret, N.; Cajgfinger, T.; Gregoire, T.; Grau, E.; Feret, J.-B.; Lopes, M.; Guilleux, J.; Dedieu, G.; et al. Discrete anisotropic radiative transfer (DART 5) for modeling airborne and satellite spectroradiometer and LIDAR acquisitions of natural and urban landscapes. *Remote Sens.* **2015**, *7*, 1667–1701. [CrossRef]
26. Verhoef, W. Light scattering by leaf layers with application to canopy reflectance modeling: The SAIL model. *Remote Sens. Environ.* **1984**, *16*, 125–141. [CrossRef]
27. Verhoef, W.; Bach, H. Simulation of hyperspectral and directional radiance images using coupled biophysical and atmospheric radiative transfer models. *Remote Sens. Environ.* **2003**, *87*, 23–41. [CrossRef]
28. Verhoef, W.; Bach, H. Coupled soil–leaf-canopy and atmosphere radiative transfer modeling to simulate hyperspectral multi-angular surface reflectance and TOA radiance data. *Remote Sens. Environ.* **2007**, *109*, 166–182. [CrossRef]
29. Jacquemoud, S.; Baret, F. PROSPECT: A model of leaf optical properties spectra. *Remote Sens. Environ.* **1990**, *34*, 75–91. [CrossRef]
30. Li, X.; Strahler, A.; Woodcock, C. A hybrid geometric optical-radiative transfer approach for modeling albedo and directional reflectance of discontinuous canopies. *IEEE Trans. Geosci. Remote Sens.* **1995**, *33*, 466–480.
31. Ni, W.; Li, X.; Woodcock, C.; Caetano, M.; Strahler, A. An analytical hybrid GORT model for bidirectional reflectance over discontinuous plant canopies. *IEEE Trans. Geosci. Remote Sens.* **1999**, *37*, 987–999.
32. Rautiainen, M.; Stenberg, P. Application of photon recollision probability in coniferous canopy reflectance model. *Remote Sens. Environ.* **2005**, *96*, 98–107. [CrossRef]
33. Kuusk, A. The hot spot effect of a uniform vegetative cover. *Sov. J. Remote Sens.* **1985**, *3*, 645–658.
34. Knyazikhin, Y.; Kranigk, J.; Myneni, R.B.; Panfyorov, O.; Gravenhorst, G. Influence of a small-scale structure on radiative transfer and photosynthesis in vegetation canopies. *J. Geophys. Res.* **1998**, *103*, 6133–6144. [CrossRef]
35. Knyazikhin, Y.; Martonchik, J.V.; Myneni, R.B.; Diner, D.J.; Running, S.W. Synergistic algorithm for estimating vegetation canopy leaf area index and fraction of absorbed photosynthetically active radiation from MODIS and MISR data. *J. Geophys. Res.* **1998**, *103*, 32257–32274. [CrossRef]
36. Kuusk, A. The hot spot effect in plant canopy reflectance. In *Photon-Vegetation Interactions: Applications in Optical Remote Sensing and Plant Ecology*; Myneni, R.B., Ross, J., Eds.; Springer: Berlin, Germany, 1991; pp. 139–159.
37. Knyazikhin, Y.; Marshak, A.; Myneni, R.B. Three-dimensional radiative transfer in vegetation canopies and cloud–vegetation interaction. In *Three-Dimensional Radiative Transfer in the Cloudy Atmosphere*; Marshak, A., Davis, A.B., Eds.; Springer: Berlin, Germany, 2005; pp. 617–652.

38. Bergen, K.M.; Goetz, S.J.; Dubayah, R.O.; Henebry, G.M.; Hunsaker, C.T.; Imhoff, M.L.; Nelson, R.F.; Parker, G.G.; Radeloff, V.C. Remote sensing of vegetation 3-D structure for biodiversity and habitat: Review and implications for lidar and radar spaceborne missions. *J. Geophys. Res.* **2009**, *114*. [CrossRef]
39. Meroni, M.; Rossini, M.; Guanter, L.; Alonso, L.; Rascher, U.; Bolombo, R.; Moreno, J. Remote sensing of solar-induced chlorophyll fluorescence: Review of methods and applications. *Remote Sens. Environ.* **2009**, *113*, 2037–2051. [CrossRef]
40. Koch, B. Status and future of laser scanning, synthetic aperture radar and hyperspectral remote sensing data for forest biomass assessment. *ISPRS J. Photogramm. Remote Sens.* **2010**, *65*, 581–590. [CrossRef]
41. Hansen, M.; Loveland, T.R. A review of large area monitoring of land cover change using Landsat data. *Remote Sens. Environ.* **2012**, *122*, 66–74. [CrossRef]
42. Wulder, M.A.; White, J.C.; Nelson, R.F.; Næsset, E.; Ørka, H.O.; Coops, N.C.; Hilker, T.; Bater, C.W.; Gobakken, T. Lidar sampling for large-area forest characterization: A review. *Remote Sens. Environ.* **2012**, *121*, 196–209. [CrossRef]
43. Verrelst, J.; Camps-Valls, G.; Muñoz-Marí, J.; Rivera, J.P.; Veroustraete, F.; Clevers, J.G.P.W.; Moreno, J. Optical remote sensing and the retrieval of terrestrial vegetation bio-geophysical properties—A review. *ISPRS J. Photogramm. Remote Sens.* **2015**, *108*, 273–290. [CrossRef]
44. Schimel, D.; Pavlick, R.; Fisher, J.B.; Asner, G.P.; Saatchi, S.; Townsend, P.; Miller, C.; Frankenberg, C.; Hibbard, K.; Cox, P. Observing terrestrial ecosystems and the carbon cycle from space. *Glob. Chang. Biol.* **2015**, *21*, 1762–1776. [CrossRef] [PubMed]
45. Stenberg, P.; Mõttus, M.; Rautiainen, M. Photon recollision probability in modelling the radiation regime of canopies—A review. *Remote Sens. Environ.* **2016**, *183*, 98–108. [CrossRef]
46. Liang, S. (Ed.) *Comprehensive Remote Sensing*; Elsevier: Amsterdam, The Netherlands, 2018; p. 3134.
47. Evans, K.F.; Marshak, A. Numerical Methods. In *Three-Dimensional Radiative Transfer in the Cloudy Atmosphere*; Marshak, A., Davis, A.B., Eds.; Springer: Berlin, Germany, 2005; pp. 243–281.
48. Camps-Valls, G.; Bioucas-Dias, J.; Crawford, M. A special issue on advances in machine learning for remote sensing and geosciences (from the guest editors). *IEEE Geosci. Remote Sens. Mag.* **2016**, *4*, 5–7. [CrossRef]
49. Knyazikhin, Y.; Schull, M.A.; Stenberg, P.; Mõttus, M.; Rautiainen, M.; Yang, Y.; Marshak, A.; Carmona, P.L.; Kaufmann, R.K.; Lewis, P.; et al. Hyperspectral remote sensing of foliar nitrogen content. *PNAS* **2013**, *110*, E185–E192. [CrossRef] [PubMed]
50. Nilson, T.; Kuusk, A. A reflectance model for the homogeneous plant canopy and its inversion. *Remote Sens. Environ.* **1989**, *27*, 157–167. [CrossRef]
51. Tian, Y.; Wang, Y.; Zhang, Y.; Knyazikhin, Y.; Bogaert, J.; Myneni, R.B. Radiative transfer based scaling of LAI retrievals from reflectance data of different resolutions. *Remote Sens. Environ.* **2002**, *84*, 143–159. [CrossRef]
52. Knyazikhin, Y.; Schull, M.A.; Xu, L.; Myneni, R.B.; Samanta, A. Canopy spectral invariants. Part 1: A new concept in remote sensing. *J. Quant. Spectrosc. Radiat. Transf.* **2011**, *112*, 727–735. [CrossRef]
53. Davis, A.B.; Knyazikhin, Y. A primer in three-dimensional radiative transfer. In *Three-Dimensional Radiative Transfer in the Cloudy Atmosphere*; Marshak, A., Davis, A.B., Eds.; Springer: Berlin, Germany, 2005; pp. 153–242.
54. Myneni, R.B.; Asrar, G.; Kanemasu, E.T. Light scattering in plant canopies: The method of Successive Orders of Scattering Approximations [SOSA]. *Agric. For. Meteorol.* **1987**, *39*, 1–12. [CrossRef]
55. Shabanov, N.V.; Knyazikhin, Y.; Baret, F.; Myneni, R.B. Stochastic modeling of radiation regime in discontinuous vegetation canopies. *Remote Sens. Environ.* **2000**, *74*, 125–144. [CrossRef]
56. Huang, D.; Liu, Y. A novel approach for introducing cloud spatial structure into cloud radiative transfer parameterizations. *Environ. Res. Lett.* **2014**, *9*, 124022. [CrossRef]
57. Vainikko, G.M. The equation of mean radiance in broken cloudiness. *Trudy MGK SSR Meteorol. Investig.* **1973**, *21*, 28–37. (In Russian)
58. Huang, D.; Knyazikhin, Y.; Wang, W.; Deering, D.W.; Stenberg, P.; Shabanov, N.; Tan, B.; Myneni, R.B. Stochastic transport theory for investigating the three-dimensional canopy structure from space measurements. *Remote Sens. Environ.* **2008**, *112*, 35–50. [CrossRef]
59. Titov, G.A. Statistical description of radiation transfer in clouds. *J. Atmos. Sci.* **1990**, *47*, 24–38. [CrossRef]
60. Zuev, V.E.; Titov, G.A. *Atmospheric Optics and Climate*; The Series "Contemporary Problems of Atmospheric Optics"; Spector, Institute of Atmospheric Optics RAS: Tomsk, Russia, 1996; Volume 9. (In Russian)

61. Menzhulin, G.V.; Anisimov, O.A. Principles of Statistical Phytoactinometry. In *Photon-Vegetation Interactions: Applications in Optical Remote Sensing and Plant Ecology*; Myneni, R.B., Ross, J., Eds.; Springer: Berlin, Germany, 1991; pp. 111–138.
62. Shabanov, N.; Gastellu-Etchegorry, J.-P. The stochastic Beer–Lambert–Bouguer law for discontinuous vegetation canopies. *J. Quant. Spectrosc. Radiat. Transf.* **2018**, *214*, 18–32. [CrossRef]
63. Stoyan, D.; Kendall, S.W.; Mecke, J. *Stochastic Geometry and Its Applications*; John Wiley & Sons: New York, NY, USA, 1995.
64. Li, X.; Strahler, A. Geometrical–optical modelling of a conifer forest canopy. *IEEE Trans. Geosci. Remote Sens.* **1985**, *23*, 705–721. [CrossRef]
65. Li, X.; Strahler, A.H. Geometrical–optical bidirectional reflectance modelling of a conifer forest canopy. *IEEE Trans. Geosci. Remote Sens.* **1986**, *24*, 906–919. [CrossRef]
66. Huang, D.; Knyazikhin, Y.; Dickinson, R.E.; Rautiainen, M.; Stenberg, P.; Disney, M.; Lewis, P.; Cescatti, A.; Tian, Y.; Verhoef, W.; et al. Canopy spectral invariants for remote sensing and model applications. *Remote Sens. Environ.* **2007**, *106*, 106–122. [CrossRef]
67. Silván-Cárdenas, J.L.; Corona-Romero, N. Radiation budget of vegetation canopies with reflective surface: A generalization using the Markovian approach. *Remote Sens. Environ.* **2017**, *189*, 118–131. [CrossRef]
68. Vladimirov, V.S. *Mathematical Problems in the One-Velocity Theory of Particle Transport*; Tech. Rep. AECL-1661; At. Energy of Can. Ltd.: Chalk River, ON, Canada, 1963; 302p.
69. Panferov, O.; Knyazikhin, Y.; Myneni, R.B.; Szarzynski, J.; Engwald, S.; Schnitzler, K.G.; Gravenhorst, G. The role of canopy structure in the spectral variation of transmission and absorption of solar radiation in vegetation canopies. *IEEE Trans. Geosci. Remote Sens.* **2001**, *39*, 241–253. [CrossRef]
70. Zhang, Y.; Tian, Y.; Myneni, R.B.; Knyazikhin, Y.; Woodcock, C.E. Assessing the information content of multiangle satellite data for mapping biomes: I. Statistical analysis. *Remote Sens. Environ.* **2002**, *80*, 418–434. [CrossRef]
71. Zhang, Y.; Shabanov, N.; Knyazikhin, Y.; Myneni, R.B. Assessing the information content of multiangle satellite data for mapping biomes: II. Theories. *Remote Sens. Environ.* **2002**, *80*, 435–446. [CrossRef]
72. Wang, Y.; Buermann, W.; Stenberg, P.; Smolander, H.; Häme, T.; Tian, Y.; Hu, J.; Knyazikhin, Y.; Myneni, R.B. A new parameterization of canopy spectral response to incident solar radiation: Case study with hyperspectral data from pine dominant forest. *Remote Sens. Environ.* **2003**, *85*, 304–315. [CrossRef]
73. Disney, M.; Lewis, P.; Quaife, T.; Nichol, C. A spectral invariant approach to modeling canopy and leaf scattering. In Proceedings of the 9th International Symposium on Physical Measurements and Signatures in Remote Sensing (ISPMSRS), Beijing, China, 17–19 October 2005; pp. 318–320.
74. Lewis, P.; Disney, M. Spectral invariants and scattering across multiple scales from within-leaf to canopy. *Remote Sens. Environ.* **2007**, *109*, 196–206. [CrossRef]
75. Lewis, P.; Disney, M. On canopy spectral invariants and hyperspectral ray tracing. In Proceedings of the 2nd Workshop on Hyperspectral Image Processing: Evolution in Remote Sensing (WHISPERS), Reykjavik, Iceland, 14–16 June 2010; pp. 1–4. [CrossRef]
76. Smolander, S.; Stenberg, P. Simple parameterizations of the radiation budget of uniform broadleaved and coniferous canopies. *Remote Sens. Environ.* **2005**, *94*, 355–363. [CrossRef]
77. Ganguly, S.; Schull, M.; Samanta, A.; Shabanov, N.; Milesi, C.; Nemani, R.; Knyazikhin, Y.; Mynenia, R.B. Generating vegetation leaf area index earth system data record from multiple sensors. Part 1: Theory. *Remote Sens. Environ.* **2008**, *112*, 4333–4343. [CrossRef]
78. Ganguly, S.; Schull, M.; Samanta, A.; Shabanov, N.; Milesi, C.; Nemani, R.; Knyazikhin, Y.; Mynenia, R.B. Generating vegetation leaf area index Earth system data record from multiple sensors. Part 2: Implementation, analysis and validation. *Remote Sens. Environ.* **2008**, *112*, 4318–4332. [CrossRef]
79. Yang, B.; Knyazikhin, Y.; Mõttus, M.; Rautiainen, M.; Stenberg, P.; Yan, L.; Chen, C.; Yan, K.; Choi, S.; Park, T.; et al. Estimation of leaf area index and its sunlit portion from DSCOVR EPIC data: Theoretical basis. *Remote Sens. Environ.* **2017**, *198*, 69–84. [CrossRef] [PubMed]
80. Köhler, P.; Guanter, L.; Kobayashi, H.; Walther, S.; Yang, W. Assessing the potential of sun-induced fluorescence and the canopy scattering coefficient to track large-scale vegetation dynamics in Amazon forests. *Remote Sens. Environ.* **2018**, *204*, 769–785. [CrossRef]
81. Marshak, A. The effect of the hot spot on the transport equation in plant canopies. *J. Quant. Spectrosc. Radiat. Transf.* **1989**, *42*, 615–630. [CrossRef]

82. Verstraete, M.M.; Pinty, B.; Dickinson, R.E. A physical model of the bidirectional reflectance of vegetation canopies 1. Theory. *J. Geophys. Res.* **1990**, *95*, 11755–11765. [CrossRef]
83. Pinty, B.; Verstraete, M.M. Modeling the scattering of light by homogeneous vegetation in optical remote sensing. *J. Atmos. Sci.* **1998**, *55*, 137–150. [CrossRef]
84. Stenberg, P. Simple analytical formula for calculating average photon recollision probability in vegetation canopies. *Remote Sens. Environ.* **2007**, *109*, 221–224. [CrossRef]
85. Disney, M.I.; Lewis, P.; North, P.R.J. Monte Carlo ray tracing in optical canopy reflectance modelling. *Remote Sens. Rev.* **2000**, *18*, 163–196. [CrossRef]